



UNIVERSITY OF SOUTHERN DENMARK

**MADS CLAUSEN INSTITUTE
NanoSYD**

Master Thesis

**ULTRAFAST PULSE LASER MEASUREMENT
SYSTEM FOR LASER SCANNING
MICROSCOPY**

Author:

Paweł Cielecki

Supervisor:

Assistant Professor

Jacek Fiutowski

PREFACE

First of all, I will always be grateful to Assistant Professor Jacek Fiutowski for his patience, knowledge he shared with me and guidance during my master project. I am grateful for all the support I received and for possibility of working with him.

I would also like to express my deep gratitude to my parents for being there for me and for all kinds of support and encouragement.

ABSTRACT

The overall aim of this project was to upgrade the existing LSM setup, which is a foundation for many various scientific projects conducted at MCI (Mads Clausen Institute). During that projects, some abnormalities in the operation of the setup was observed, which were believed to be caused by irregular operation of the laser. Therefore, it was decided to extend the LSM setup with an intensity autocorrelation system. This system would provide a basic diagnostics of the laser pulsing operation as well as measurements of the pulse width. Results of these measurements were later used to investigate an influence of the pulse duration on a laser ablation of PMMA, which is commonly used field-mapping and micromachining technique.

More detailed description of all assumed objectives is presented in chapter 1. The second chapter of this thesis contains a brief theoretical introduction. This section describes phenomena such as; ablation, autocorrelation and generation of ultrashort pulses, which are a basic of this thesis and explains used nomenclature.

Chapter 3 presents designing process of autocorrelation system. It presents the constraints imposed by the LSM setup and different implementation ideas are considered. Furthermore, it explains their selection of all individual components and describe their role in the system.

Subsequent chapter 4 is related to the software for autocorrelation system. It shows the designing process from its beginning and explains thinking processes in all its phases. Moreover, it explains an operation a state machine used as a core of the software and presents two considered mechanisms of measurements. The last part of this chapter contains a short instruction for the software, which should help the inexperienced users.

Chapter 5 is related to tests of autocorrelation system. The autocorrelation function obtained during very first measurements was distorted, which is not acceptable. This chapter describes all efforts taken to improve the quality of measurements including; replacement of some components of the system, testing different configurations and verifying an influence of vibrations.

The new functionality of the LSM setup – pulse measurements was tested in the ablation mode, what is described in chapter 6. It begins with a description of a LSM setup structure. Thereafter, it presents experiments designed to verify the influence of pulse width on the ablation of PMMA. During these experiments, a special attention is paid to potential problems and irregularities related to operation of the LSM setup.

GLOSSARY

LSM – Laser Scanning Microscope

PMMA – Poly(methyl methacrylate)

BBO – Beta-barium borate (β -BaB₂O₄)

FWHM – Full width at half maximum

BNC – Bayonet Neill–Concelman

SEM – Scanning Electron Microscope

TABLE OF CONTENTS

PREFACE	I
ABSTRACT	II
GLOSSARY	III
1 GOALS OF THE PROJECT	1
2 THEORETICAL BACKGROUND	2
2.1 GENERATION OF ULTRASHORT LASER PULSES – MODE-LOCKING	2
2.2 NONLINEAR OPTICS AND SECOND HARMONIC GENERATION	4
2.3 ULTRAFAST PULSE MEASUREMENTS - AUTOCORRELATION	6
2.4 LASER ABLATION	9
3 DESIGN OF THE AUTOCORRELATION SYSTEM	10
3.1 STRUCTURE OF LSM SETUP AND ASSOCIATED CONSTRAINS	10
3.2 CONFIGURATION IDEAS	11
3.3 COMPONENTS AND SOLUTIONS APPLIED IN THE SYSTEM.....	13
3.3.1 Laser path components	13
3.3.2 Loop with a controlled delay – linear translation stage	15
3.3.3 Focusing lens and shg crystal	17
3.3.4 Equipment for intensity measurements.....	18
3.3.5 Beam termination.....	18
3.3.6 Selection of the filter.....	19
4 SOFTWARE FOR THE AUTOCORRELATION SETUP	23
4.1 REQUIRED FUNCTIONALITY	23
4.2 OVERALL STRUCTURE OF THE SOFTWARE.....	25
4.2.1 Initiation.....	25
4.2.2 Waiting for instructions	26
4.2.3 Sliding table manipulation	27
4.2.4 Measurements	27
4.2.5 Closing procedures.....	30
4.3 USER INTERFACE	30
4.4 USAGE OF THE SOFTWARE	33
5 AUTOCORRELATION SYSTEM - TESTS AND MEASUREMENTS	34
5.1 PREPARATION OF MEASUREMENTS	34
5.2 SPECTRUM MEASUREMENTS	35
5.2.1 Bandwidth calculator	37
5.3 MEASUREMENTS	38
5.3.1 Removing the optical isolator	39
5.3.2 Compensation by a glass plate	40
5.3.3 Checking geometry issues.....	41

5.3.4	Changing the beamsplitter	42
5.3.5	Testing crystal	42
5.3.6	Changing lens.....	43
5.3.7	Testing influence of vibrations (adding dc motor)	44
5.3.8	Laser.....	45
5.4	COMPARISON OF MEASUREMENT METHODS.....	46
6	ABLATION OF PMMA	48
6.1	PRESENTATION OF THE LSM SETUP	48
6.2	FABRICATION OF THE SAMPLE	49
6.3	DEFINING THE SIZE OF ABLATED AREA	51
6.4	EXPERIMENT – INVESTIGATING INFLUENCE OF A PULSE WIDTH ON AN ABLATION OF PMMA.....	54
6.4.1	Ablation for unmodulated pulse (without the beamsplitter cube)	55
6.4.2	Ablation for modulated pulse (with the beamsplitter cube).....	57
7	CONCLUSIONS AND FURTHER IMPROVEMENTS.....	61
8	INDEX OF FIGURES.....	64
9	INDEX OF TABLES.....	67
10	REFERENCES	68
11	APPENDICES	70
	APPENDIX A – DATASHEET OF TSUNAMI LASER.....	71
	APPENDIX B – BLOCK DIAGRAM OF STEP MEASUREMENT PROGRAM	72
	APPENDIX C – BLOCK DIAGRAM OF CONTINUOUS MEASUREMENT PROGRAM.....	73

1 GOALS OF THE PROJECT

The main goal of this project was to upgrade the existing LSM setup. It was desired to extend the functionality of the setup by incorporating an intensity autocorrelation system. It would provide a basic diagnostic of the laser pulsing operation, which is crucial for operation of the entire setup as well as pulse width measurements. Results of these measurements would be used to determine the influence of the pulse duration on a laser ablation of PMMA coatings using the ablation mode of LSM. Additionally, a close attention should be paid for any potential imperfections of the system and its operation, which may interfere the ablation. Taking into account all above information the following objectives of the project were formulated:

- **Designing and building the system for intensity autocorrelation measurements.**
Designing process should be started with finding a suitable position for the system, which would not disrupt the operation of the LSM setup. It should be followed by a selection of required equipment. Subsequently, all selected elements should be put together to give rise to the complete system. The last task would be to provide the required power supply for all active components of the system.
- **Developing proper software providing automatic measurements.**
The first step would be to connect all active components into one system administered by the computer. Afterwards, a suitable algorithm of measurements should be found and an additional functionality of the software should be defined. Subsequently, a proper programming environment should be selected and used for implementation. Moreover, a communication with the user should be provided by user's interface. Finally, the software should be tested in terms of repeatability of measurements
- **Testing the intensity autocorrelation system.**
The system should be properly tested and all efforts should be made in order to obtain correct results. In case of any abnormalities, the reason should be found and eliminated. If one of the used components would be a cause, it should be, as far as possible, replaced and tests should be repeated.
- **Performing ablation of PMMA.**
New functionality of the LSM setup – pulse width measurements – should be used in the ablation mode. Firstly, the ablation should be performed and the ablation threshold should be determined. Subsequently, the ablation should be repeated for extended pulse duration. A difference in results would verify if broadening of a pulse is an issue for ablation. Moreover, a special attention should be paid for potential sources of defect in ablation associated with both the system and the process.

2 THEORETICAL BACKGROUND

This chapter contains theoretical aspects related to the field of interest of the project. Its main goal is to describe the principle of applied phenomena and to clarify a nomenclature used in this thesis. The following subchapters represent four phenomena, which understanding is crucial for the project. Firstly, the principle of laser and methods used for generation of ultrashort pulses are described, which are the foundation of the project. Then, a short introduction to nonlinear optics and second harmonic generation is presented. This information is necessary to fully understand the principle of autocorrelation, which is shortly described in the third subchapter. The last part is dedicated to the ablation, which is a basic for the main experiment of this project.

2.1 GENERATION OF ULTRASHORT LASER PULSES – MODE-LOCKING

Before discussing methods of generating ultrashort pulses, a brief review of a single-mode laser operation is presented. The simplest laser geometry, presented in Figure 2.1, consist of two mirrors and a gain medium, which acts as an optical amplifier. Combined mirrors form so called cavity or resonator. Mirrors are aligned in such a way that a beam started by a spontaneous emission is reflected back and forth though the cavity. During these cycles (round-trips) the beam is amplified (gained) by externally pumped gain medium using stimulated emission phenomena. As a result a highly coherent, intense beam is created.

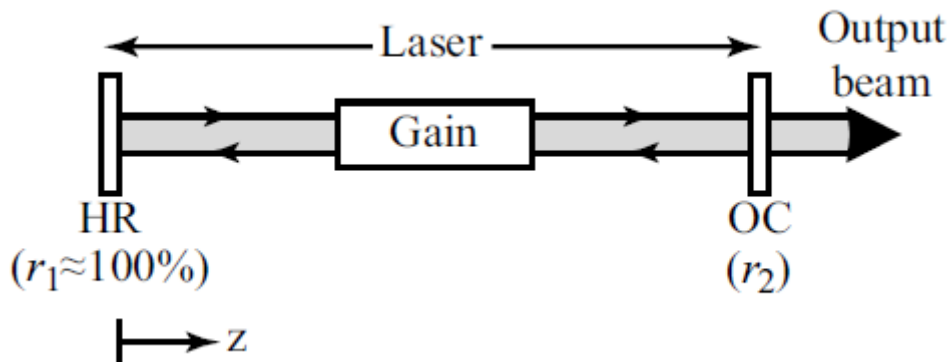


Figure 2.1 Simple laser geometry. HR – high reflector, OC – output coupler, z – direction of laser emission [1].

It is worth noting that during every cycle some part of the beam is emitted through output coupler. In order to maintain the laser operation two conditions has to be fulfilled. First of them – the gain condition, states that the round-trip gain must equal the loss [1]. The second one – phase condition implies that the laser is only allowed to oscillate with certain discrete angular frequencies, which are referred as longitudinal frequencies. Considerations of these conditions lead to the frequency domain interpretation of the laser operation, which is schematically presented in Figure 2.2. In that case cavity loss is independent of frequency, while the response of the gain has a bandpass spectrum. The output of the laser contains only these longitudinal modes, whose gain exceeds cavity loss. This laser

operation mode is called multimode because the beam contains simultaneously multiple frequencies.

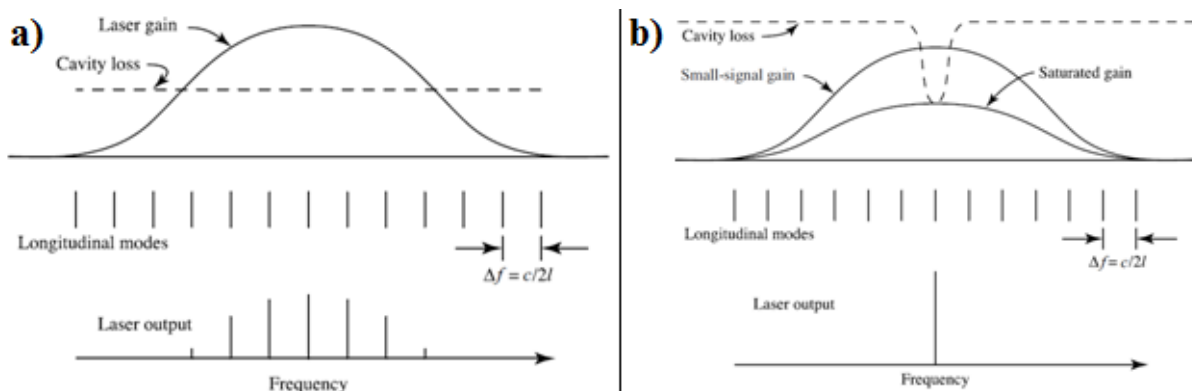


Figure 2.2 Operation of the laser in a frequency domain a) multimode b) single-mode [1].

The single-mode (monochromatic) laser radiation can be obtained by inserting a frequency-dependent loss element (filter) into the system [1]. This filter should have a narrow bandpass characteristic to ensure that the gain of just one longitudinal mode exceed loss and therefore is the only component of the output signal. This situation is illustrated in the following Figure 2.2.

Since time characteristics of the laser pulse are bounded to its frequency characteristics by Fourier transform, pulse duration (width) and bandwidth cannot vary independently [2]. Properties of the Fourier transform imply that ultrashort pulses can be obtained only for the broad bandwidth. Previously described single-mode lasers are a source of a monochromatic light and therefore, they are unable to produce ultrashort pulses. Even removing the bandwidth-limiting filter and operating in the multimode is not sufficient for ultrashort pulses generation. Therefore some more sophisticated methods of increasing the amount of mode involved in laser operation and hence broadening the bandwidth has to be applied. These methods are based on inserting pulse-forming elements (modulators) to the system and are referred as mode-locking [3]. In general, two different mechanisms of mode-locking can be distinguished:

- Active mode-locking – this method uses an electronic modulator to periodically modulate cavity losses. Ultrashort pulses can be obtained if the modulator is synchronized with round-trips of the system. In is worth noting that a typical pulses duration obtained by this method is in picoseconds range.
- Passive mode-locking – in this method a passive element – saturable absorber is added to the cavity. This optical component absorb incident light until it get saturated. In that case it transmits a light for a short moment before it recovers and the cycle is repeated. Passive mode-locking is able to produce much shorter pulses than active mode-locking. The merit goes to saturable absorber, which operation is faster than any electronic modulator.

2.2 NONLINEAR OPTICS AND SECOND HARMONIC GENERATION

Nonlinear optics studies phenomena, in which the response of the material system does not depend linearly on strength of applied optical field. Since, in general, only lasers are able to produce a light with a sufficient intensity to induce nonlinear phenomena, this field of science started to develop rapidly after a production of the first laser (1960) [1]. Nonlinear optical phenomena are usually described by expressing the polarization $\tilde{P}(t)$ (dipole moment) in terms of strength of applied electric field $\tilde{E}(t)$. In the conventional (linear) optics, relation between these two parameters is given by the following formula:

$$\tilde{P}(t) = \epsilon_o \chi^{(1)} \tilde{E}(t) \quad (1)$$

Where, $\chi^{(1)}$ is a linear (first order) susceptibility and ϵ_o is a permittivity of vacuum. It is worth noting that for simplicity polarization and strength of electric field are represented by scalar quantities.

However, in nonlinear optics, a generalized form of the above equation has to be applied. In that case a polarization is expressed as a power series in the field strength:

$$\begin{aligned} \tilde{P}(t) &= \epsilon_o [\chi^{(1)} \tilde{E}(t) + \chi^{(2)} \tilde{E}^2(t) + \chi^{(3)} \tilde{E}^3(t) + \dots] \\ &\equiv \tilde{P}^1(t) + \tilde{P}^2(t) + \tilde{P}^3(t) + \dots \end{aligned} \quad (2)$$

Where, $\chi^{(2)}$ and $\chi^{(3)}$ are susceptibility of second- and third- order respectively. $\tilde{P}^2(t)$ is a polarization of second-order and similarly $\tilde{P}^3(t)$ is a third-order polarization.

The main reason of using polarization for describing an optical phenomenon is that a time-varying polarization can act as a source of an electromagnetic radiation. It is confirmed by the following wave equation for a nonlinear optical medium [1]:

$$\nabla^2 \tilde{E} - \frac{n^2}{c^2} \frac{\partial^2 \tilde{E}}{\partial t^2} = \frac{1}{\epsilon_o c^2} \frac{\partial^2 \tilde{P}^{NL}}{\partial t^2} \quad (3)$$

Where, n is a linear refractive index, c is a speed of light in a vacuum and \tilde{P}^{NL} is a nonlinear polarization.

➤ Second Harmonic Generation

Assuming a laser beam with the electric field strength given by:

$$\tilde{E}(t) = E e^{-i\omega t} + c. c. \quad (4)$$

Which is incident upon a medium with a nonzero second-order susceptibility $\chi^{(2)}$. In that case a nonlinear polarization, which is created in such a medium, takes the following form:

$$\tilde{P}^2(t) = 2\epsilon_o \chi^{(2)} E E^* + (\epsilon_o \chi^{(2)} E^2 e^{-i2\omega t} + c. c.) \quad (5)$$

The above equation shows that polarization consists of two terms. The first one is a constant term (frequency = 0), while the second one varies with a frequency 2ω . In accordance with

the previously presented wave equation for a nonlinear optical medium the second term gives rise to the generation of radiation at the second-harmonic frequency. This phenomenon is known as second harmonic generation (SHG). Since the second derivative of the first term vanishes, this contribution does not result in generation of the optical wave. Under proper condition second harmonic generation process can be very efficient. In that case almost the entire power of incident light with frequency ω is change into the radiation with frequency 2ω . Second harmonic generation can be also considered as a exchange of photons between components of the field with different frequencies. This situation is visualized in Figure 2.3 b). In that case two photons with a frequency ω turns into one photon of 2ω frequency.

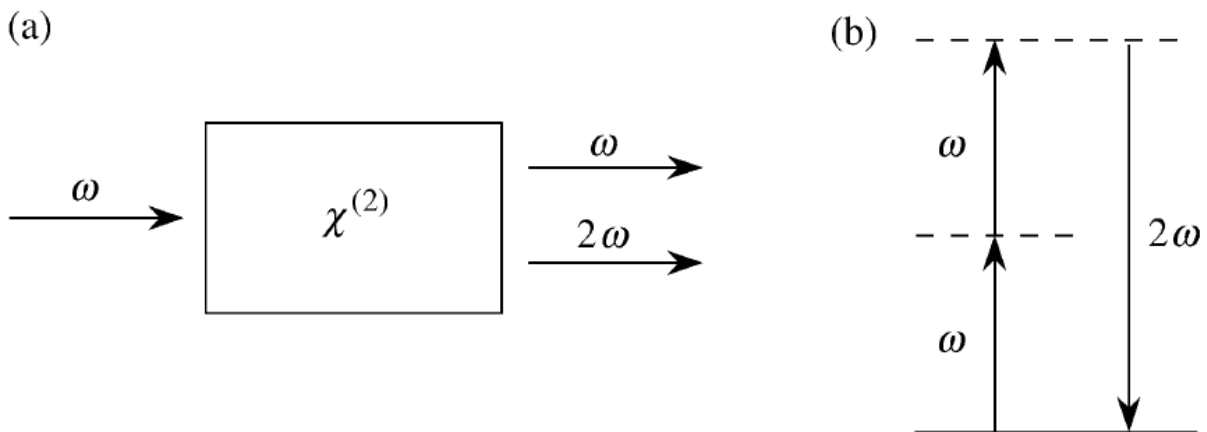


Figure 2.3 Second harmonic generation a) general concept b) energy-level diagram.

Second harmonic generation is extremely phase-sensitive process. The high efficiency can be obtained only if there is a phase matching between interacting waves (wave incident upon the medium and created second harmonic wave) [2]. The phase matching can be achieved using materials, which do not exhibit inversion symmetry-birefringent (centrosymmetric) crystals. Some examples of birefringent crystals are [1]: beta barium borate (BBO), lithium niobate (LiNbO_3), gallium arsenide (GaAs). It is worth noting that in contrast to second-order nonlinear phenomena, third-order optical interactions can occur in centrosymmetric as well as noncentrosymmetric.

Second harmonic generation has an application in many different fields, few examples are presented below:

- It can be used to convert the wavelength of radiation of laser. Nd:YAG laser operates at $1,06 \mu\text{m}$, which is outside the visible spectrum. Using SHG a visible radiation with wavelength of 530 nm is created. This may be very useful during adjustment of the laser path.
- It can be used for imaging. As it was reported in [6], SHG combined with multiphoton imaging was found useful for investigating the three-dimensional structure of macromolecules within living tissue.
- SHG crystals are commonly used in intensity autocorrelation [7], which is a common pulse width measurement technique.

2.3 ULTRAFAST PULSE MEASUREMENTS - AUTOCORRELATION

Femtosecond pulses are far beyond the reach of the conventional electronic systems. Therefore, some more sophisticated techniques have to be used for their characterisation. It was noticed that the temporal profile of an optical signal can be easily determined using a shorter pulse with a well known shape as a reference. It can be achieved by measuring intensity correlation, which is given by the following equation:

$$A_c(\tau) = \int_{-\infty}^{\infty} I_s(t) I_r(t - \tau) dt \quad (6)$$

Where A_c is an obtained correlation function, I_s is an intensity of measured signal and I_r is an intensity of reference signal.

As it is presented in the above equation, correlation function is independent of time. Instead, it depends on a time shift between the pulses, which can be easily implemented by moving the optical components. This trick allows avoiding necessity of using ultrafast measurement equipment.

However, in case of femtosecond pulses, shorter pulses are assumed not available from practical matters. Therefore, it was proposed to use the measured signal itself as a reference. This approach is called autocorrelation and it is commonly used measurement and diagnostic technique [8]. Autocorrelation measurements are performed using interferometer and SHG crystal, whose nonlinearity provides intensity multiplication of two beams. In that case measured time-integrated (time-averaged) SHG power can be described by the following formula [7]:

$$\begin{aligned} \langle P_{SHG}(t) \rangle \sim & 2\langle |a(t)|^2 \rangle + 4\langle |a(t)|^2 |a(t - \tau)|^2 \rangle \\ & + \left\{ 2\langle (|a(t)|^2 + |a(t - \tau)|^2) \times a(t)a^*(t - \tau) \rangle e^{j\omega_0\tau} \right. \\ & \left. + \langle [a(t)a^*(t - \tau)]^2 \rangle e^{2j\omega_0\tau} \right\} + c. c. \end{aligned} \quad (7)$$

The first term (green) of the above equation does not depend on τ . The second term (brown) depends on it by varies very slowly. The third term (blue) together with the fourth term (red) are interferometric contributions for ω_0 and $2\omega_0$ respectively. Based on a treatment of these terms, two different autocorrelation methods can be distinguished:

- Interferometric autocorrelation – in these methods all four terms are measured. Obtained autocorrelation function contains information about pulse width, phase and coherence [7]. This approach requires fast measurement in order to avoid averaging rapidly oscillating interferometric terms.
- Intensity (fringe-averaged) autocorrelation – interferometric terms in this method are suppressed by averaging SHG signal over few optical periods. Autocorrelation function obtained by this approach is an even function of τ , which unfortunately, is not unequivocal (many different signal can give the same autocorrelation function [9]). As a result, the autocorrelation function

does not provide complete information about the measured pulse (e.g. phase). However, it is a useful tool for determining pulse duration. Since this method is much easier in implementation, it was decided to use it in the project. Therefore the following information are relate to the intensity (fringe-averaged) autocorrelation.

The implementation of an intensity autocorrelation measurement is very simple and do not require any sophisticated and expensive equipment. At the beginning, the measured pulse has to be split into two equal signals. It can be achieved by using a simple beamsplitter. Thereafter, signals are guided into the two different delay loops wherein, one of them has a variable delay, which together create a simple interferometer. Finally, signals are connected back into one and its intensity is measured for different values of a delay. There are two commonly used configurations of intensity autocorrelation system, which differ in structure and what is even more important in obtained signal.

➤ **collinear geometry (with background)**

In this geometry, the signals leaving delay loops are guided to a beamsplitter, which orients them collinearly. Afterwards signals are focused onto a SHG crystal using a lens. Then an intensity of created second harmonic signal is measured. The obtained second harmonic signal is a sum of two terms. First of them represents the intensity autocorrelation function of two pulses, while the second one is related to SHG from two pulses individually. The second term forms a constant background, which is a significant weakness of this configuration. The sample implementation of the collinear geometry is presented in the following Figure 2.5.

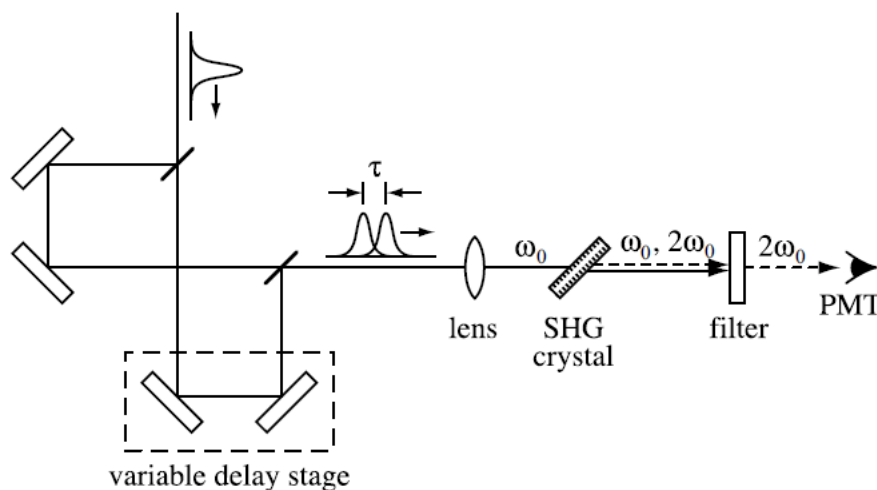


Figure 2.4 Sample of collinear geometry of an autocorrelation system [2].

➤ **noncollinear geometry (background-free)**

Instead of “merging” two signals on the beamsplitter, noncollinear geometry uses an additional mirror to reflect one of signals and orient it parallel to the other. Subsequently, parallel signals are focused onto the SHG crystal by a lens. Second

harmonic signal related to the autocorrelation of two signals is going straight to the intensity sensor. However, signals representing two individual pulses are spreading away from the sensor. These signals can be easily terminated using an iris (or screen) and hence they do not interfere with the measurement. Therefore, measured signal is an autocorrelation function itself (it is background-free). The following Figure 2.5 illustrates a sample structure of the noncollinear geometry.

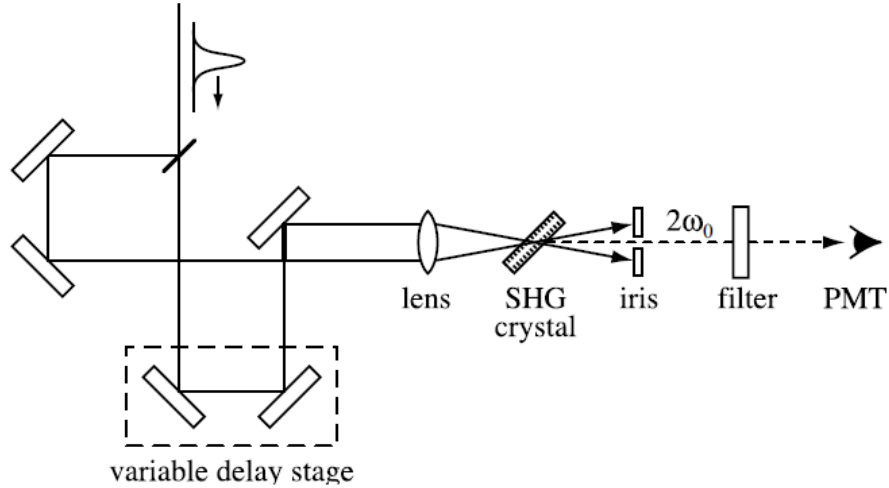


Figure 2.5 Sample of noncollinear geometry of an autocorrelation system for background-free measurements [2].

As it was previously stated, the autocorrelation function can be used to determine duration of the measured pulse. In order to obtain that information the following procedure has to be performed. At the beginning, the shape of the measured pulse has to be “assumed” (one can use a shaped used by the laser manufacturer during a characterization of the device). In general, sech^2 and Gaussian are the most common and accurate shapes [8]. Subsequently, the autocorrelation function has to be fitted to the assumed pulse shape and its FWHM has to be determined. Thereafter, FWHM of the autocorrelation function has to be divided by a deconvolution factor corresponding to the pulse shape. Table 2-1 presents deconvolution factors of the most common pulse shapes. The result of the performed calculation is FWHM of the measured pulse.

Table 2-1 The most common pulse profiles with corresponding autocorrelation functions and deconvolution factors [2].

$I(t)$	$G_2(\tau)$	$\frac{\Delta\tau}{\Delta t}$
$\text{sq}(t)$	$1 - \tau $ for $ \tau \leq 1$, 0 otherwise	1
e^{-2t^2}	$e^{-\tau^2}$	$\sqrt{2}$
$\text{sech}^2(t)$	$\frac{3(\tau \cosh(\tau) - \sinh(\tau))}{\sinh^3(\tau)}$	1.543
e^{-t} for $t \geq 0$, 0 otherwise	$e^{- \tau }$	2

^a Δt and $\Delta\tau$ are full widths at half maximum of the intensity $I(t)$ and the intensity autocorrelation function $G_2(\tau)$, respectively. $\text{sq}(u)$ is defined as a unit square pulse such that $\text{sq}(u) = 1$ for $|u| \leq \frac{1}{2}$ and 0 otherwise; and t and τ are in normalized units.

2.4 LASER ABLATION

Laser ablation (also referred as photoablation) is a process in which a material is removed under the influence of incident light. It was first reported in 1982 [10] and since then it has been carefully studied by many research teams. However, despite many years of a research, the mechanism of ablation was not fully recognized. There are many different models, which consider ablation as photothermal processes, photochemical reactions or even photophysical process [10]. However, it is certain that in order to remove the part of a material, laser pulse should deliver enough energy to break the bonds between atoms [11]. Therefore the crucial parameter for ablation is so called ablation threshold, which is related to a minimum energy required to start the process. The ablation threshold is commonly given in form of a peak intensity:

$$I_{peak} = \frac{P_{peak}[W]}{A [cm^2]} \quad (8)$$

Where, I_{peak} is peak intensity, P_{peak} is a peak power and A is a focal spot area.

Another commonly used form of presenting ablation threshold is fluence, which is given by the following formula

$$F = \frac{E [J]}{A [cm^2]} \quad (9)$$

Where, F is fluence, E is an energy of the pulse and A is a focal spot area.

Another important matter in ablation is so called incubation. It was revealed that for longer exposure duration the ablation threshold decreases [12] [13].

During almost 25 years of research, ablation has been used in numerous applications. It is worth noting that femtosecond lasers had a crucial role in a rapid development of ablation applications because in the femtosecond second regime there is no (or a little) heat conduction [10]. The most important fields in which laser ablation is applied are:

- Field-mapping [12] – ablation of polymer thin films is used to examine the field enhancement caused by the occurrence of plasmonic resonances.
- Micromachining – ablation is commonly used tool in microfabrication. A sample application of local material removal provided by laser ablation is making a channels and other structures for microfluidics [15]. Moreover, ablation can be also used in bottom-up fabrication using so called ablation deposition [16].
- Medicine [17] – laser ablation has application in repairing human organs. It can be used during a heart operation to remove a small area that can cause heart rhythm problems.

3 DESIGN OF THE AUTOCORRELATION SYSTEM

The first main task of the project was to upgrade the laser scanning microscope (LSM) setup with an autocorrelation system. The primary function of the autocorrelation system is to monitor a pulse width during LSM operation. Functionality of this system will be tested in so called ablation mode of the LSM, which is further described in chapter 6. Moreover, the autocorrelation system will be used as a diagnostic tool to verify operation of the laser and detect pulse defects.

3.1 STRUCTURE OF LSM SETUP AND ASSOCIATED CONSTRAINS

Since the goal was to upgrade existing LSM setup, it is necessary to familiarize with its structure and to recognize associated design constraints for the designed autocorrelation system. The outline of the laboratory stand containing most important dimensions is illustrated in Figure 3.1. Entire LSM setup is placed on an optical table, which is divided into two sections. The first section contains the LSM with associate equipments. Moreover, this part of the table is almost fully occupied by some other research setups therefore; it could not be used in this project. The second section, marked in Figure 3.1 as a yellow area, contains the laser and the major part of the laser path. As it is presented in the following figure, this part of the table has plenty of a free space hence; it is a perfect place for the designed system.

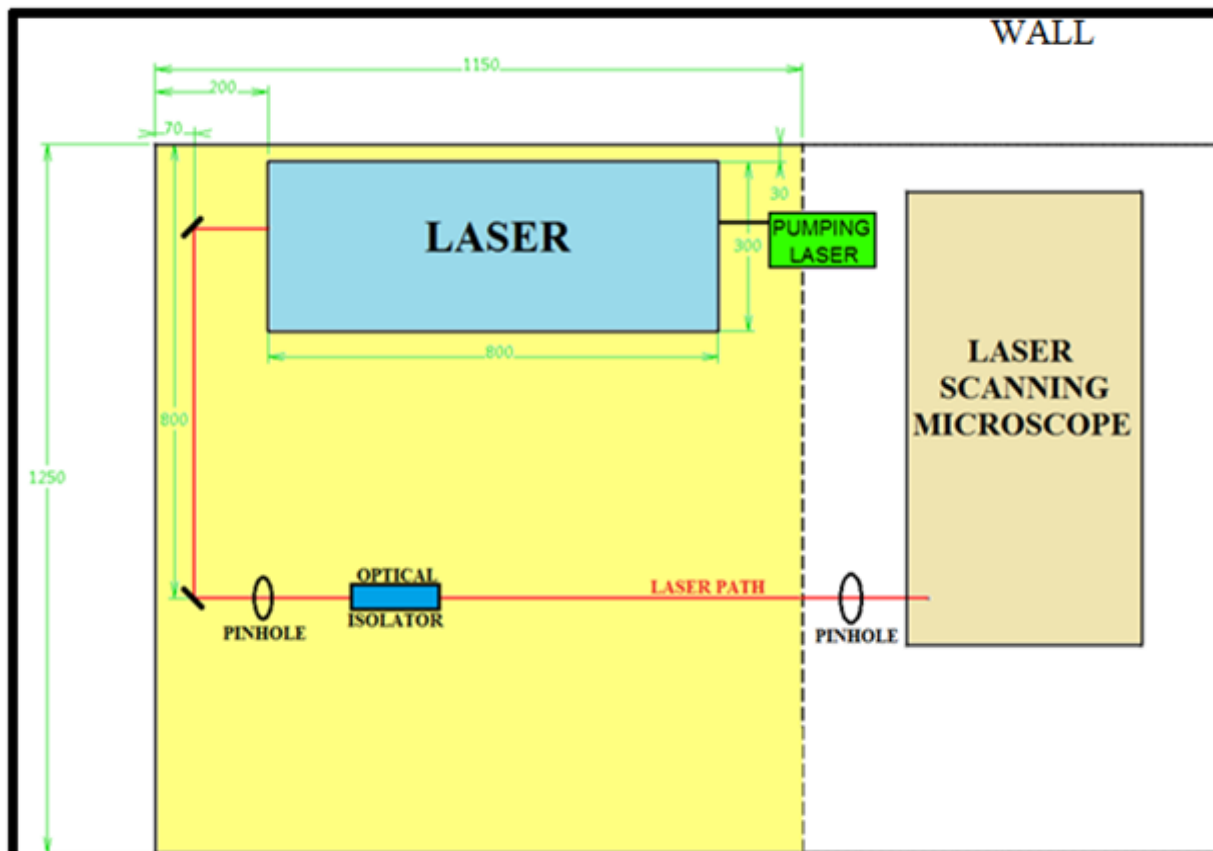


Figure 3.1 Schematic drawing of the laboratory stand.

The laser applied in the LSM setup is Tsunami 3941-35-M3S produced by Spectra-Physics. This unit has a tuneable wavelength range 780–820 nm, max power 700 mW at 800 nm, nominal repetition rate 82 MHz and sub 35 fs pulse width [appendix A]. The Tsunami laser is pumped Millennia Vs Js, 5W Nd:YAG laser. The laser path contains many various optical components. Some of them have to be taken into account during designing process. The first important component is an optical isolator I-7090C-M produced by Isowave. The main function of this device is to prevent the laser beam travelling back to the laser, which may disrupt its operation. Since, the optical isolator is quite large comparing to the other optical components and therefore it cannot be placed anywhere, its position has to be carefully considered during designing process. Furthermore, the laser path is equipped with few pinholes, which are used to restore an adjustment of the laser beam. However, these devices are rather small and fitting it into the design should not be challenging. The last but also the most important component of the system is the LSM and associate equipments. Because this part of the setup is not directly related to the designing of the autocorrelation system it will not be describe in this chapter. The precise description of LSM is contained in chapter 6.

3.2 CONFIGURATION IDEAS

After defining system constrains resulting from the laboratory conditions and becoming acquainted with the setup, the next task was to find a suitable place for the system and to design its structure. At the beginning of these considerations, it was noticed that previously presented in Figure 2.5 geometry is an optimal configuration in respect of used equipment (mirrors). The main reason for that is an applied position of the beamsplitter. There are two possible configuration of this component. In the first one the beam is reflected towards the intensity sensor, while in the other the beams is reflected in the opposite direction. As it is illustrated in Figure 3.2 a), the first configuration requires as much as 8 mirrors to create delay loops, which are equal in length. On the other hand, the second configuration requires just 6 mirrors, which makes it a better choice.

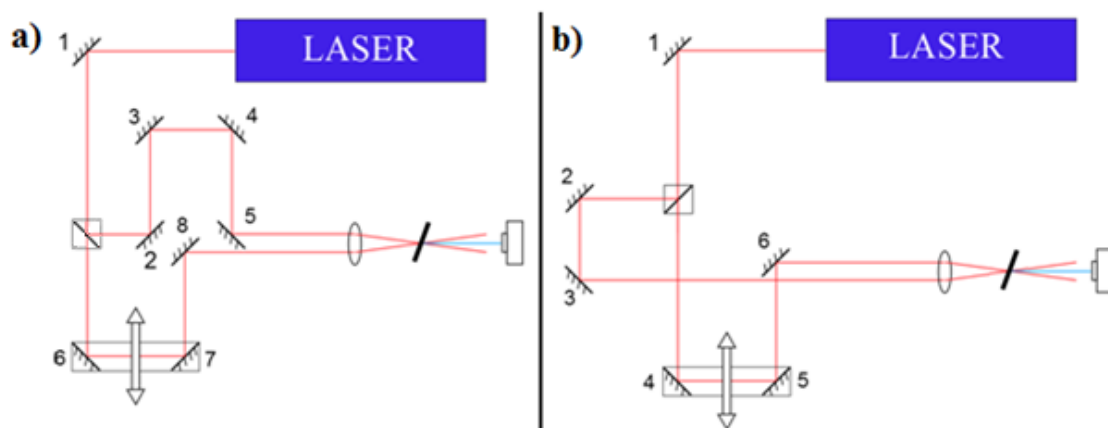


Figure 3.2 Two possible configuration of autocorrelation system a) beam reflected in the direction of the intensity sensor b) beam reflected in the opposite direction.

The next step was to find a suitable location for the entire autocorrelation system. Figure 3.3 presents three considered positions.

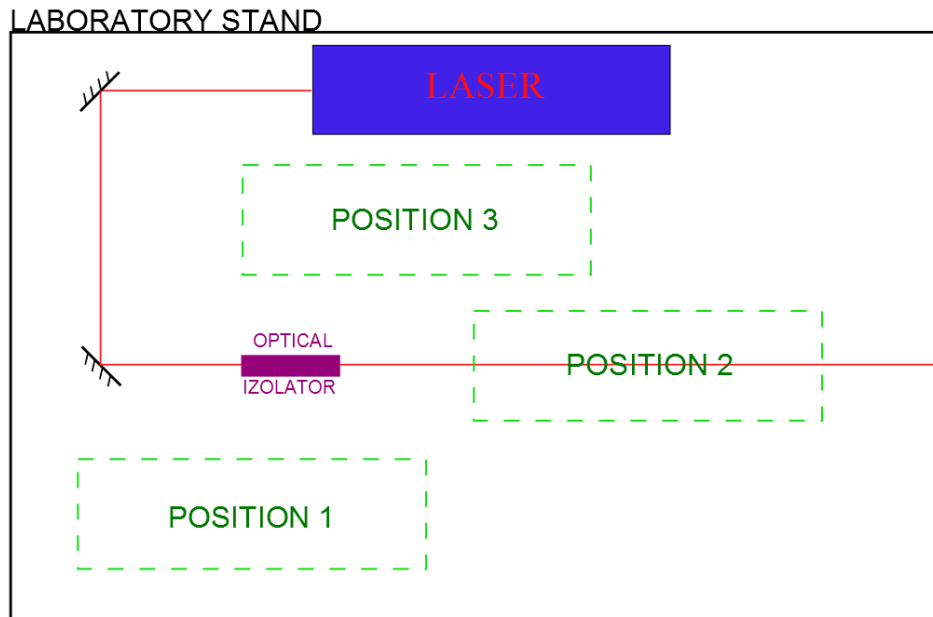


Figure 3.3 Considered locations for autocorrelation system.

➤ Position 1 is located at the edge of the laboratory stand, which provides an easy access to the system and ease of adjustment. Moreover, it has the greatest area from all considered locations. However, placing the autocorrelation system in that location would hinder an access to the central part of the table and hence, prevent a further development of the LSM system. Furthermore, the system does not require so much space and placing it in this position would be a huge waste of resources.

➤ Position 2 assumes to use the existing laser path as a delay loop of the autocorrelation system. This approach should significantly reduce the amount of space occupied by the system. However, this configuration has one very important disadvantage. As it is illustrated in Figure 3.4, the laser path for LSM is blocked by the three very important components of the autocorrelation system: lens, SHG crystal and intensity sensor. Usage of the LSM setup requires removing these components, which make this configuration hard to implement.

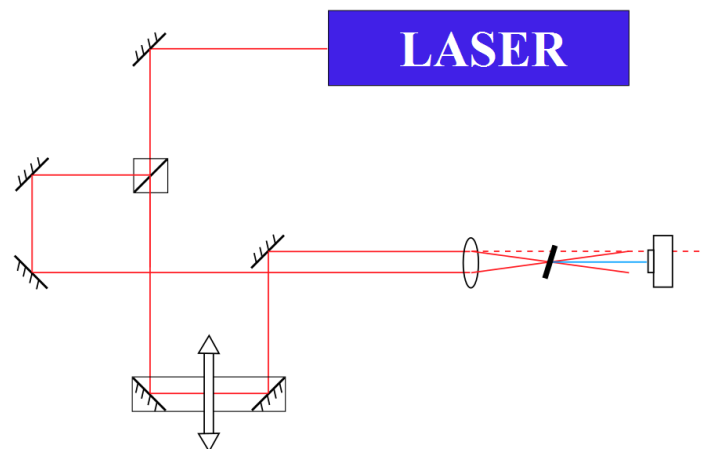


Figure 3.4 Considered system configuration for position 2.

➤ Position 3 is located between the Tsunami laser and the existing laser path. Because it is placed in the centre of the laboratory stand it would not prevent the further development of

the setup. Moreover, the area of this location is proper for the dimensions of the autocorrelation system. The only disadvantage of this position is a poor access to the system caused by a large distance to the edge of the laboratory stand. However, it would affect only the construction phase and should not hinder the usage of the system.

Deep analysis of all arguments presented above has led to selection of the position 1. The main reason for that choice was an easy implementation and possibility of the further development of the LSM setup. The last task was to fit, the previously found optimal configuration into the selected location. The following Figure 3.5 shows two considered structures of the system. The main difference between presented structures is a way of guiding the beam from the existing laser path. The first idea requires placing two optical elements in that path while, the second uses only one component for that purpose. Moreover, the first idea assumes placing a delay loop near to the edge of the laboratory stand, what may be hard to achieve. Therefore, the second configuration presented in Figure 3.5 b) was chosen as the final structure of the system.

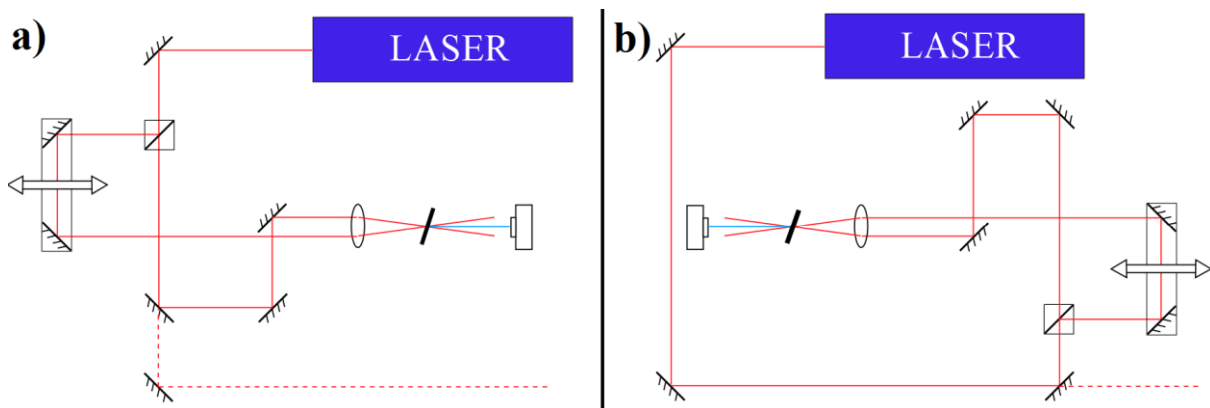


Figure 3.5 Considered configurations of the system for position 1.

3.3 COMPONENTS AND SOLUTIONS APPLIED IN THE SYSTEM

This subchapter describes components and solutions used in the intensity autocorrelation setup. Moreover, it explains thinking processes, calculations and measurements, which have led to the selection of the equipment. Components are presented in the order related to their position in the system; starting from the guiding the laser beam to the system and finishing at the intensity measurement. It is worth noting, that due to economical aspects, it was intended to mostly use equipment from university resources.

3.3.1 LASER PATH COMPONENTS

The first important task in laser path designing process was related to guiding the beam from LSM setup towards the autocorrelation system. Two solutions were considered. The first idea, assumes using a beamsplitter to split the main beams into two secondary beams. One of them would be guided towards the LSM setup while the other would be used for autocorrelation measurements. The main advantage of using a beamsplitter is a possibility

of using both systems simultaneously. However, the intensity of the beam is distributed between these two systems. It should not affect the autocorrelation measurements (it does not require the entire power of the beam) although, it might be important for ablation experiment. The second approach assumes using a mirror mounted to the kinematic mount, which ensures high accuracy of assembling. In this idea, the post acts as a switch. If it is assembled, the beam is reflected by the mirror and guided towards the autocorrelation system. If the post is disassembled nothing blocks the laser path and the entire beam is guided towards LSM setup. The greatest advantage of this solution is that the entire power of the beam can be directed to the LSM setup. Unfortunately it also means that systems cannot be used simultaneously. The third option was to use a polarizing beamsplitter together with a half-wave plate. By rotating the half-wave plate intensity of a transmitted and reflected light can be adjusted. This method allows using both systems simultaneously as well as directing the whole power to the LSM setup. However, it requires adding two optical components to the system.

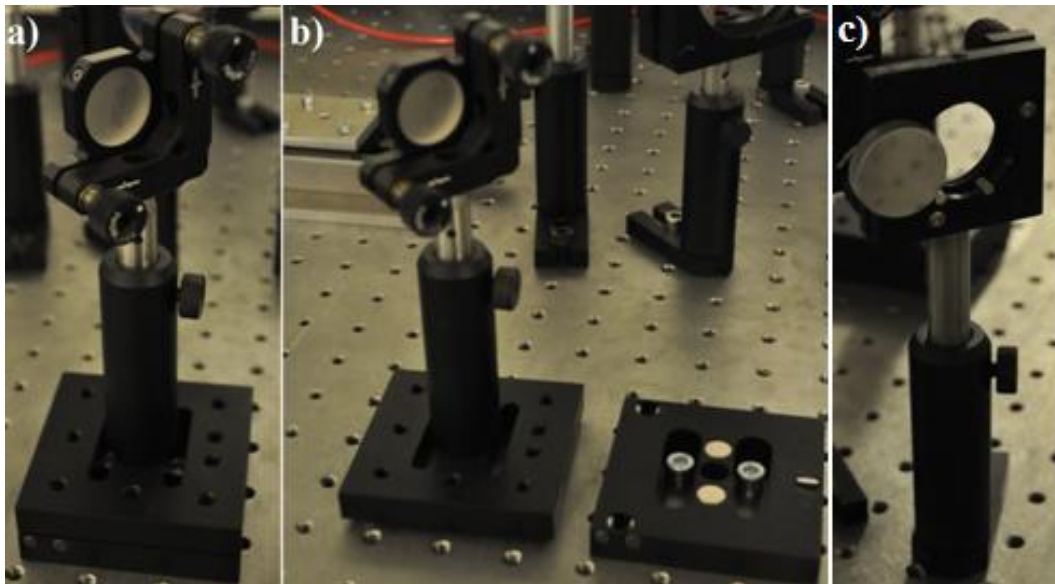


Figure 3.6 Mirror mounted to a kinematic mount used for guiding the laser beam to the autocorrelation setup a) post assembled b) post disassembled c) mirror stuck to the frame.

After considering pros and cons of presented solutions, the second idea based on the demountable mirror was found the most reasonable choice. The First important argument was a possibility of using the entire beam power for LSM system. It was noticed that it is enough to run pulse measurements before the experiment with ablation, which indicates that system do not have to be used simultaneously. Moreover, this configuration requires just one additional component. Implementation of the chosen solution is presented in the Figure 3.6 a) and b). It is worth noting that the accuracy of the demountable post was verified during later tests of the system. Performed test has shown that disassembling and assembling of the post does not affect the adjustment of the system and no adjustment corrections are required.

According to the previously chosen configuration of the system the next element in the laser path is a beamsplitter. Since a spectra of femtosecond pulses are wide (beam is not truly monochromatic), a dispersion caused by the thick optical elements may widen the pulse and hence, interfere the measurements. Therefore, cube beamsplitters should be avoided and only

thin plates should be considered. In order to avoid problems with dispersion, the thinnest available (1 mm) 50/50 beamsplitter has been selected. According to the data presented by the manufacturer this thickness is not sufficient for the desired pulse width. Unfortunately, at the beginning of this project, the other equipment could not be bought. Therefore, previously mentioned 1 mm plate beamsplitter was applied in the system. Furthermore, the operation of the selected beamsplitter was verified. Intensity measurements of the transmitted and the reflected beams revealed that the splitting ratio is 60/40, which may lead to the error in measurements of the pulse width.

Two beams created by the beamsplitter are guided to separate delay loops. The first loop has a controlled delay (the principle of controlled delay loop is further described in chapter 3.3.2), while a delay of the other is constant. The stationary delay loop is created by the group of mirrors, which are embedded to the adjustable frames and mounted to the posts. At the end of the stationary loop, the beam has to be reflected and guided parallel to the one from the adjustable loop. These beams have to be in a small distance to be later focused by the lens. Therefore, a mirror used for the reflection cannot be embedded in the standard frame. Instead it has been stuck to the frame with a wax as it is illustrated in Figure 3.6 c)

3.3.2 LOOP WITH A CONTROLLED DELAY – LINEAR TRANSLATION STAGE

An ability to control the delay of the beam is a fundamental aspect of the pulse width measurement in the autocorrelation system. However, before suitable equipments were selected, some calculations were performed in order to determine the required properties of the delay loop.

The first important parameter is the distance that has to be scanned in order to obtain autocorrelation function. Tsunami laser applied in the system is able to produce pulses down to 35 fs. Nevertheless, the width at the base of the signal is required in this calculation. In order to simplify calculations (the main goal is just to know the scale of the required delay), the width of the pulse at its base was assumed as 100 fs. The autocorrelation function is obtained by measuring the intensity of two overlapping pulses therefore, the scanned distance has to be twice as long as width of the one pulse. Moreover, the scanned area has to be larger in order to measure the background level and to verify if there are no anomalies in the around the signal. Therefore, the scanned width can be assumed as 500 fs. Using this value for calculating the scanned distance gives the following result:

$$S = 2,998 \cdot 10^8 \frac{m}{s} \cdot 5 \cdot 10^{-13} s = 149,9 \mu m = 0,1499 mm$$

Obtained result shows that the entire measurement takes place at the very small distance. It means that the equipment responsible for a delay must have a very good resolution. Another useful parameter is a distance between two consecutive pulses. That information can be obtained using a pulsing frequency of the laser unit. The nominal frequency of the laser according to the data sheet [appendix A] is 82 MHz however, the last maintenance revealed that the real

frequency is 75,5 MHz. Knowing the pulsing frequency, the time between two pulses can be easily calculated:

$$t = \frac{1}{f} = \frac{1}{75,5 \text{ MHz}} = 1,32 \cdot 10^{-8} \text{ s}$$

The distance between the pulses can be obtained by inserting the obtained time and the speed of the light into the equation for the velocity in uniform motion:

$$v = \frac{S}{t} \quad \text{hence,} \quad S = v \cdot t = 2,998 \cdot 10^8 \frac{\text{m}}{\text{s}} \cdot 1,316 \cdot 10^{-8} \text{ s} = 3,95 \text{ m}$$

Performed calculation shows that distances between the consecutive pulses are very large. It indicates that the loop has to be equal in length because there is not possible to correlate two consecutive pulses. Moreover, both performed calculations revealed that the first task related to the autocorrelation measurements will be to find a very small point where the delay of the two loops is equal.

It was decided to use a motorized linear sliding table T-LSR150B produced by Zaber Technologies Inc. [Figure 3.7 a)] as a core of the controlled delay loop. The parameters of this device are very promising. The step size is 0,496 μm and the minimum speed is 4,65 mm/s. Moreover, it has a manual control knob, which was found useful during the initial tests of the system. The only disadvantage of the sliding table is its working distance, which is too large for this application. However, there was found enough space to apply this device in the system.

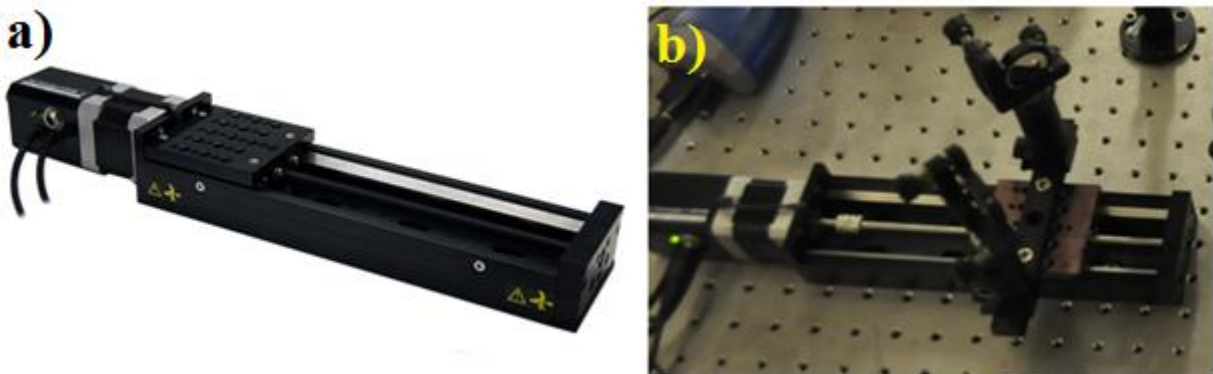


Figure 3.7 Sliding table used for modifying length of the laser path a) manufacturer`s image [2] b) with mirrors on a rail.

After selecting a suitable movable device, the next task was to construct an optical delay loop. The first step was to screw a special rail to the platform of the sliding table. The main function of this rail is to provide an easy positioning of the mirrors. Subsequently, mirrors were mounted to the posts with sliding bases and embedded on the rail. The entire implementation of the controlled delay loop is illustrated in Figure 3.7 b).

Using the data provided by the manufacturer of the motorized sliding table, the theoretical resolution of the designed autocorrelation system can be calculated. It is worth

noting, that in the applied configuration the single step of the sliding table increases the delay by two lengths of the step.

$$t = \frac{S}{v} = \frac{(0,496 \cdot 10^{-6} \text{ m}) \cdot 2}{2,998 \cdot 10^8 \frac{\text{m}}{\text{s}}} = 3,31 \cdot 10^{-15} \text{ s} = 3,31 \text{ fs}$$

The above calculations shows, that the selected motorized sliding table provide a very good resolution. As it was previously mentioned, the autocorrelation function of the 35 fs pulse is stretched on about 200 fs. That indicates that a relative resolution of the autocorrelation system is $\approx 1,7\%$.

3.3.3 FOCUSING LENS AND SHG CRYSTAL

Applied noncollinear geometry of the autocorrelation system requires a lens to focus split beams onto a SHG crystal. Despite the fact that a focal length is not imposed by the geometry, it has a great significance for the structure of the system. For smaller focal lengths, crossing beams are spreading at a larger angle. It means that a photomultiplier can be placed closer to the crystal without a threat of an impact from these beams. However, a focal length cannot be too small because a short distance between the lens and the SHG crystal may cause problems with adjustment of these elements. After considering these arguments it was decided to use a double-convex, 1" lens with a focal length 35 mm. The lens was embedded to the frame that allows its angular adjustment and mounted to a sliding table [Figure 3.8 a)]. This configuration allows easily focusing laser beams onto a crystal.

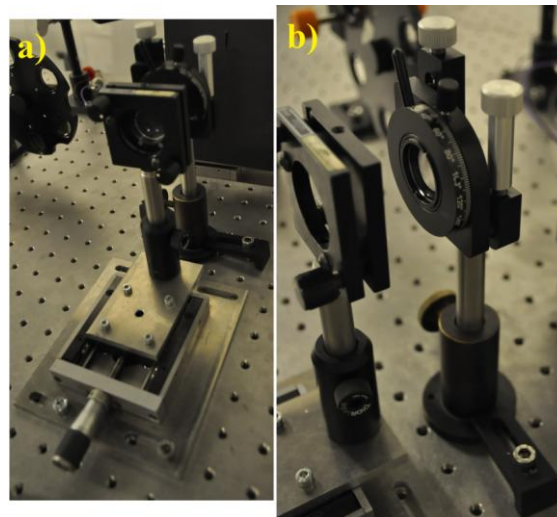


Figure 3.8 a) Lens mounted to the sliding table b) BBO crystal embedded in rotary frame.

The next important element of the system is a non-linear optical element used for the generation of a second harmonic signal. The idea was to use one of two available BBO crystals. First of them is 1 mm thick while the other is 0,5 mm. According to the data provided by the manufacturer, none of these crystals is suitable for 35 fs pulses because they are too thick. The required crystal thickness for the desired pulse duration is 0,1 mm (Table 5-1). Unfortunately, at the beginning of the project, that kind of the crystal could not be afford (It was later replaced by the new crystal, what is described in chapter 5). As a result, it was

decided to use 0,5 mm crystal because its thickness is closer to the required value. The selected crystal was embedded into a special frame as it is presented in Figure 3.8 b). Structure of this frame allows to rotate the crystal with a great precision, which makes it easier to find a position that provide a maximum efficiency of second harmonic generation.

3.3.4 EQUIPMENT FOR INTENSITY MEASUREMENTS

The next important task was to find appropriate equipment for intensity measurements. Two different sensors were considered; a photodiode and a photomultiplier. After considering pros and cons of these devices, the photomultiplier was selected. The main reason for that was a higher sensitivity and a bigger sensing area, which are crucial for measurements and should significantly facilitate finding the signal. Since the photomultiplier requires a high-voltage (up to 2kV), it is connected to the power supplier, which offers a voltage up to 6,5 kV. Moreover, the it is connected to the electrometer with an analogue display, which was found extremely helpful during firsts adjustments of the system. The photomultiplier together with other equipments related to intensity measurements is presented in Figure 3.9.

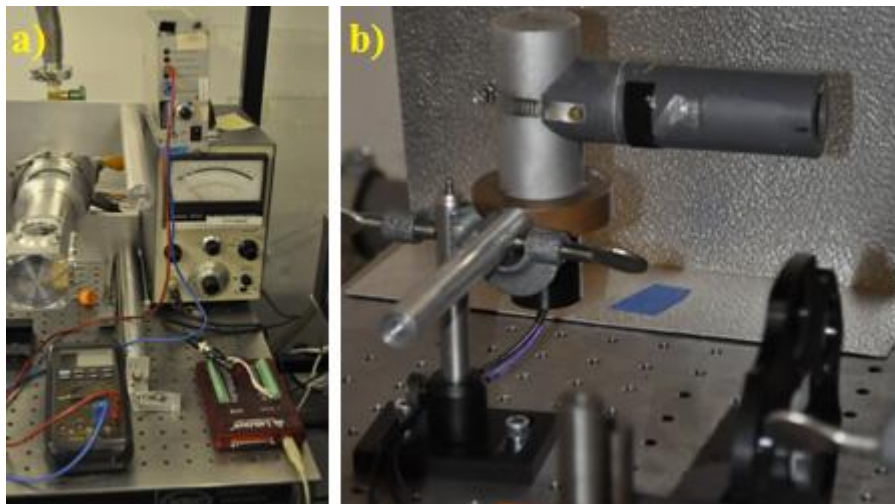


Figure 3.9 Equipment used for intensity measurements a) electrometer with analogue display, power supplier (on the top of the amplifier) and LabJack – analogue-digital converter b) photomultiplier.

The only method to effectively store, manage and process the obtained measurement signal is its digitization. In the designed autocorrelation system, analogue-digital conversion is provided by LabJack U12, which is a multifunctional data acquisition station. The main reason for choosing LabJack was its ease of use, an ability to integrate it with different programming environments such as: C/C++, LabVIEW, Visual Basic and MATLAB. Moreover, there is a big community of LabJack users and plenty of available tutorials. It is worth noting that because of the large size, components associated with the measurement of intensity were placed on the other laboratory table.

3.3.5 BEAM TERMINATION

According to laser safety standards [2] it is required to terminate all beams at the end of their path. In order to achieve that, a simple protective screen was designed. The main idea was to construct one screen that would terminate both laser beams. The screen was made of

a black, light-absorbing paper with a hole and a carton, which acts as a support structure. In the first implementation, a width of the hole was just slightly smaller than spacing between the beams. However, first tests revealed, that the constant component from one of the beams was interfering the measurements. In order to prevent it, a width of the hole was significantly decreased and the screen took the form presented in the Figure 3.10 a). Further tests shown, that measurements are very sensitive to the position of the screen. Even the smallest displacement may result in either a reduction of the signal intensity or an occurrence of the constant component. Therefore, in order to provide an easier positioning, the screen was mounted to a sliding table. Moreover, a support structure made of carton was replaced with an angled aluminium plate that ensures the stability and allows easily connecting the screen to the sliding table. The final structure of the protective screen is illustrated in the following Figure 3.10 b).

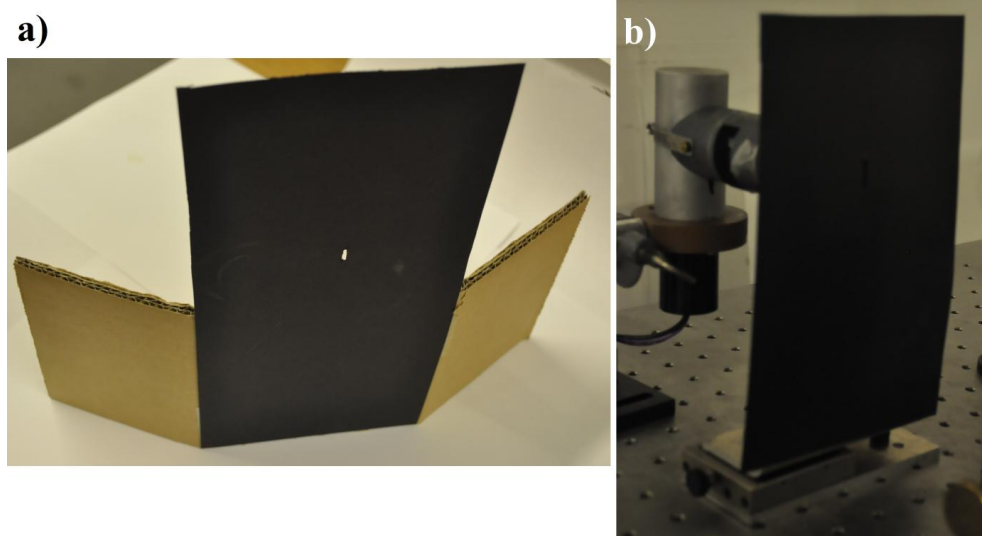


Figure 3.10 Beam-terminating, protective screen with a slit a) temporary solution made from carton b) final solution embedded on the sliding-table.

3.3.6 SELECTION OF THE FILTER

The photomultiplier, used for intensity measurements of a second-harmonic signal, is a very precise and light-sensitive device. It means that even the smallest reflection formed in the laser path may interfere with measurements, while main beam falling on the photomultiplier's cathode may damage the equipment. Previously presented protective screen with a slit should suppress a significant part of the incident light; however, a full protection can be achieved only by using an optical isolation. This kind of isolation can be provided using an optical filter. Required filter should show a high absorption for the operation wavelength of the laser (≈ 780 nm) and a high transmission in the spectra region related to the second-harmonic (≈ 390 nm). In order to select the most suitable optical filter, spectroscopic measurements were performed. Each of four considered filters were mounted to the post and placed between a light source and a probe of a spectrometer while computer software was plotting and archiving spectra of a transmitted light. It is worth noting that during these measurements, two different light sources were used to cover a required spectra; a deuterium arc lamp which covers the lower part of the spectra (≈ 200 - ≈ 680) and halogen lamp which is

used for its upper part ($\approx 400 - \approx 900$). Results of measurements with usage of the deuterium arc lamp are presented in Figure 3.11 while results for the halogen lamp are illustrated in Figure 3.12.

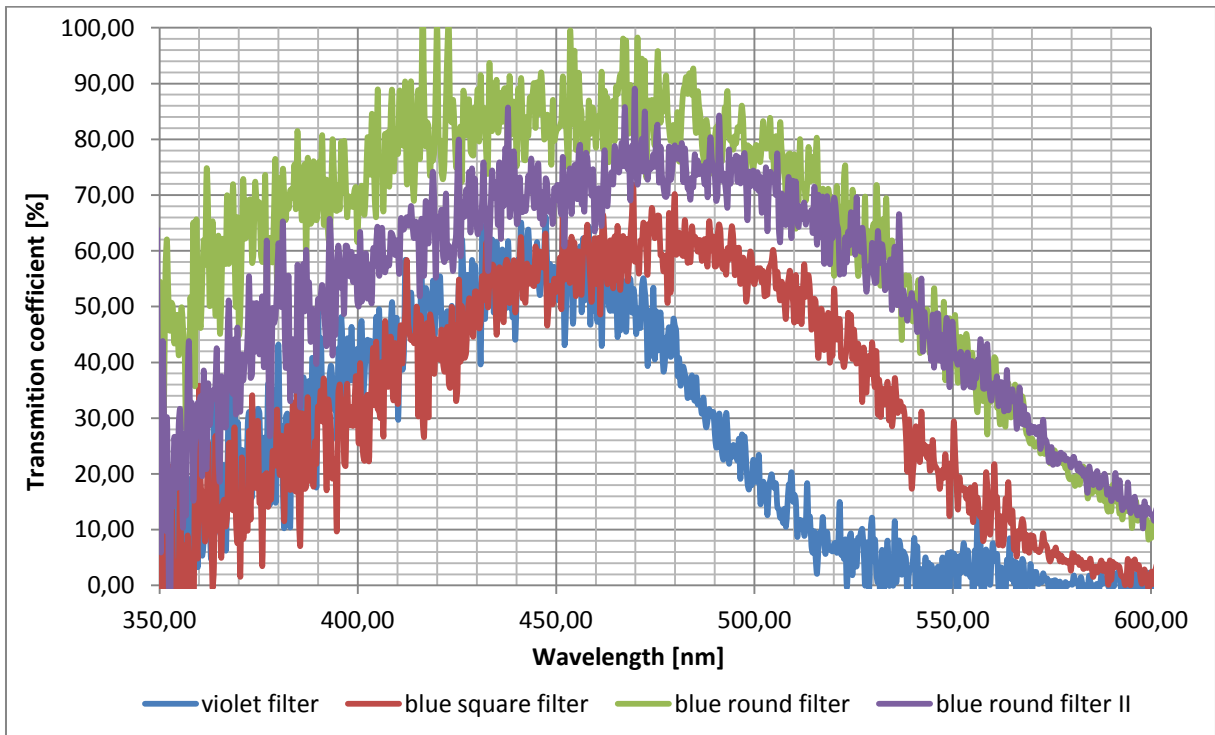


Figure 3.11 Light spectra measurements performed for various optical filters. Deuterium arc lamp used as a light source.

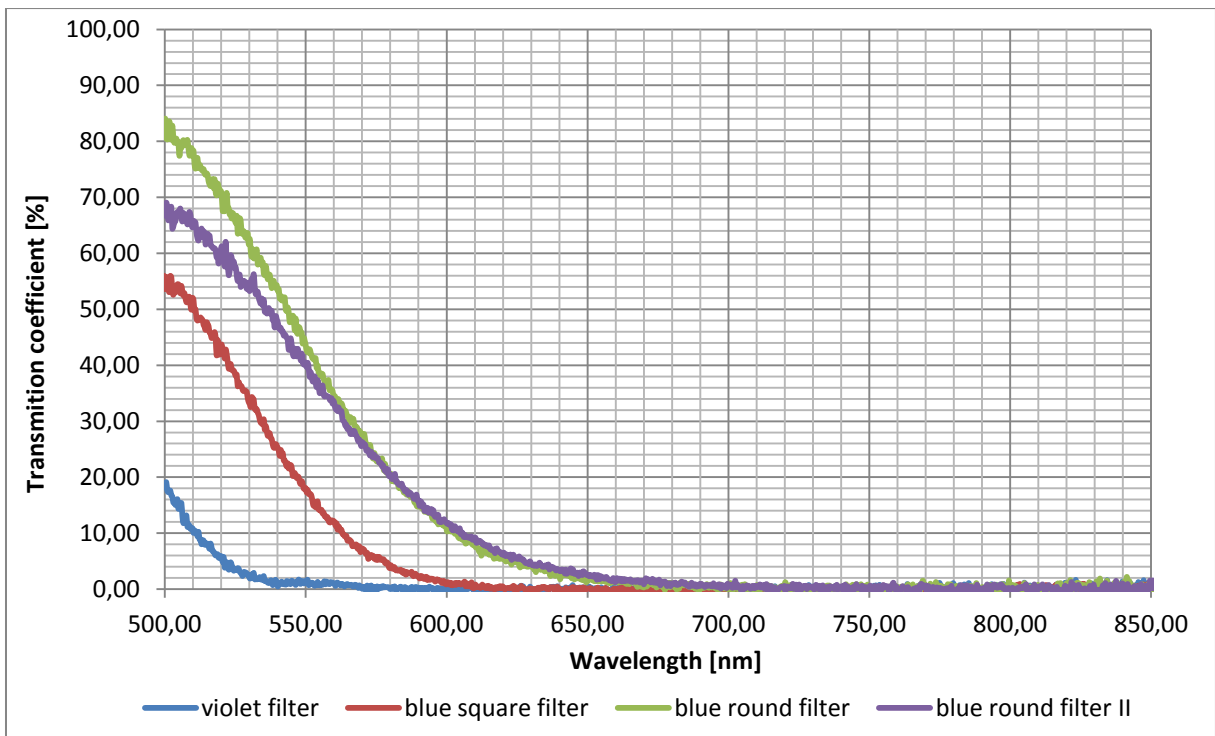


Figure 3.12 Light spectra measurements performed for various optical filters. Halogen lamp used as a light source.

Performed measurements show that all of considered filters have a band-pass characteristic. It means that they pass wavelengths within a certain, bilaterally limited range and attenuates wavelengths outside that range. Figure 3.11 shows that lower boundary wavelengths for all tested filters are 350 nm or less. Their upper boundary wavelengths are significantly different. Both blue round filters have the widest transmission spectra and its upper boundary wavelength is about 700 nm, which is much lower than the laser's operation wavelength. Figure 3.12 confirms that all tested filters show a perfect absorption in that region. However, their behaviour differs much in the second-harmonic spectra region. The main difference is related to the transmission coefficient, which represents a fraction of the incident light that is transmitted. Some filters such as: violet round filter and blue square filter transmit only less than a half of the light in the region of second-harmonic occurrence. The most efficient in this manner is blue round filter which transmits about 70% of the incident light. Considering all of above observations, blue round filter has been selected to provide an optical isolation of photomultiplier.

The next task was to find an appropriate place for the filter. The distance between the photomultiplier and the SHG crystal is not large and some part of it has been already reserved for the protective screen. Therefore, it was decided to use a special structure of the photomultiplier's tube. This tube consists of two smaller tubes connected by a thread. Since the internal thread is not made on the entire length, there is a small space that can be used for embedding the filter. Moreover, screwing on the second tube presses the filter and ensures its stable position.

By combining all components described in this chapter, the complete autocorrelation system was created. The following figures present the structure of the designed system.

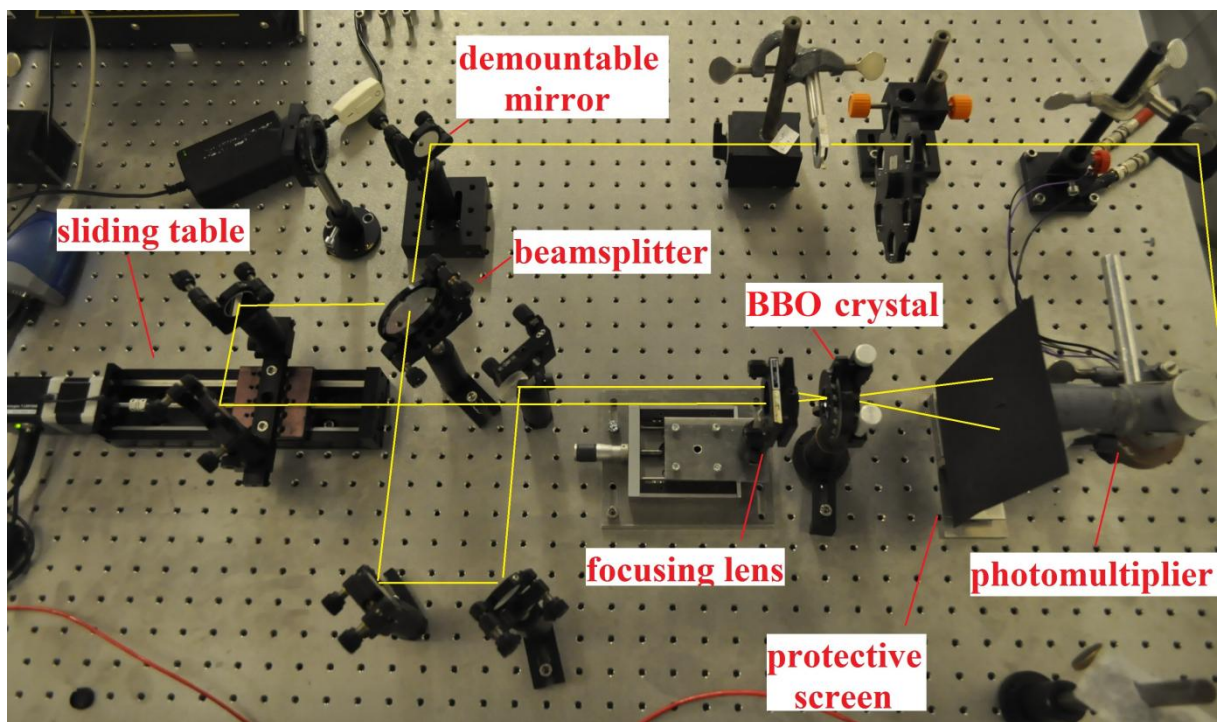


Figure 3.13 Entire autocorrelation setup with desired laser path.

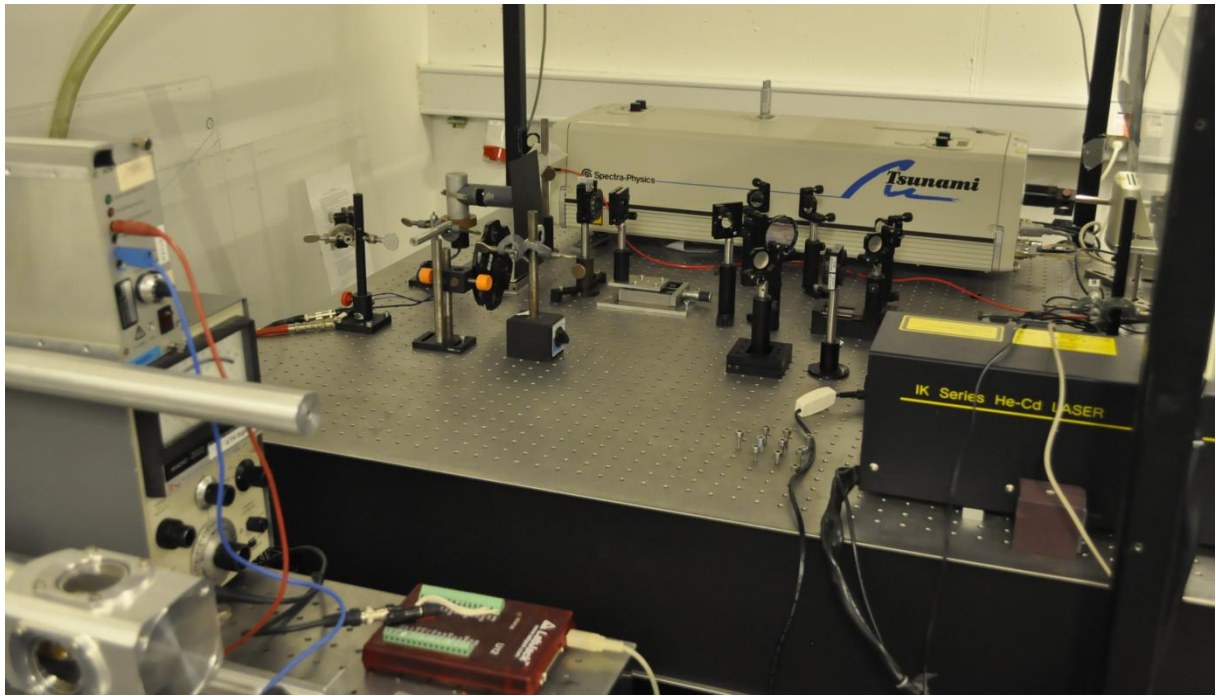


Figure 3.14 Completed autocorrelation system.

4 SOFTWARE FOR THE AUTOCORRELATION SETUP

After constructing the hardware of the autocorrelation system, the next task was to design proper software for control and data acquisition. However, before proceeding to the programming part, it is important to familiarize with connections and interactions between active components of the measurement system, which is going to be controlled.

The system consists of two independent units connected by the computer, which manage them and process the received data. The first unit is the motorized sliding table, which controls the delay between autocorrelated beams. The sliding table is equipped with RS-232 port, which allows communication with other devices. Since the computer (laptop) does not have this type of a serial port, an adapter RS-232 / USB has been used. This kind of connection provides bidirectional communication between these two devices, which is required for the measurement process. Computer has to send instructions regarding a movement of the motorized table, while the sliding table informs the computer when the instructions are completed. The second unit is related to intensity measurements. It consists of the photomultiplier, the analogue electrometer with a display, and LabJack. The signal from photomultiplier is sent through the BNC cable to the electrometer, which shows measured intensity on the display. Then the signal is transmitted to LabJack, which digitize and send it to the computer by the USB cable. The connection between the LabJack hence, the entire intensity measurement system and the computer is also bidirectional. The LabJack sends the results of the intensity measurements, while the computer instructs LabJack about digitization parameters and when the transition of data should be started. The structure of the entire measurement system and interactions between its components is graphically presented in Figure 4.1.

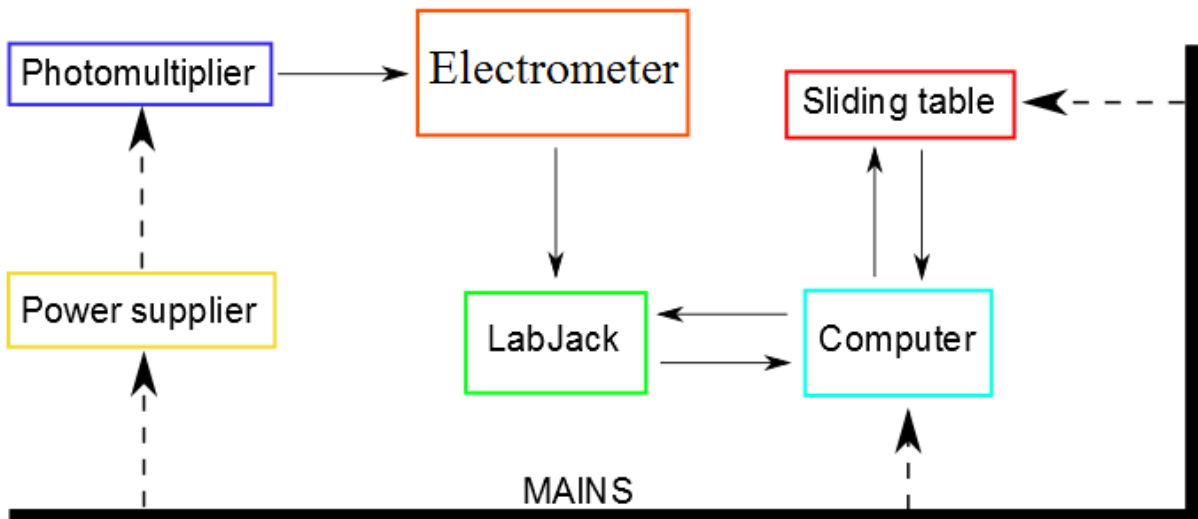


Figure 4.1 Signal flow diagram of the measurement system. Solid lines – data flow. Dashed lines – power supply.

4.1 REQUIRED FUNCTIONALITY

The first step in the designing process of the software was to select the suitable programming environment. Since both motorized sliding table and LabJack are strongly

supported by LabVIEW, which provides adequate libraries to these devices, it was decided to use this programming environment. Moreover, LabVIEW is based on a graphical programming rather than writing a code, which provides much faster implementation of the software. Another argument for using this programming tool was simplicity of creating user interface, which in this case is made semi-automatically.

After selecting a working environment, there was a time to define the initial requirements for functionality of the designed software. It is noteworthy that the software was constantly developing. Performed tests provided information about new functionalities that have to be implemented in the program. The following list contains assumptions, which were defined both at the beginning of the programming as well as resulting from performed tests of the system.

- The software has to work in the continuous mode. Many laboratory programs programmed in LabView are designed for single operation (starting the program, performing an action, ending the program), which is highly cumbersome for the user. Designed program after finishing the operation should wait for other instructions.
- The software must allow both autocorrelation measurements and manipulation of the sliding table. The user should be able to control the behaviour of the device without starting the measurement.
- The user must be able to define the parameters of the measurement.
- The software must allow running multiple measurements in the loop. This functionality should significantly facilitate preparing statistics and hence investigating precision and repeatability of measurements.
- A communication between the software and the user has to be provided by the user interface, which is easy and intuitive in usage.
- During the measurement, major information about this process must be shown to the user. This information should contain; an obtained resolution, measurements remaining, progress of the measurement.
- The obtained data has to be presented in a graphical form. An additional advantage would be to plot a data in the real time.
- The data obtained during measurement must be stored on a computer disk. Moreover, the data has to be saved in a suitable file format, which provides an easy processing. The accepted formats are: .csv and .xlsx used by Microsoft Excel.
- During the measurement the intensity is measured for different positions of the sliding table however; it is more intuitive for the user to use a time instead of a distance. Therefore, the program has to convert the distance between two scans to the time that light needs to travel that distance.
- Before ending, the program should release all resources used during its execution. This mainly concerns the communication ports because without terminating

a connection between the software and devices, there might be a problem with using devices by other programs.

4.2 OVERALL STRUCTURE OF THE SOFTWARE

Taking into account all software requirements described in the previous chapter, a suitable structure of the program has been chosen. It was decided to base the program on a simple state machine, whose structure is graphically presented in the following Figure 4.2. The state machine consists of five states. Three of them are main states, which are responsible for operation of the system, while two remaining states are subsidiary states used for configuration purposes. Principle of operation as well as implementation of states is further described in following subchapters.

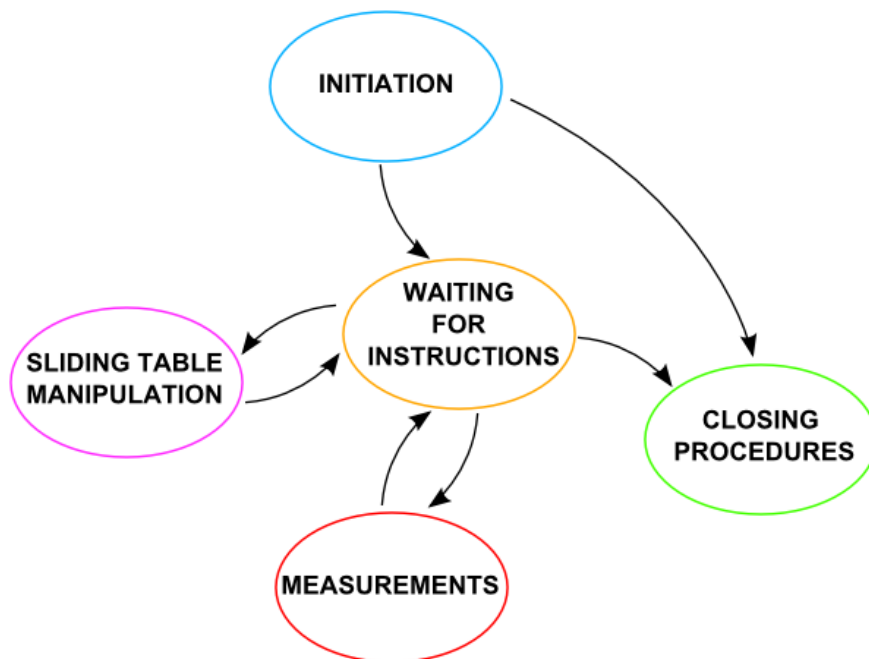


Figure 4.2 State machine applied in the software.

4.2.1 INITIATION

The initiation state is the starting state of the program, which cannot be later re-entered. Its structure is illustrated in Figure 4.3. As the name of the state may suggest, its main function is to initiate devices and prepare them for further operations. Since LabJack does not need any initiation, this state is focused only on preparing the motorized sliding table. At the beginning “initialize” function block from Zaber library is called. It establishes communication with a device and clears the serial buffer. This function takes as a parameter the name of the port, which sliding table is connected to. Afterwards, default setting of the device is restored by using an adequate command in the “CMD ZABER” block. This procedure is intended to avoid measurement problems caused by changing the parameters of the device by previous users. It is worth noting that “request” block from Zaber library has many parameters, whose functionality is not used in the designed software therefore, it was reduced to the “CMD ZABER” block. More information about Zaber library and associated

function blocks can be found in [4]. The next step in the initiation process is sending the sliding table to the home position. Since the sliding table is not equipped with an encoder, reaching a home sensor is the only method to reset the internal position of the device.

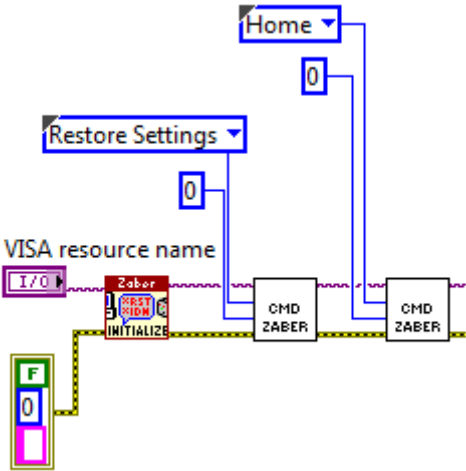


Figure 4.3 Implementation of initiation state.

The initiation state has an additional functionality that is not presented in the Figure 4.3. The error code is connected to the “if” loop that contains the rest of the program. If the initiation would not succeed, the entire program stops. This procedure should prevent possible damages of the equipment.

4.2.2 WAITING FOR INSTRUCTIONS

After completing initiation procedures, the program switches to the waiting state. It is a transition state that waits for a user action in order to shift to the one of the active states related with either manipulation or measurement. This state is implemented as a while loop, which can be left only by pressing “STOP PROGRAM” button. This action starts closing procedures and leads to ending the program. By using a timer, the loop is executed once per 50 ms, which reduces the usage of operation system resources. Inside the while loop, the switch structure is implemented. Each case of the switch structure corresponds to the different state. Cases and therefore states can be entered by using a related button. Pressing “RUN MEASUREMENT” button changes the state to the measurement state, while pressing “RUN CONTROL” button switches to the manipulation state. If none of the buttons is pressed, the program enters the default case, which does not do anything. Since the switch structure is located inside the while loop, the program goes to the beginning of this loop after the case is finished. This structure has very useful consequences. Once the program enters the waiting state, it stays there since the user decides to either perform measurements or control the sliding table. After finishing the operation, the program returns to the waiting state and waits for another instruction. That provides the constant work of the program, which was one of initial requirements. The waiting loop has one additional function. All the parameters related to the measurements and control of the sliding table can be entered only during the waiting state. This approach prevents changing the parameters during performed action. Moreover, inserted parameters are used to calculate properties of the measurement (e.g. resolution),

which are later presented to the user. It is worth noting that, calculations are repeated with every cycle of the loop, which means that results are refreshed once per 50 ms (20 Hz).

4.2.3 SLIDING TABLE MANIPULATION

As it was previously mentioned, the software beside autocorrelation measurements must allow manipulating the sliding table. This functionality was found extremely important during signal searching. In order to provide that functionality the manipulation state was implemented in the program. This state can be entered from waiting state by pressing “RUN CONTROL” button. In this state, the sliding table performs one previously defined action and the software goes back to the waiting state. The user can choose from a predefined list of actions that contains inter alia; move at constant speed, move absolute, move relative, go home position and define the necessary parameters. It is noteworthy that the action and its details can be changed only during waiting state and after a transition to the manipulation state the change is not possible. This approach was implemented to prevent an accidental modification of parameters.

4.2.4 MEASUREMENTS

The measurement state is the most important part of the software. The main task of this state is to manage and synchronize operations of the sliding table and LabJack in order to perform autocorrelation measurements. The measurement state can be entered from waiting state by pressing “RUN MEASUREMENT” button. When the measurement is done, the state is automatically switched back to the waiting state. Two different approaches to the measurement process have been considered during designing of the software. Both approaches have some stronger and weaker points therefore, two versions of the software has been created.

- CONTINUOUS MEASUREMENT

An initial idea for autocorrelation measurements was to move the sliding table with the constant speed and measure the intensity of the light in the equal intervals. Knowing the speed and the frequency of sampling, the distance between two measurement point and hence the time can be calculated. This approach requires the following parameters to be defined by the user:

- NUMBER OF MEASUREMENTS,
- INITIAL POSITION,
- SCAN RATE (sampling frequency),
- SPEED.

After entering the measurement state, the sliding table is moved to the INITIAL POSITION, which has been previously defined by the user. Simultaneously, time-shifts corresponding to the movement of the sliding table are calculated. Afterwards it starts moving with the constant SPEED. The movement of the sliding table is realized using “request” block from Zaber library with a procedure “move at constant speed”. When the sliding table is moving the LabJack starts to collect the data in a stream with a desired SCAN RATE. It is

worth noting that during the stream is active LabJack is unable to perform any other actions. This task is performed by “AStreamStart” function (LJ stream start block). More information regarding LabJack library are available in [5]. When the determined (4096 – max value) number of measurements is performed by the stream, the function AStreamRead transfer the data from LabJack to the computed at saves it in the table. Subsequently, obtained results are saved to the file. In the meanwhile, the sliding table is stopped using “stop” function in “request” block. Then the stream is cleared by AStreamClear function. The last step in the measurement process is plotting all data in a graph. If only one measurement was requested the program ends the measurement state and switches back to the waiting state. Otherwise other measurements are performed until previously defined NUMBER OF MEASUREMENTS is reached. Presented sequence of operations of designed software is illustrated in Figure 4.4.

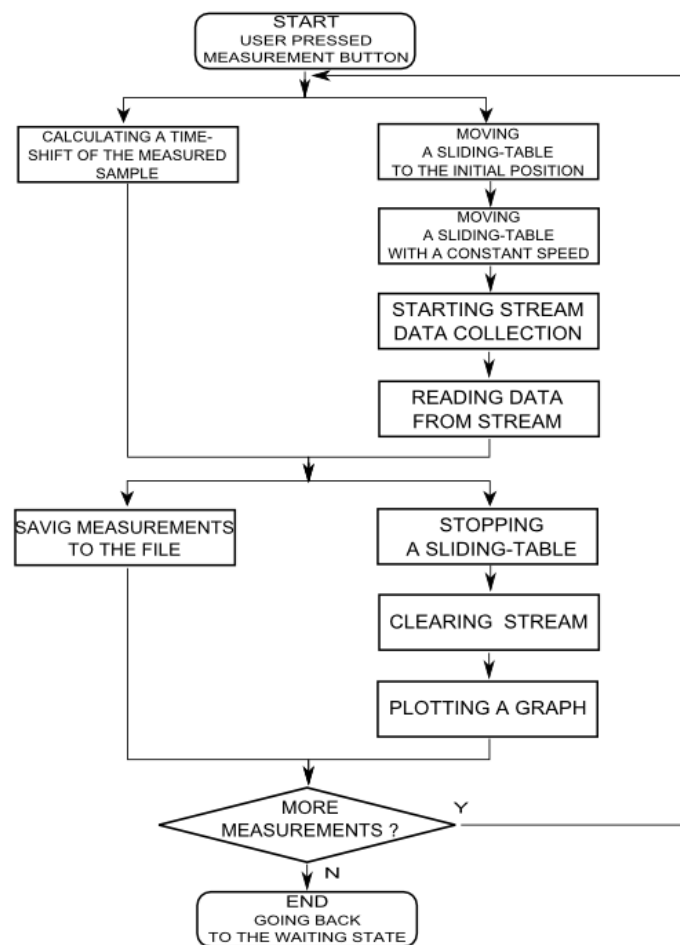


Figure 4.4 Process diagram for continuous measurements.

Presented approach allows performing measurements very fast. The time of one measurement is less than 10 s (depends of scan rate and speed). Unfortunately, the usage of stream functions prevents plotting results in the real time. Moreover, the large scan rate makes it possible to perform the measurement few times during the single step of the sliding table. Since the states between steps are not established, it was expected that continuous measurement method may give noisy or imprecise results. Structure of the continuous measurement program is presented in [appendix C].

- STEP MEASUREMENT

Being aware that continuous approach may affect the precision of the measurements, the other measurement method was introduced. This method is based on the well-known step and repeat tactics. The sliding table is moved by a certain distance and the intensity is measured. The presented operations are repeated since a required distance is scanned. In this approach the user has to determine the following parameters:

- NUMBER OF MEASUREMENTS,
- INITIAL POSITION,
- STEP SIZE,
- NUMBER OF ITERATIONS (iterations).

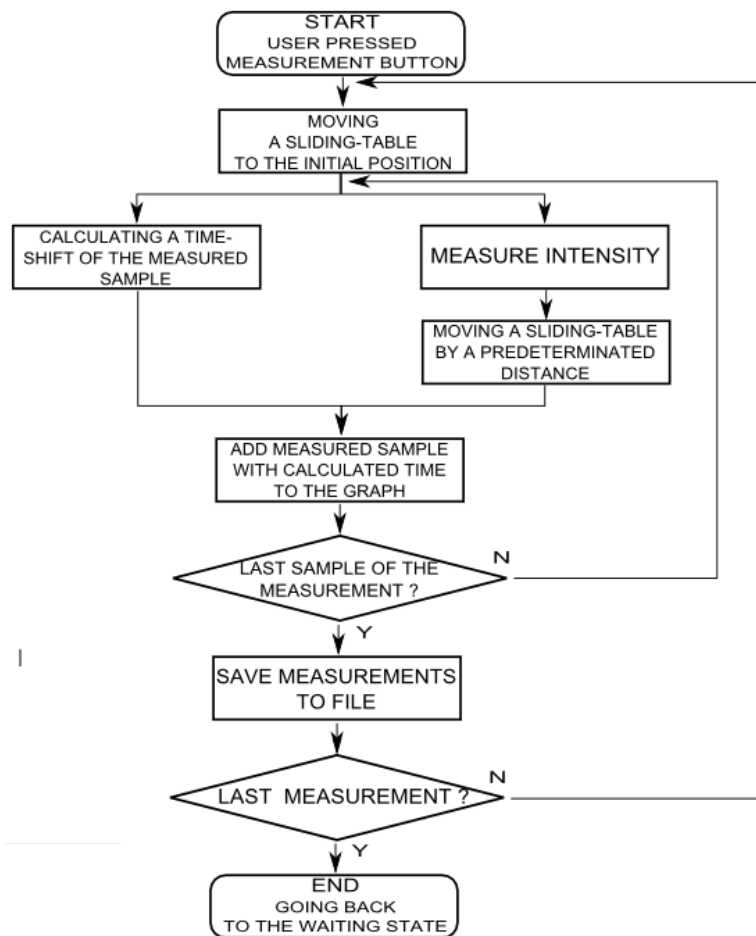


Figure 4.5 Process diagram for step measurements.

Similarly to the previous measurement method, the first step is to move the sliding table to the INITIAL POSITION. Then, the intensity is measured using “EAnalogIn” function (LJ EAI block), which reads the voltage from one analogue input of LabJack. After the measurement is done the sliding table is moved by user defined STEP SIZE. Simultaneously, the program calculates the time-shift related to the movement of the sliding table. Subsequently, the measured sample and corresponding time-shift are added to the table in the memory and plotted on the graph. The operation is repeated until the user defined NUMBER

OF ITERATIONS is reached. In that case, the measured data is saved to the file. All presented algorithm is located in the “for” loop that is related to the amount of measurements (scans). If the user set more than one measurement the program returns to the beginning of the loop and the entire procedure is repeated until the counter of measurements reaches the defined value (NUMBER OF MEASUREMENTS). Figure 4.5 graphically presents described sequence of operation for step measurement approach.

This method is definitely slower than the previous one, since the “EAnalogIn” function does not provide as high sampling frequency as the stream. However, since the measurement is performed step by step, it is possible to plot the curve on the graph in a real time and the progress of measurement can be easily followed by the number of a current iteration. Moreover, the intensity is measure only in the established points (steps of the sliding table), which should reduce the noise of the obtained signal. The complete structure of the software for step measurements is presented in [appendix B]

4.2.5 CLOSING PROCEDURES

Closing state is entered after pressing the “STOP PROGRAM” button while the waiting state is active. It is executed before the program ends to release occupied resources. Similarly to the initiation only the motorized sliding table need closing procedures because it is using the serial port that has to be configured. Closing procedures consists from only two function blocks. First of them is a “close” block from Zaber library, which terminates the connection between the software and the device. The second one is an error handler, which shows details about potential errors. It is worth noting that closing procedures can be started automatically if the initiation process fails.

4.3 USER INTERFACE

Another important part of the software is the user interface. It is a graphical panel that is used for communication between the user and the program. User interface allows the user to manage the program (define measurement parameters, start measurement, control sliding table etc.) and present him details about the program and performed measurements. Since there are two versions of the software, two different interfaces were created. Each of them is adapted to the measurement mechanism applied in the associated version of the program. However, both user interfaces are based on the same scheme. The interface can be divided into two main sections. First of them is related to the manipulation (control) of the sliding table, while the other is connected with measurements. Sections are located on the two separated tabs that can be switched by clicking on the name of the tab. This structure was invented to prevent user`s mistakes (changing the parameters of measurement but starting the manipulation). In that configuration user can be sure that all parameters presented on the screen are related to the activity, which he is going to perform.

Since the manipulation of the sliding table does not require many parameters, the structure of the control tab is very concise. It contains only three elements. There is a drop-down list of commands that can be executed, a control named DATA, which is used to define

additional information related to the chosen command (e.g. speed or absolute position) and RUN CONTROL button, which starts the manipulation. The control tab is illustrated in the Figure 4.6. It is worth noting that control section is identical for two versions of the software.

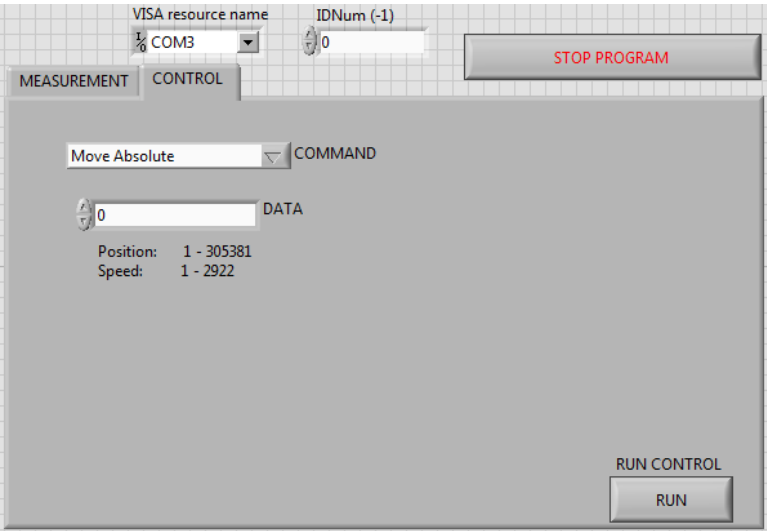


Figure 4.6 User interface – control tab.

The measurement section for continuous measurements presented in Figure 4.7 contains the following elements. On the right hand side there is a panel associated with LabJack. It is used to define the channel that takes part in the measurements and to choose the suitable gain. Moreover, there are for controls that correspond to main parameters of continuous measurements. They are: number of measurements, starting position, scan rate and speed. Additionally, the tab is equipped with few indicators, which inform the user about details of the measurement. These indicators show: number of currently performed measurement, scanned distance, distance between two measurement points, speed converted to $\mu\text{m/s}$ and approximate time of one measurement. Moreover, after each measurement cycle the actual scan rate is shown. This functionality was added to detect some potential LabJack errors.

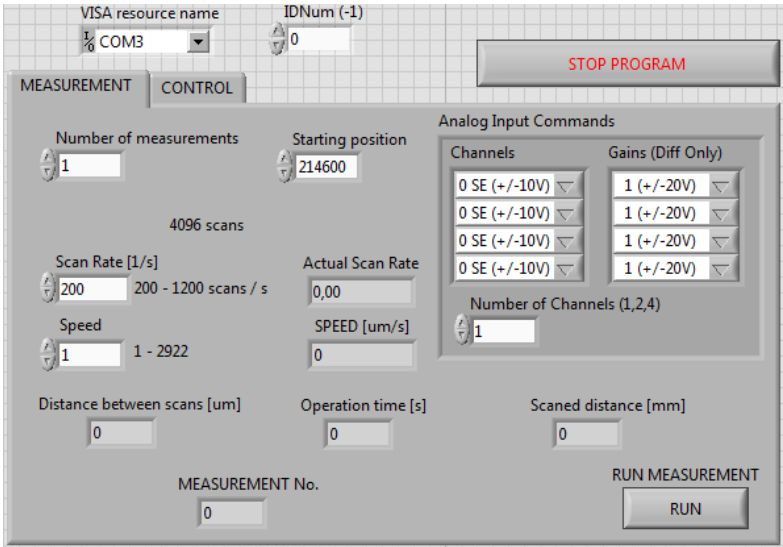


Figure 4.7 User interface – continuous measurement software, measurement tab.

The measurement tab of the step mechanism software (Figure 4.8) has also got a panel associated with LabJack located on the right. This panel is much different from the one presented above (it is a result of using different LabJack functions); however its functionality remains unchanged. It is used to determine the channel used for measuring and the gain. The tab contains four controls adapted to the step approach: number of measurements, starting position, step size and iteration. Indicators located on the tab show: number of currently performed measurement and iteration, scanned distance, step size converted to μm and resolution of the measurement. It is worth noting that, the previously presented measurement tab for continuous measurement does not present the resolution. During the continuous scan, intensity is also measured in not established positions of the sliding table; therefore, estimation of the resolution is much more complex. It is worth noting that, the indicator showing the approximate time of one measurement is not present in this version of software. Since the realization time of “EAnalogIn” function applied in the program is not established, the time of the measurement cannot be estimated. Moreover, there are two buttons located on the tab. “RUN MEASUREMENT” button starts measurements, while “STOP MEASUREMENT” stops the single measurement. Adding this functionality was required because the scan in step approach may last much longer than using the continuous method.

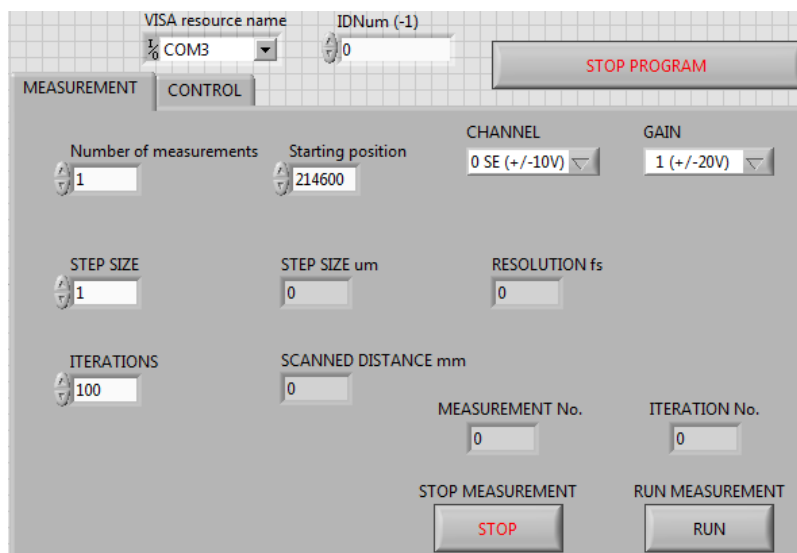


Figure 4.8 User interface – step measurement software, measurement tab.

Besides described sections, the interface has a few general elements that could not be fitted into the described sections (these elements are present in both versions of the software). Two of them are related to the communication between the program and the devices. “VISA resource name” is a drop-down list, from which the user has to choose the serial port that provides connection with the sliding table. “IDNum” is control, where the ID number of the LabJack used in the measurements has to be inserted. Another element is a graph, which is used for plotting obtained data. Due to its big size, the graph is not presented in any figure. The last element is a “STOP PROGRAM” button, which is used to safely end the program.

4.4 USAGE OF THE SOFTWARE

The user's interface of the designed software is very clear and intuitive. However, the beginner user might have some problems or doubts regarding the operation of the program. Therefore, a brief instruction regarding performing measurements has been made.

- Before starting the program the user should choose the serial port, which provides connection with the sliding table from the drop-down list named VISA resource name. Moreover, ID of LabJack has to be inserted in the "IDNum" control. When these actions are done, the program is ready for start.
- After pressing "Run" button in the LabVIEW menu (standard starting procedure in LabVIEW), the software automatically starts initiation procedures.
- Initiation is completed while the motorized sliding table reaches the home position, which may be recognized by behaviour of its diodes (or RS 232 / USB converter diodes). If the diodes stop blinking the sliding table reached its destination point. It is worth noting that a movement of the sliding table may take several second.
- Then, the program enters the waiting state, where the user may define all parameters related to the measurement.
- When all parameters are set, the user can start the measurement by pressing "RUN MEASUREMENT" button.
- The first operation during measurement process is moving the sliding table to the initial position of the measurement. This operation might take several seconds. After reaching that point, the actual measurement begins.
- In case of the software using step approach, the progress of the measurement can be easily followed by the indicator "ITERATION No." If the number shows by this indicator matches user defined iteration number, the measurement is done. In case of using a continuous approach, the progress is not presented. However, if the measurement is over, the LabJack diodes stop blinking and shine steadily.
- While the measurement is over, the data are saved to the file in the predefined folder. The software goes back to the waiting state and it is ready to perform another action.
- The program can be ended by pressing the "STOP PROGRAM" button during the waiting state. It is worth noting that this button will not work during the measurement or control is performed.

5 AUTOCORRELATION SYSTEM - TESTS AND MEASUREMENTS

After designing the structure and creating the adequate software, there was a time to test the autocorrelation system as a diagnostic and measurement tool. This chapter contains precise descriptions of: performed preparation of the system, conducted measurements and actions taken to improve an obtained signal. Moreover, at the end of the chapter, there is a comparison between two designed measurement methods.

5.1 PREPARATION OF MEASUREMENTS

Before first measurements can be performed, the system has to be properly prepared. The first step of the preparation was to adjust the individual elements of the system. This operation is very important for a proper operation of the system, especially in the controlled delay loop. If beams in that part of the setup are not reflected at the right angle and guided perpendicular to the BBO crystal, the delay would be different from the step of the motorized sliding table. As a result the precision of the measurement would be lowered.



Figure 5.1 Gantry used in adjustment process.

The adjustment of components was performed in the same direction in which the laser beam is guided into the autocorrelation system. At the beginning, the demountable mirror was adjusted, then the beamsplitter, mirrors creating a delay loop, lens and at the end, the BBO crystal. The main idea was to use a 2D holes pattern of the laboratory table to guide beams parallel or perpendicular to each other as it was presented in Figure 3.5 b). In order to achieve that, a simple gantry was constructed (Figure 5.1). This device has a post with a marked target which is used to adjust the height. Moreover, it is equipped in two translation axes parallel to the table. Principle of operation of the gantry is very simple. Firstly, the device is mounted to the laboratory table in such a way that a longer axis is parallel to the desired direction of the beam. Then, the post with a target is positioned as close to the centre of the adjusted element

as possible. Subsequently, the beam is adjusted to hit the target. Thereafter, the gantry is moved far from the adjusted component along the longer axis and the operation is repeated. This approach should result in positioning of the beam precisely parallel to the holes of the laboratory table. It is worth noting that the adjustment process does not have to be performed before every single measurement. However, because of the vibrations caused by various laboratory equipment, it is recommended to repeat this process periodically.

Another step in the preparation process was to find the initial position of the sliding table (starting point of the measurements). At the beginning, the length of the stationary loop was measured using a ruler. That action allowed marking an approximate point on the sliding table in which, the signal should be created. Subsequently, that position was converted into a distance in steps, which is the primary unit used by the sliding table. It was achieved by repeatedly moving the sliding table by a set number of steps until the desired position was reached. Then, measurements on the wide (relatively) distance around marked point were performed. Measurements were performed in the step mode. When the signal was found, the number of iterations, the step size and the previously obtained starting position were used to calculate the number of steps where the signal is created. The number in steps obtained in that way was used as a starting point allowed to perform measurements in the very narrow distance range.

5.2 SPECTRUM MEASUREMENTS

Another activity preceding tests of the autocorrelation setup was a measurement of a spectrum of the laser beam. Since spectral and temporal characteristics of the pulse are associated with each other by Fourier transform, there is also a relation between the bandwidth and the pulse width [8]. These relations implied that there is a minimum duration-bandwidth product (also called time-bandwidth product) that cannot be exceeded [9]. Duration-bandwidth product is strongly dependent of the pulse shape and it is given by the following formula:

$$\Delta\omega_p \tau_p \geq 2\pi c_b \quad (10)$$

Where, ω_p is a bandwidth, τ_p is a pulse duration (both are FWHM) and c_b is a numerical constant related to the pulse shape. For a Gaussian shape c_b is 0,441 while for a sech^2 shape it is 0,315.

The equality in the above formula is preserved if the frequency of the pulse was not modulated. In that case a pulse is only limited by the Fourier transform. Obviously, not all pulses are transform-limited. Deviations (chirps) of the beam caused by e.g. chromatic dispersion in thick optical elements can lead to increasing the pulse width without affecting the bandwidth [8].

The above equation implies that a spectrum measurement does not lead to precise information about the pulse width. However, knowing the bandwidth and the pulse shape, a minimum possible (transform limited) duration of the pulse can be calculated. It would reveal if minimum pulse width specified by the laser manufacturer is possible to achieve.

The measurement itself is very simple. The laser beam was terminated (just after the laser) using the screen and the probe of the spectrometer was directed to the scattered beam. The spectrum was measured and saved using USB Avantes spectrometer. Subsequently, the obtained spectrum was processed using OriginPro 9.0; it was fitted to the Gaussian shape (it was the closest match, GaussAmp fit was used) and the FWHM of bandwidth was calculated. Processed result is presented in Figure 5.2 a). Knowing a bandwidth of the pulse, minimum pulse duration was calculated using the following formula:

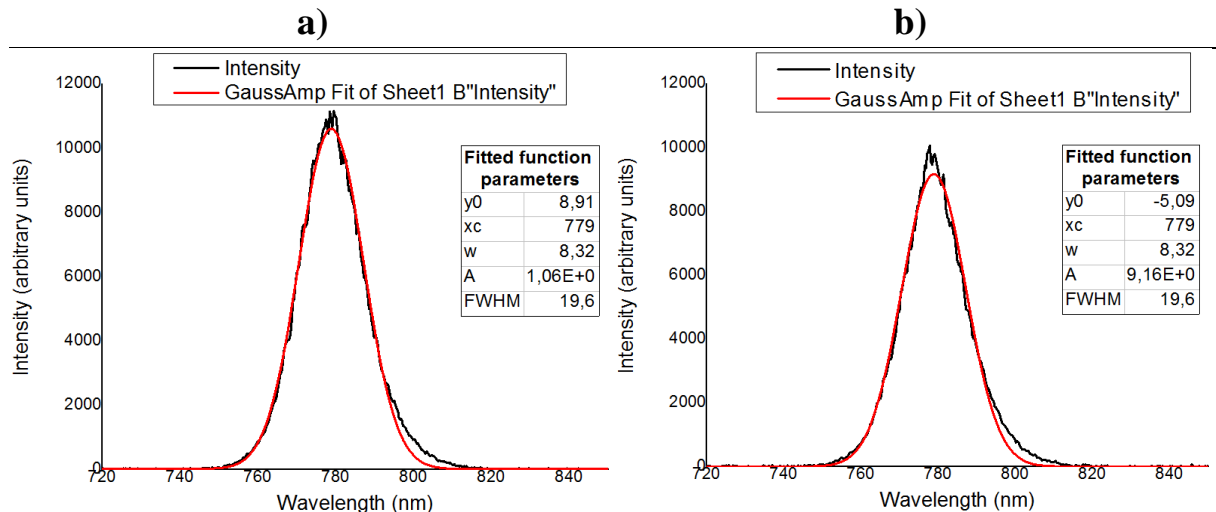
$$\tau_p = \frac{c_b \cdot \lambda_c^2}{\omega_p \cdot c} \quad (11)$$

Where, ω_p is a bandwidth, τ_p is a pulse duration (both are FWHM), c_b is a numerical constant related to the pulse shape, λ_c is a central wavelength and c is the speed of light. The formula is using the reverse analogy to the one presented in [10].

$$\tau_p = \frac{0,441 \cdot (7,79 \cdot 10^{-7}m)^2}{19,6 \cdot 10^{-9}m \cdot 2,998 \cdot 10^8 \frac{m}{s}} \approx 45,4 \cdot 10^{-15} = 45,4 \text{ fs}$$

Performed calculation shows that for the measured bandwidth, a transform-limited pulse has a duration 45,4 fs. It means that for that setting, laser is not able to achieve the pulse width reported by the manufacturer. Moreover, it should be remembered that chirped pulses may have a longer duration.

Additionally, the spectrum of the beam was measured in three different parts of the autocorrelation setup; after the optical isolator in the loop with constant delay and in the controlled delay loop (both just after the beamsplitter). This operation was performed to inspect if none of used components was suppressing some part of the spectrum. In that case the improper component should be replaced in order to not interfere with intensity autocorrelation measurements. Results of the spectrum measurements are presented in the following figure.



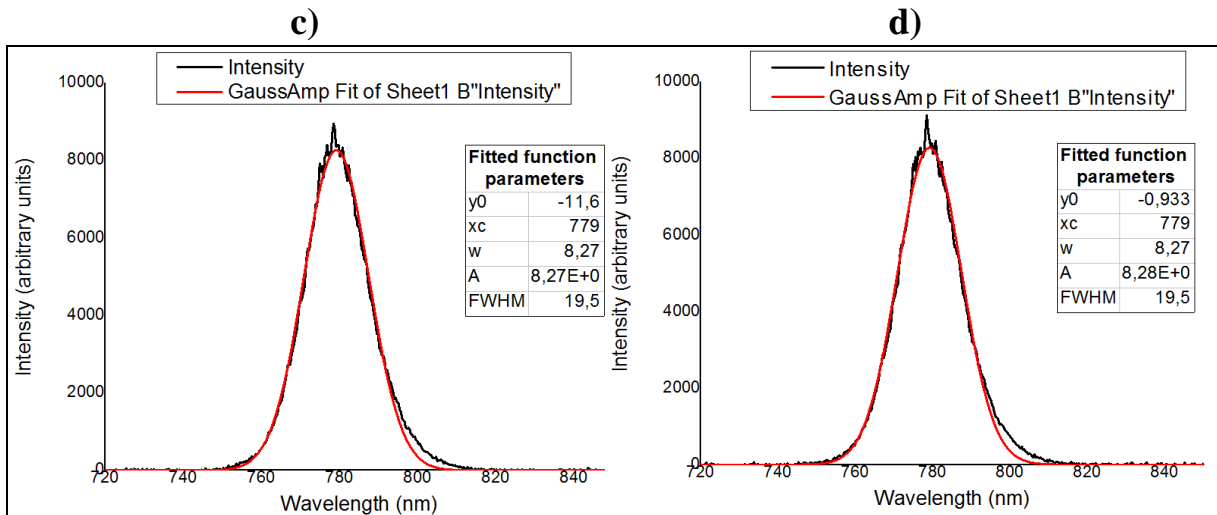


Figure 5.2 Spectrum measurements in a different parts of the system a) after laser b) after optical isolator c) after a beamsplitter – stationary delay loop d) after a beamsplitter – controlled delay loop.

Figure 5.2 shows that all spectra have a similar shape, which can be approximated as a Gaussian. Moreover, FWHM of intensity of these spectra are very similar. It means that none of the optical components, in the measured part of the setup, is not suppressing the spectrum. However, one irregularity has been noticed. All obtained spectra are not symmetrical, which may indicate some issues with a pulsing operation of the laser. Nevertheless, it cannot be stated just based on the spectrum measurement.

5.2.1 BANDWIDTH CALCULATOR

In order to facilitate calculations of the minimum pulse width that can be obtained for the certain bandwidth, a simple “bandwidth calculator” was created. Similarly to the main software of this project, this program was made using LabVIEW. The structure of the program is very simple. All calculations are included in a while loop, which is refreshed every 50 ms (20 Hz). The loop can be broken using a “STOP PROGRAM” button, which also ends the program. The complete structure of the entire program is presented in Figure 5.3.

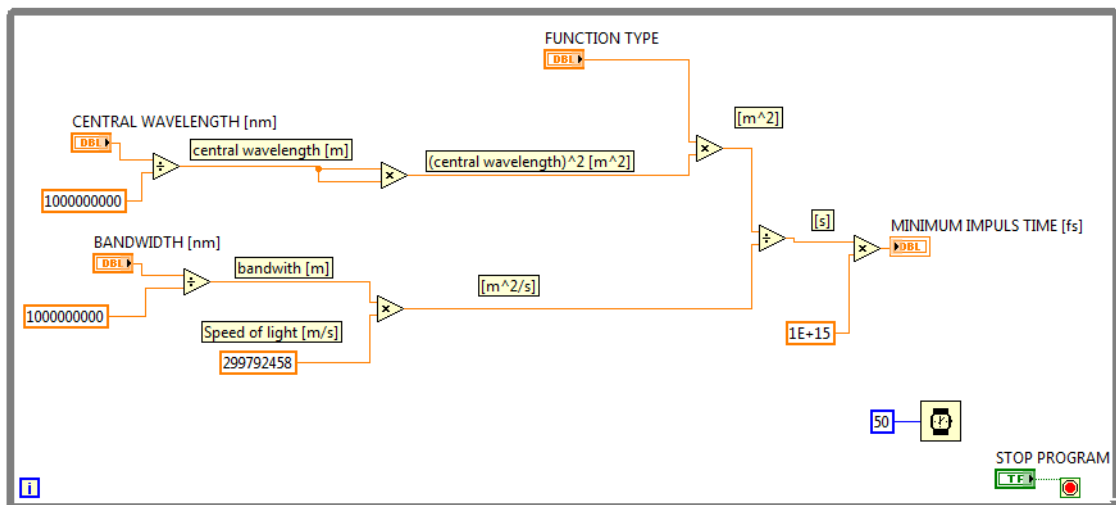


Figure 5.3 Implementation of bandwidth calculator.

The user can communicate with a program using a compact user's interface. It contains three controls, which are used to input bandwidth [nm], central wavelength [nm] and a function type that fit to the spectrum. For now, the user can choose from only two shapes (Gaussian and sech^2) however, if necessary more function types can be easily added to the program. Furthermore, user's interface contains an indicator, which shows calculated pulse width and the "STOP PROGRAM" button that ends the program. The interface is presented in the following Figure 5.4.

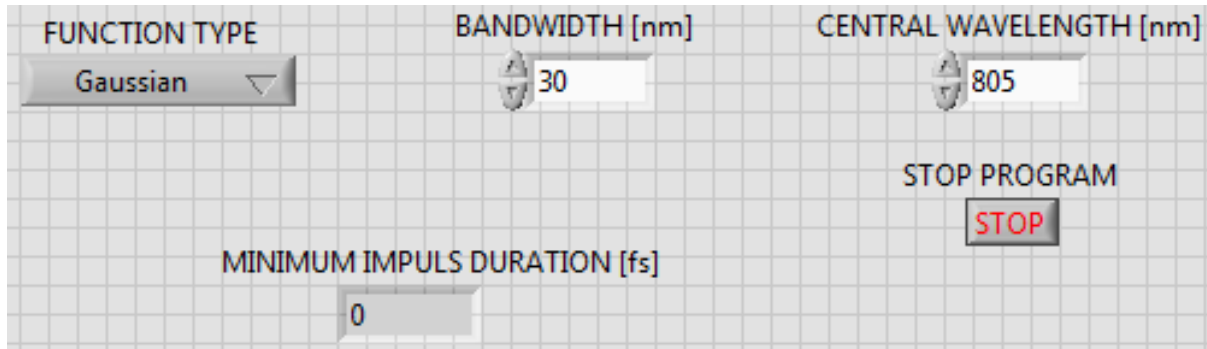


Figure 5.4 User interface of bandwidth calculator.

The bandwidth calculator is very simple and intuitive in usage. In order to start the program, the user has to press the "Run" button in the LabVIEW menu. This action instantly starts calculations using default parameters. The user may change parameters at will during an operation of the program. Since calculations are refreshed every 50 ms, the new result should be displayed almost immediately after new parameters are defined. If the program is no longer needed, it can be ended by pressing the "STOP PROGRAM" button.

5.3 MEASUREMENTS

Performed adjustment of the setup as well as spectra measurements prepared the entire autocorrelation system for measurements of the pulse width. Since the step approach is said to be more reliable, test measurements were conducted using the software based on this approach. When the measurement was completed, the obtained data was fitted to the "assumed" pulse shape using OriginPro 9.0. The manufacturer of the laser used and recommend to use the sech^2 shape during measurements. Unfortunately, OriginPro 9.0 does not support sech^2 as a fitting function therefore, a Gaussian shape (GaussAmp) was used for fitting. These two functions are very similar, their FWHM are almost identical. The only noticeable difference is that sech^2 has bigger wings at the base. Nevertheless, the duration-bandwidth product of these functions are different (Gaussian 1,41; sech^2 1,543) therefore, the final pulse width for Gaussian fitting will be slightly larger than for sech^2 . The autocorrelation function obtained during the first measurement together with a fitted Gaussian function is presented in the below figure.

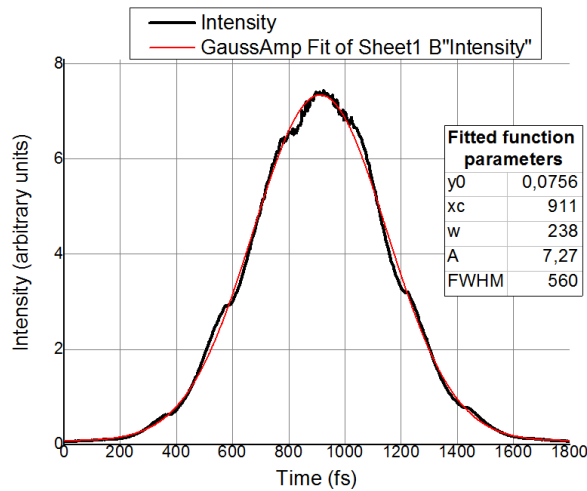


Figure 5.5 The result of the very first measurement performed using autocorrelation system.

The above Figure 5.5 shows that the autocorrelation function has roughly a Gaussian shape; however it is much distorted. Moreover, the FWHM of intensity is 560 fs. After dividing this value by a deconvolution factor gives a pulse width equal 395 fs, which is far above expectations. Both the shape as well as the pulse width was found not acceptable, therefore some further steps have been taken to improve the obtained signal. The following subchapters describe these steps and present associated thinking processes.

5.3.1 REMOVING THE OPTICAL ISOLATOR

The first idea was to remove the optical isolator from the laser beam path. These device is extremely important for a proper operation of LSM, however it is not required for intensity autocorrelation measurements. It is based on a Faraday Effect, which uses a magnetic field to rotate the polarization of the beam while it transmits through a glass. The dispersion on the glass component of the isolator may cause a significantly increase the pulse width [11]. After removing the optical isolator from the laser path the intensity autocorrelation measurement was repeated and the obtained function is presented in Figure 5.6.

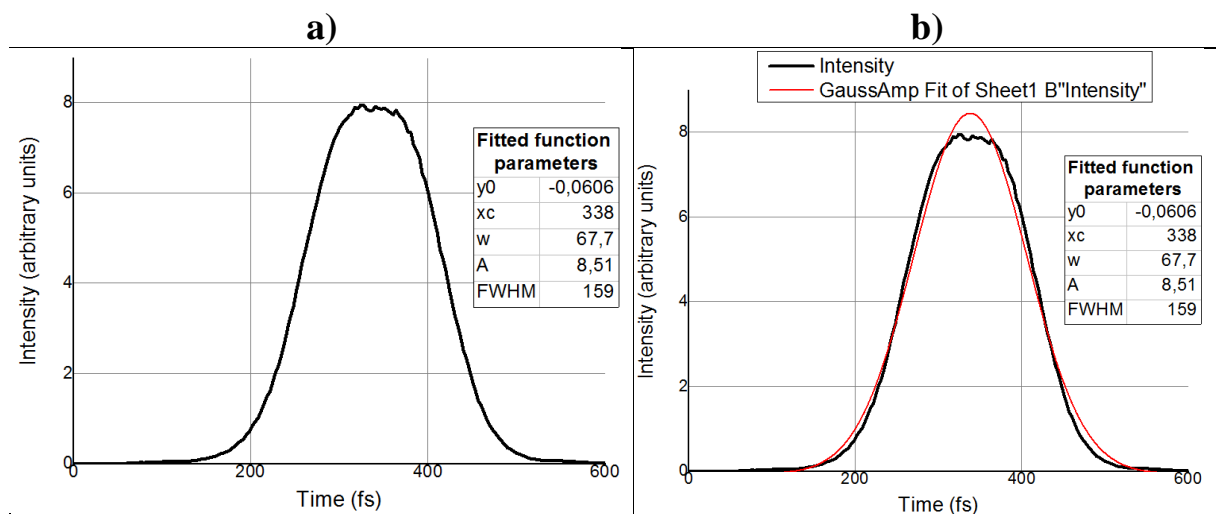


Figure 5.6 Autocorrelation function after removing the optical isolator from the setup a) without fitted function b) with fitted function.

At first sight, the profile of obtained autocorrelation function seems to have a Gaussian shape. Moreover, the FWHM of intensity significantly decreased to 159 fs, which after calculations gives a pulse width about 112 fs. However, performed fitting revealed that function shape is not a true Gaussian. The wings at the base are slightly narrower while, a top of the function is wider than fitted shape. It appears that a noise, which was previously distributed on the entire profile, is now accumulated on the top of the profile. Removing the optical isolator highly improved the pulse width therefore; this change to the setup has been preserved. Nevertheless, the shape issue was not solved thus some other changes to the setup has to be considered.

5.3.2 COMPENSATION BY A GLASS PLATE

It was noticed that, the thickness of the beamsplitter does not affect both delay loops equally. The transmitted beam, which goes through it (constant loop), is certainly affected by a dispersion, while the reflected beam (controlled loop) is not. This changes an autocorrelation into a correlation because pulses in the loops are not equal. In order to compensate the thickness of the beamsplitter, a glass was applied in the controlled loop. Thereafter, an intensity autocorrelation measurement was repeated again. Results of this measurement are presented in Figure 5.7.

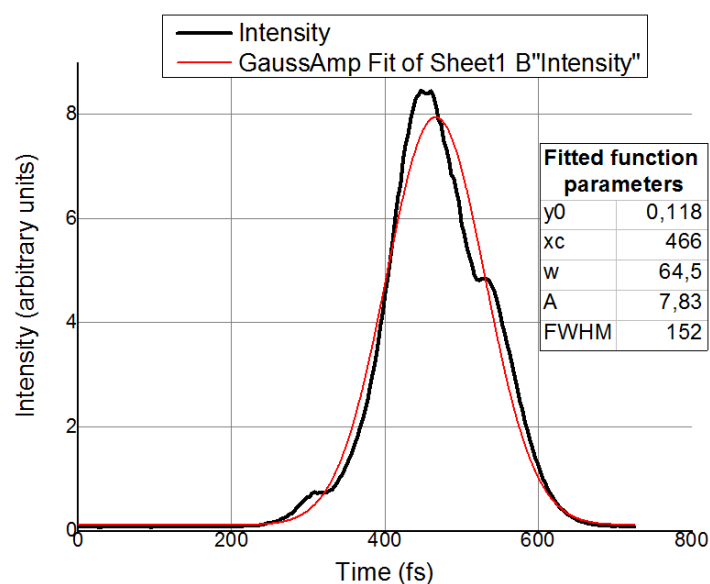


Figure 5.7 Autocorrelation function obtained with a compensating mirror applied in the setup.

The profile of the autocorrelation function drastically changes after adding the compensator to the system. The noise, which was previously accumulated in the top of the function spread to the entire profile as it occurred in the first measurement (with optical isolator). Moreover, the FWHM of the intensity slightly decreased; however it may be a result of a fitting, which does not work so precisely in case of so complex shapes. Test with an additional mirror shown that, lack of the thickness compensation is not the main issue of the system as well as it is not a reason of distorted shape of obtained signal.

5.3.3 CHECKING GEOMETRY ISSUES

Observed displacement of the distortions caused by the inserted glass plate may suggest that the system has some issues related to the geometry. In order to verify this hypothesis, the geometry of the setup was slightly changed. It was achieved by small movements of the most crucial components of the setup such as; BBO crystal, lens, mirrors on the mounting table and the last mirror in constant delay loop. The movement of these components was provided by adjustable frames, which allow very precise rotations around two axes.

During a long adjustment of components, no geometry change, which eliminates distortions, was noticed. However, it was observed that distortions move along the autocorrelation function during the movement of some components (mostly mirrors from both loop but also the lens). Therefore, a few more attempts were made to move distortions outside the autocorrelation function. Unfortunately, when distortions are moved to the one edge the function profile, the another one appears on the opposite edge. It may imply that the geometry of the setup is not a cause of distortions. Since the noise cannot be fully eliminated by geometry changes, some efforts were made to at least reduce its influence on measurements. It was found that the autocorrelation function is the most exposed and the least misshapen when distortions are moved to its edges. The centre part of autocorrelation function is then a true Gaussian and a fitting is much easier. The final result of reducing the influence of distortions via geometry changes is presented in Figure 5.8. It is worth noting that, since the central part of the function is not affected by distortions, the FWHM of intensity of the fitted function decreased to 129,1 fs, which after dividing by deconvolution factor gives a pulse duration equal 91,3 fs. From this point of tests, all further changes was performed together with a small geometry changes. Even if these changes will not eliminate distortions it is important to obtain the presented optimal profile of the autocorrelation function.

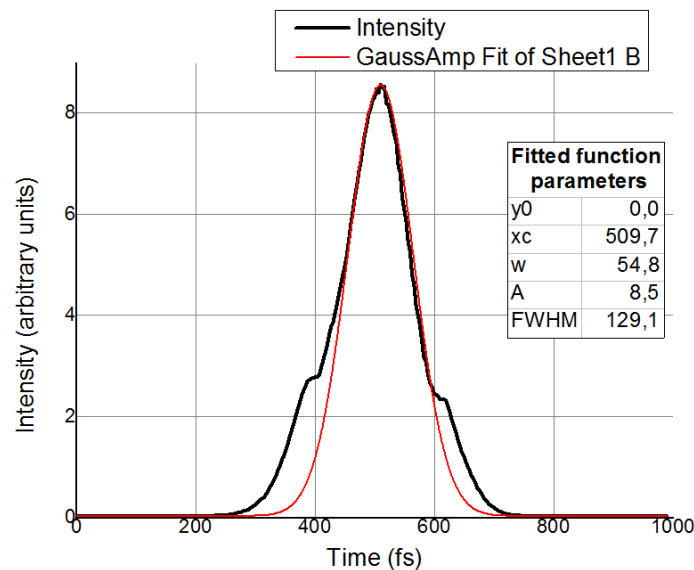


Figure 5.8 The most optimal profile of autocorrelation function obtained during geometry changes.

5.3.4 CHANGING THE BEAMSPLITTER

Since the dispersion is the biggest issue in the femtosecond optics [12], a usage of the thick optical components is not acceptable. Therefore, another idea to improve the obtained signal was to replace the thick beamsplitter. It was found that ultrathin pellicle beamsplitter (BP245B2) manufactured by ThorLabs is an optimal solution for this application. Unfortunately, according to the datasheet, a nominal reflection-transmission ratio of these device is 45:55. However, its transmission coefficient spectrum, which is illustrated in the following Figure 5.9, shows that the splitting ratio is not constant and strongly depends on a wavelength. Performed tests revealed that the splitting ratio for applied laser adjustment is nearly 50:50, which make this device a perfect choice.

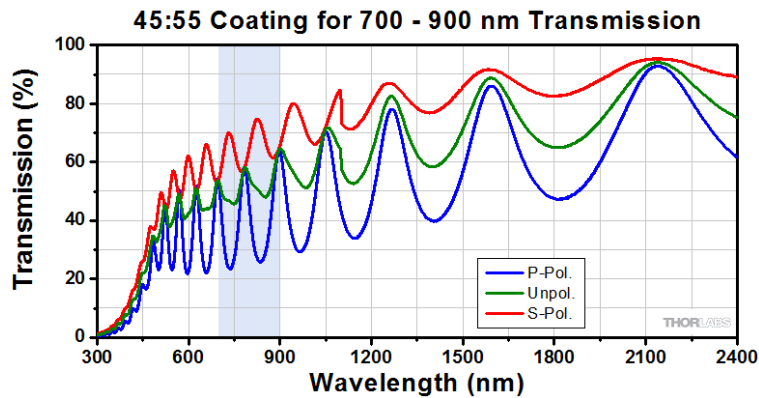


Figure 5.9 Transmission coefficient of beamsplitter applied in the autocorrelation system [13].

Unfortunately, intensity autocorrelation measurements performed with a new beamsplitter shown no improvement in case of distortions. The only difference was in the FWHM of intensity, which decreased by a few femtoseconds.

5.3.5 TESTING CRYSTAL

As it was previously noticed, the thickness of the BBO crystal (0,5 mm) is too big for such sort pulses. The following Table 5-1 presents a crystal thickness, which is required for the certain pulse duration. Previously conducted calculations based on the spectrum measurement and duration-bandwidth product revealed that the laser can emit pulses with duration down to 45,5 fs. According to the data from the table, crystal with thickness of 0,1 mm has to be used for this pulse duration. Taking it into account, previously used crystal was replaced with a more suitable, 0,1 mm thick BBO crystal (BBO-601H Eksma Optics).

Table 5-1 Thickness of the BBO crystal required for certain the pulse duration [12].

Application	Pulse duration, fs	Thickness, mm
Type 1, SHG@800 nm, $\theta=29.2^\circ$, $\varphi=90^\circ$	10	0.05
Type 1, SHG@800 nm, $\theta=29.2^\circ$, $\varphi=90^\circ$	20	0.1
Type 1, SHG@800 nm, $\theta=29.2^\circ$, $\varphi=90^\circ$	50	0.2
Type 1, SHG@800 nm, $\theta=29.2^\circ$, $\varphi=90^\circ$	100	0.5
Type 1, SHG@800 nm, $\theta=29.2^\circ$, $\varphi=90^\circ$	200	1

The intensity autocorrelation measurements were repeated using the upgraded setup. Results of these measurements are presented in the following Figure 5.10.

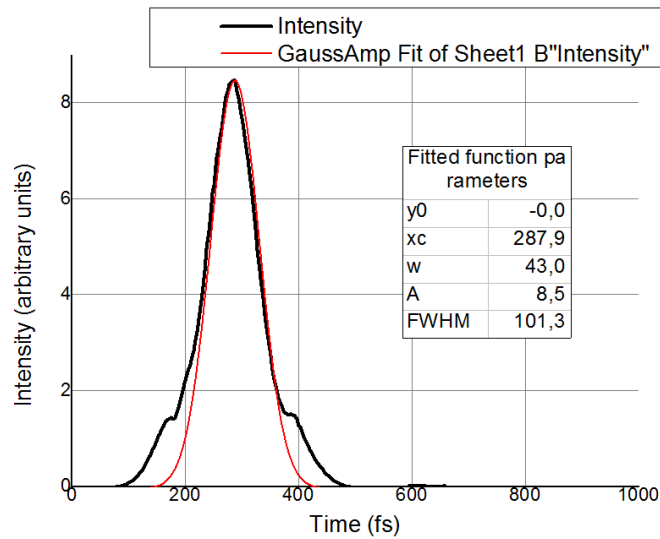


Figure 5.10 Autocorrelation function obtained after replacing the BBO crystal.

The replacement of the prism resulted in a significant improvement of the measured signal. First of all, the FWHM of intensity decreased to about 101,3 fs, which after taking into account the deconvolution factor gives a pulse width 71,6 fs. This value is quite close to expected 45,4 fs. Moreover, the distortions located on the sides of the function were reduced (the signal-noise ratio increased).

5.3.6 CHANGING LENS

Another idea to improve the shape of obtained autocorrelation function was to test different lenses. It was possible that due to spherical aberrations, the beams are not focused in one point, what could be a potential source of distortions. Moreover, replacement of a lens substantially changes the geometry of the setup (the changes are more radical than in case of previously describe adjustment). It would definitely eliminate all potential back-reflections from lens to the crystal. Tests were performed for three various lenses:

- Double-convex lens, focal length = 35 mm, diameter 1" (initial choice),
- Plano-convex lens, focal length = 50 mm, diameter 1",
- Plano-convex lens, focal length = 70 mm, diameter 2".

The lenses was sequentially inserted into the setup and adjusted to ensure that beams are equally distant from an axis of the lens. Moreover, for the third lens, which has the biggest diameter, an additional test has been performed. The distance between two beams was change by adjusting the last mirror in the constant delay loop. As a result, beams were focused at the different angle, which should also verify an influence of possible reflections.

Unfortunately, performed tests have not shown any changes in the profile of the autocorrelation function. It implies that neither spherical aberration of the lens nor back-reflections from lens to crystal is a cause of distortions. However, information obtained during

performed tests resulted in a permanent replacement of the lens. It was noticed that, plano-convex lens ensures better control over the reflection. Moreover, the larger focal length, the harder is to focus beams onto the BBO crystal. Taking these into account, the initially chosen lens with replaced with the plano-convex lens, $f = 50$ mm.

5.3.7 TESTING INFLUENCE OF VIBRATIONS (ADDING DC MOTOR)

The motorized sliding table during its normal operation may generate vibrations, which may be a cause of observed distortions of the autocorrelation function. In order to verify that, it was decided to add another source of vibrations and observe its influence on the function profile. Moreover, so prepared vibration test should definitely allay concerns about geometry issues. In case of geometry problems, the vibration should distribute noise distortions (average them) on the entire signal. Vibrations were applied by mounting a small DC motor to the frame of each individual mirror of the system. Connection between the motor and the frame was provided by double-sided tape. Moreover, a shaft of the motor was asymmetrically loaded to increase vibrations. Intensity autocorrelation measurements were performed for three different voltages (and therefore frequencies of vibrations) applied to the DC motor; 1,5 V, 3 V and 4,5 V. The following Figure 5.11 presents results of the test for the last mirror in the constant delay loop.

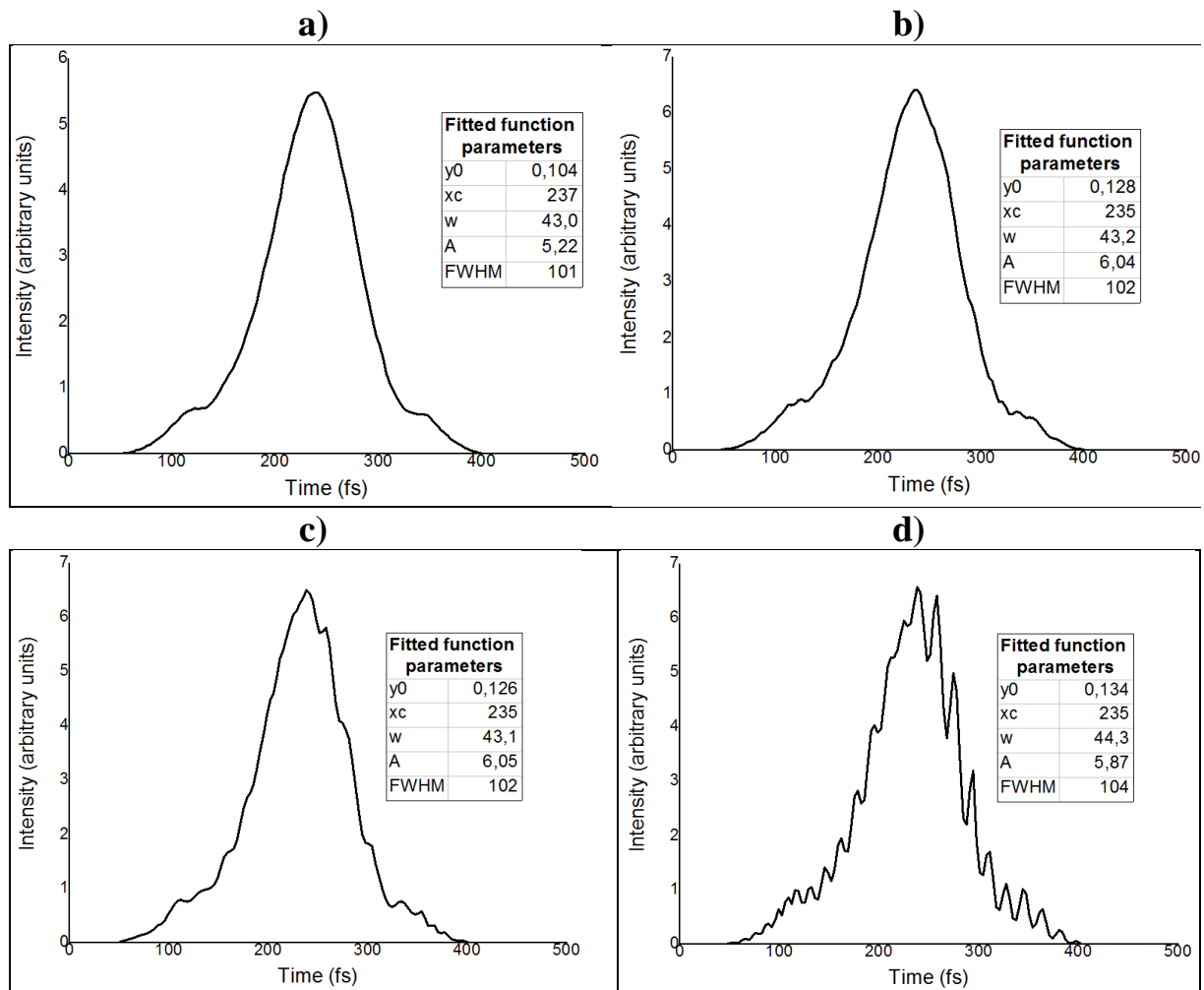


Figure 5.11 Autocorrelation function for various voltages applied to the DC motor mounted to the last mirror in the constant delay loop a) 0 V – motor turned off b) 1,5 V c) 3 V and d) 4,5 V.

The influence of vibrations is larger for higher voltages applied to the DC motor and therefore, for higher frequencies. Moreover, the entire profile of the function is similarly affected by the vibrations. It implies that distortions of the autocorrelation function are not caused by the motorized sliding table. Furthermore, it unambiguously proves that geometry is also not a cause of distortions.

It is worth noting that for the DC motor mounted to other mirrors, results were very similar. However, in some cases, vibrations with lower frequency caused a larger noise. Probably, it was a result of meeting the resonant frequency of the post.

5.3.8 LASER

When all other elements of the system have been tested, it was a time to go back to the laser. Previously performed spectra measurement revealed that spectrum of the emitted beam is not symmetrical in the frequency domain. In order to verify the operation of the laser in the time domain, an ultrafast photodiode (Alphas UPD-500-UP) connected to oscilloscope has been used. It is worth noting that, the operation frequency of this device is not sufficient to observe an individual pulse; however the plotted profile should approximately match the shape of the pulse. The following Figure 5.12 illustrates the results of the mentioned measurement.

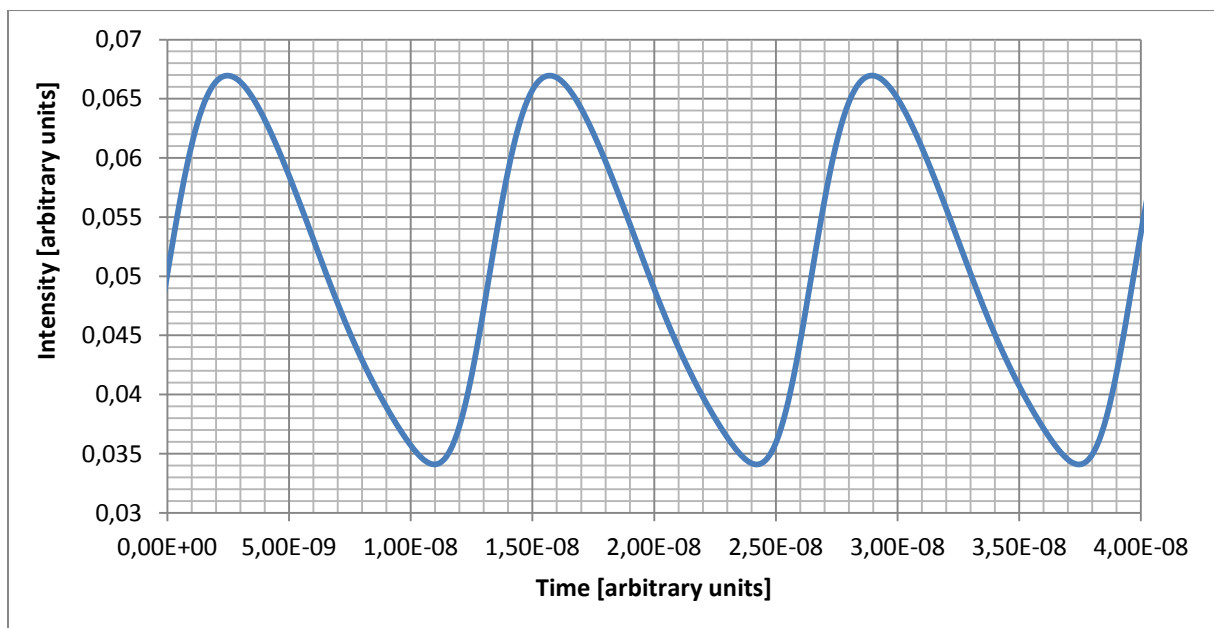


Figure 5.12 Approximate pulse shape obtained using GHz oscilloscope.

The data acquired using the ultrafast photodiode shows that the pulse shape is highly asymmetric. This information together with results from spectra measurements and performed tests of the setup may indicate that there are some issues with an operation of the laser. Since no other diagnostic tool, which might be used to unambiguously disprove or confirm this hypothesis, the previously presented (Figure 5.10) autocorrelation function with associated pulse duration of 71 fs is assumed to be the final result of intensity autocorrelation measurements.

5.4 COMPARISON OF MEASUREMENT METHODS

When the best possible shape of the measured signal was achieved, there was a time to compare two versions of software and hence measurements methods described in chapter 4.2.4. The following Figure 5.13 illustrates intensity autocorrelations functions obtained by using these methods. As it was expected, the profile of the function for continuous approach is rugged, while for the step approach the obtained profiles are smoother. The roughness in the continuous method is definitely the result of measuring the intensity when the sliding table is not establishing (between its steps).

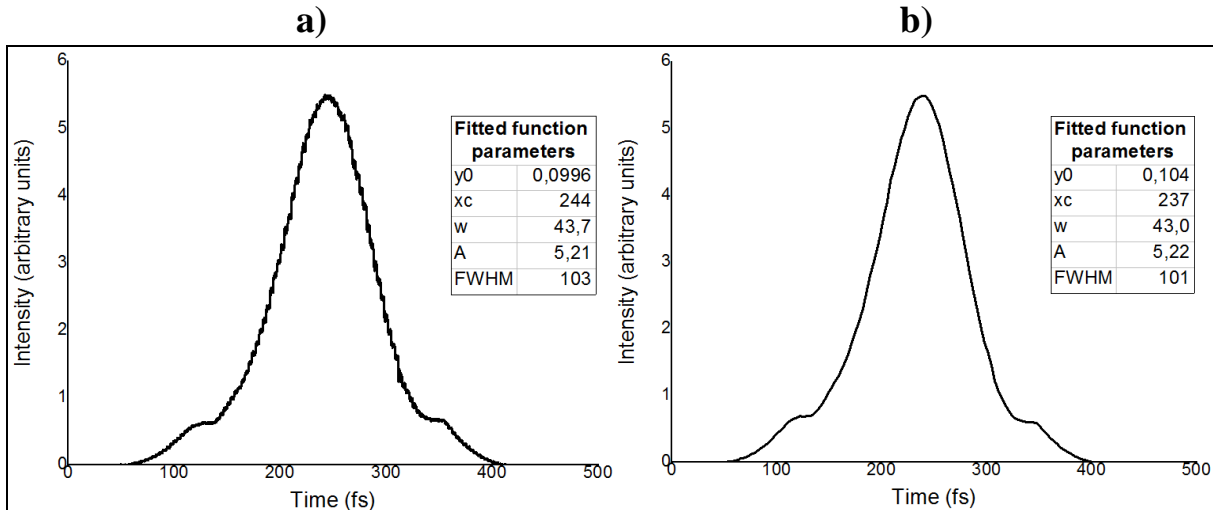


Figure 5.13 Intensity autocorrelation function obtained using a) continuous approach b) step approach.

Since, individual results are not reliable it was decided performed 20 measurement using each method and use them to conduct some static calculations. Autocorrelation functions obtained during that measurements were fitted to the GaussAmp shape using OriginPro 9.0 and their FWHM were calculated. Thereafter, simple statistical calculations were performed (mean and standard deviation). Table 5-2 presents the results for continuous measurements while, results corresponding to step measurements are shown in Table 5-3.

Table 5-2 Results of measurements obtained using continuous method with corresponding statistics.

CONTINUOUS MEASUREMENTS – FWHM OF INTENSITY									
102,9	103	103,1	103,4	103,8	103,4	103,6	102,6	104,6	103
102,7	103,9	103,1	103,5	103,5	103,3	103,5	103,5	103,4	103,6
MEAN VALUE					STANDARD DEVIATION				
103,37					0,45				

Conducted statistics shows that both methods give very similar results. Calculated mean values differ by around 2 %. It means that both methods and therefore programs may be used interchangeably, depending on user preference. Moreover, small standard deviations imply that both approaches give repeatable results. Therefore, both programs may be used for intensity autocorrelation measurements depending on user's preferences.

Table 5-3 Results of measurements obtained using step method with corresponding statistics.

STEP MEASUREMENTS – FWHM OF INTENSITY									
101,2	101,2	101,6	101,4	101,2	102,2	101,5	101,8	101,3	101,4
101,9	101,3	101,6	100,9	100,5	101	101,3	100,5	102,1	101,2
MEAN VALUE					STANDARD DEVIATION				
101,36					0,45				

6 ABLATION OF PMMA

After the operation of the autocorrelation system has been verified, the new functionality of the LSM setup had to be tested in practice. The main goal was to verify the influence of the pulse width on the ablation. Beside the final experiment, this chapter consists a detailed description of the LSM setup; structure of the sample used for the experiment and performed preparation. Moreover, a special attention is paid on potential problems and inconveniencies of the system during the ablation mode.

6.1 PRESENTATION OF THE LSM SETUP

During the previous considerations about the autocorrelation system and its position in the setup (chapter 3.1), the structure of the LSM was not sufficiently described. Therefore, it is important to familiarize with the structure and operation details of LSM setup before performing experiments with ablation. It is worth noting that this chapter does not cover all details related to the LSM setup, instead it is focused on these components, which are necessary for ablation mode. The structure of the LSM setup is presented in Figure 6.1.

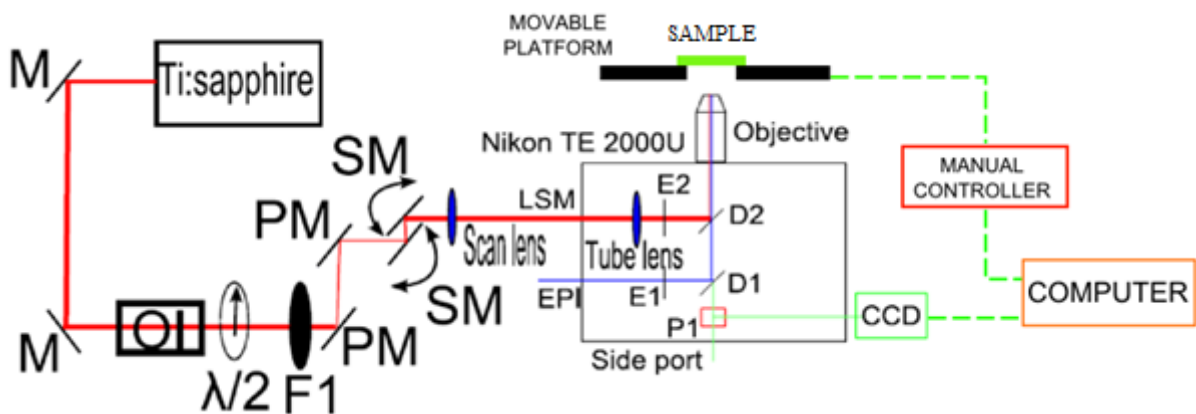


Figure 6.1 Schematic drawing of the LSM setup [20]. M – mirror, PM – periscope mirror, SM – scanning mirror, D – dichromatic mirror, F – adjustable neutral density filter.

The LSM setup is based on an inverted Nikon Eclipse TE 2000U microscope, which is equipped with a rotary turret containing various infinity corrected objectives (4X, 10X, 20X, 40X and 60X; 40X objective is mostly used for ablation). The sample is placed above the objective on a movable x-y-z platform and mounted in the clamp. The platform is controlled using manual controller, which is connected to the computer (controller can be also programmed to provide automatic operation). The path of the laser beam from Tsunami laser to LSM contains many components important for the ablation process. The first element in this path is the optical isolator. As it was previously explained, this device prevents the beam from returning to the laser, which may suppress its pulsing. Then, the beam goes through an adjustable half-wave plate, which allows rotating the polarization of the beam and adjustable neutral density filter, which is used to control the intensity of the beam. The neutral density filter was very useful during finding the ablation threshold. Afterwards, the beam is elevated using an optical periscope constructed of two mirrors. The elevation of the beam is necessary to guide the beam to the next component of the setup, which is located much higher than the

laser path. In order to facilitate alignment of the beam two pinholes were added to the setup first is located before the optical isolator, while the other before the periscope. The next component is crucial for the ablation. It is a 6210H galvanometric scanner produced by Cambridge Technology. The scanner consists of two mirrors, which are controlled with A510 3-X DAC computer card from ISS. The control is performed from computer using SimFCS software developed by Globals Software. Structure of the program allows defining various parameters of ablation such as: number of points in the scan, sampling frequency, size of scanned area, etc. After being deflected by mirrors of the scanner, the beam is guided through the telescope to the LSM. The telescope consist of two lenses (scanning lens and tube lens) mounted in the optical tubing. In the LSM the beam is reflected by the dichromatic mirror and focused onto the sample with one of objectives included in LSM. The observation of the sample is performed using either an eyepiece or a CCD camera. Since usage of the oculus during ablation is forbidden because of the laser hazard, the CCD camera was mostly used of observation of the sample during the project. The LSM setup is presented in the following Figure 6.2

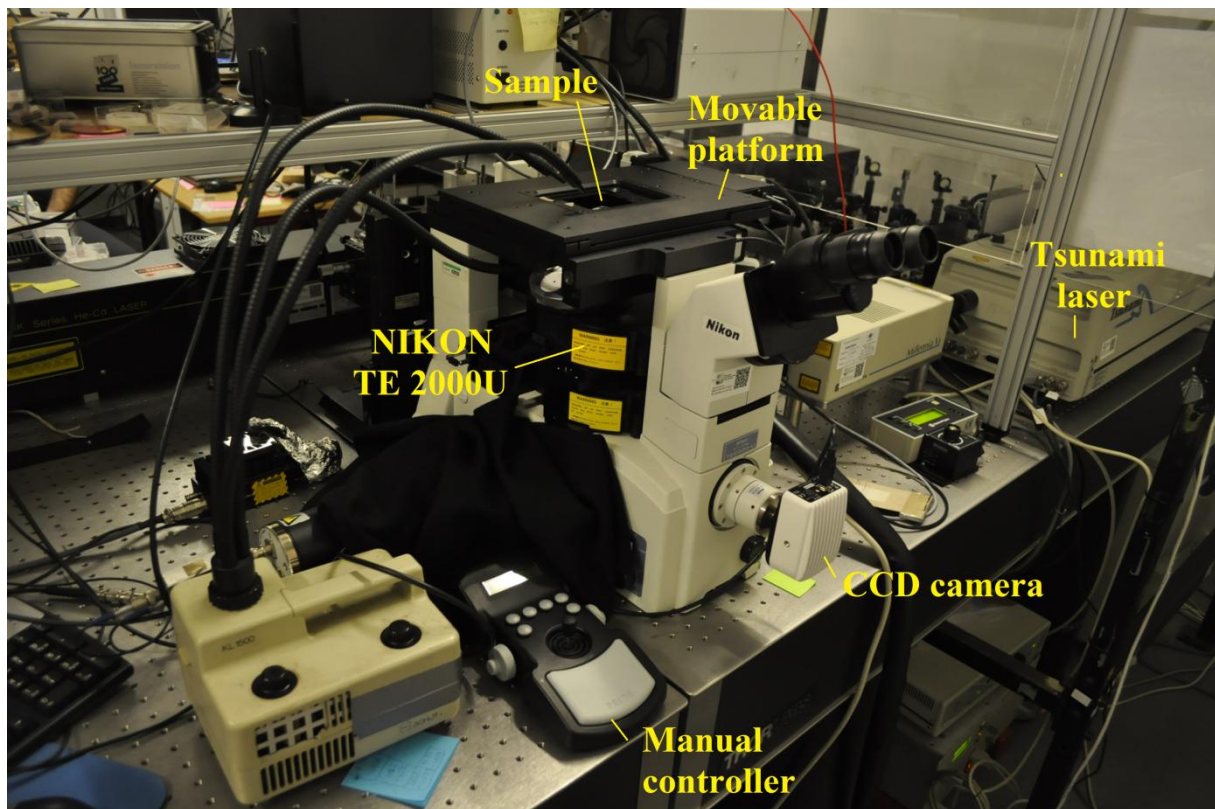


Figure 6.2 LSM setup.

6.2 FABRICATION OF THE SAMPLE

The next step was to find a suitable sample for ablation. The main idea was to use already tested sample, whose usefulness in PMMA ablation has been already proven. After long considerations, it was decided to use a sample pattern, which were proposed in [20] [21] [22] for near-field mapping. This sample is based on a silicon substrate (1 cm x 1cm) covered with 70 nm gold. Moreover, six two-dimensional arrays of nano-squares with size of

50 μm x 50 μm were fabricated on the top. The details regarding the structure of the individual array are presented in Figure 6.3. At the end, the entire sample was covered with 200 nm of PMMA.

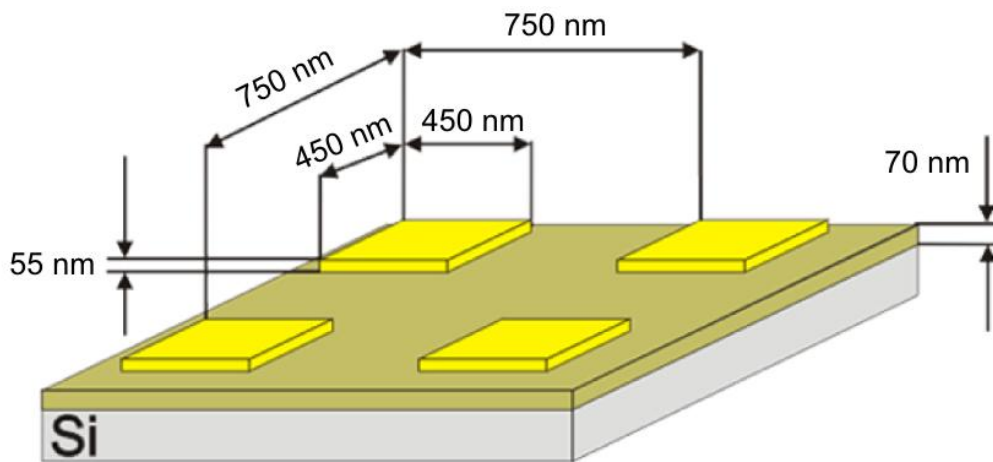


Figure 6.3 Schematic drawing of the nano-squares array located on the sample [20].

It was reported in [31] that used nano-array pattern cause a local field enhancement for wavelengths around 800 nm due to an occurrence of localized surface plasmons. According to this information, it was decided to extend the content of the project. An additional goal was to performed the ablation of PMMA located on nanostructures. Results of this operation would verify the influence of the pulse width on near-field mapping process.

The following list contains the complete recipe used during a fabrication of samples:

- **Photolithography (positive) on the silicon substrate to create a pattern for gold pads:**
 - Spin coating photoresist, first 500 rpm for 5 s, then 4000rpm for 30s.
 - Bake 90°C, 60 s,
 - Exposure \approx 5 s,
 - Development,
 - Followed by ICPRIE dry etching,
- **E-beam deposition of 70 nm gold:**
 - Deposition performed using Cryofox Explorer 600 LT,
 - 5 nm of Ti deposited on the bottom to increase adhesion,
 - Followed by lift-off,
 - Spin dry,
- **Dicing,**
- **E-beam lithography to create a pattern for structures:**
 - Spin coating 200 nm of PMMA A4,
 - First 1000 rpm, 5 s,

- Then 7000 rpm, 45 s,
- Baking 200°C 90 s,
- E-beam lithography performed using Hitachi S-4800 SEM,
- **E-beam deposition of 55 nm gold – structures;**
 - Deposition performed using Cryofox Explorer 600 LT,
 - Followed by lift-off,
 - Spin dry,
- **Spin coating of 200nm PMMA A4;**
 - First 5 s, 1500 rpm,
 - Then 45 s, 7000 rpm,
 - Baking 200°C, 90 s,

A complete sample fabricated using the above process is shown in the following Figure 6.4.

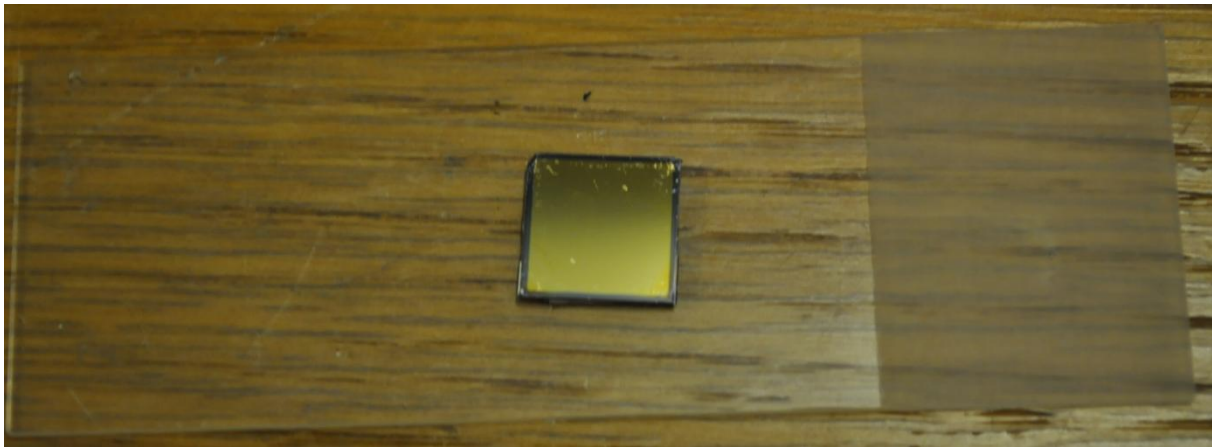


Figure 6.4 Sample used in the ablation experiment.

6.3 DEFINING THE SIZE OF ABLATED AREA

In the scanning mode (ablation can be also performed in one spot, without scanning), the size of the ablated area depends on the voltage applied to scanning mirrors [24]. There are different possible modes of scanning; circular, square, rectangular and linear. The very first tests revealed that finding a focus, which is very time-consuming, is much easier for ablation of squares because individual lines of the scan can be tracked. Therefore it was decided to use this scanning mode in the project. The first task was to define the relation between the size of the ablated area and voltage applied to the scanning mirrors. It is noteworthy that this task is not directly connected with the main thread of this project however; this simple experiment would definitely help to familiarize with the operation of LSM system and ablation process. Moreover, obtained results will help other users of the LSM setup, which are willing to perform similar experiments.

The first step of this experiment was to ablate squares for different values of the voltage. As a substrate for ablation process, samples presented in the previous subchapter (6.2) were used. Ablation was performed in the range of voltages from 400 V_{x_fs} to 1000 V_{x_fs} (V_{x_fs} – an unit related to the voltage applied in the ablation controlling system) with intervals every 100 V_{x_fs} . For each voltage three holes in different places on the sample were made in order to perform a simple statistics and prevent random error caused by local irregularities. It is worth noting that in this experiment ablation was performed only in the flat area (without structures) of the sample. Subsequently, the sample was taken to the cleanroom, where it was observed and imaged using SEM (Hitachi S-4800). Sample SEM images of the ablated areas are presented in the following Figure 6.5.

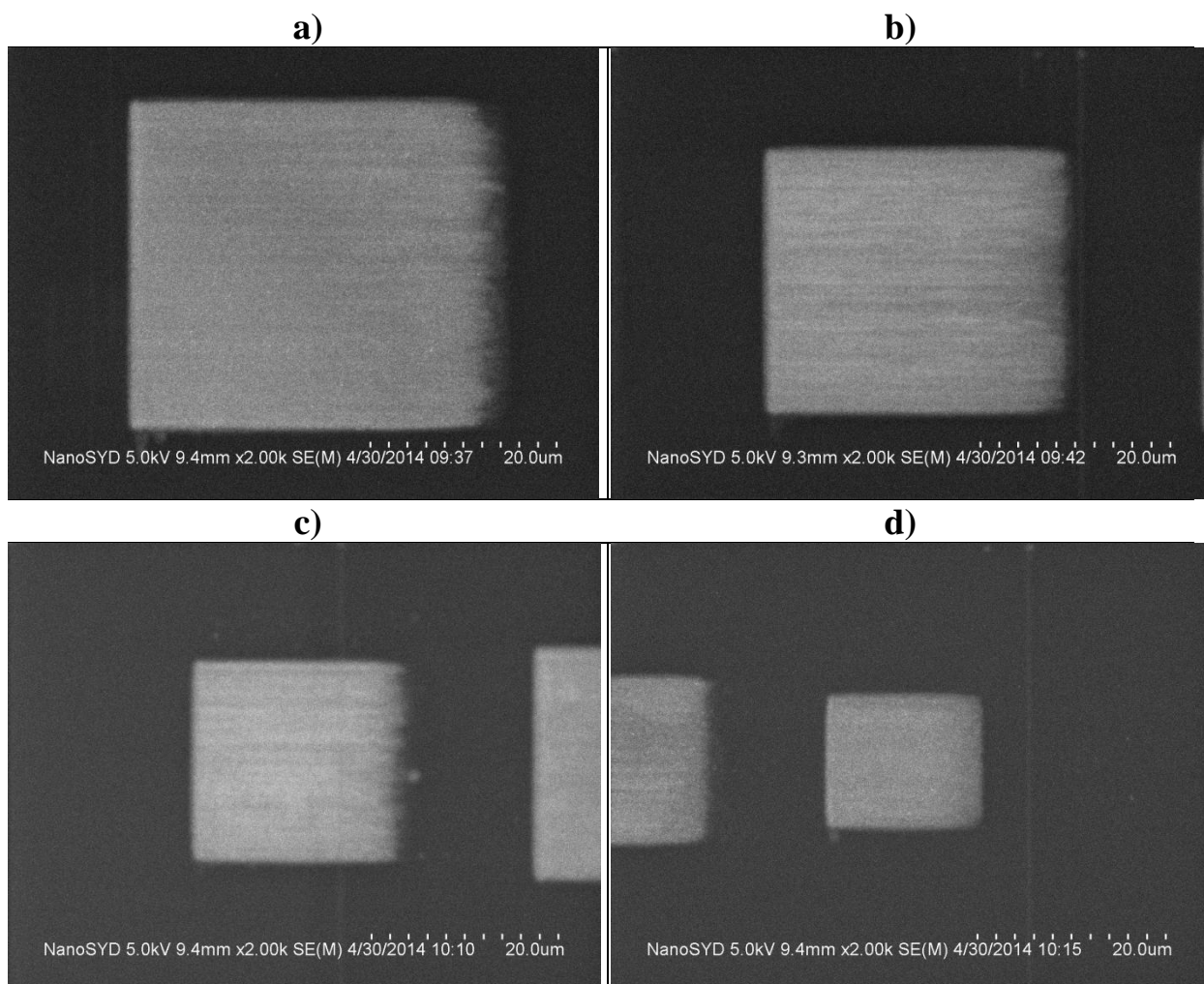


Figure 6.5 SEM images of ablated squares for different values of voltage applied to scanning mirrors a) 1000 b) 800 c) 600 d) 400.

Obtained imaged shows that the material on the right side of the ablated area is, in almost any case, not completely removed and the edge is irregular. The reason for that is probably associated with the operation of the scanning system. Horizontal direction is a fast axis of the scan and it is scanned from the left to the right side. After reaching the last point in the lane, the scanning point is transferred to the beginning of the next line. It is possible that the very last point in the line is not completely ablated because some part of its ablation time is taken by this movement. Another possible reason of observed irregularities is a tilt of the

sample, which results from the method of mounting the sample in the LSM. Additionally, it was observed that a horizontal dimension slightly differs from a vertical, which should be further investigated in this experiment.

Subsequently, SEM images were investigated and measured using ImageJ software. Since, a potential difference between vertical and horizontal dimension has been noticed, they were measured separately. Results of performed measurements for horizontal dimension are presented in Table 6-1, while Table 6-2 shows measurements of vertical dimension.

Table 6-1 Horizontal dimension of the ablated are depending on various voltages applied to scanning mirrors.

		Voltage [Vx_fs]						
		400	500	600	700	800	900	1000
Horizontal	1	16,36	18,28	22,98	28,15	31,85	37,42	40,60
		16,49	18,48	22,98	28,15	32,05	37,22	40,60
	2	16,37	18,42	23,04	28,54	32,19	36,82	40,53
		16,44	18,75	23,37	28,74	32,05	37,02	40,86
	3	16,44	18,35	22,71	26,60	32,15	35,70	41,65
		16,50	18,15	23,04	27,13	31,88	35,56	41,72
	mean	16,43	18,40	23,02	27,88	32,03	36,62	40,99

Table 6-2 Vertical dimension of the ablated are depending on various voltages applied to scanning mirrors.

		Voltage [Vx_fs]						
		400	500	600	700	800	900	1000
Vertical	1	14,37	17,75	20,99	24,77	27,82	31,52	34,77
		14,31	17,68	21,39	24,98	28,08	31,66	34,70
	2	14,06	17,56	20,99	24,64	27,95	31,06	34,44
		14,19	17,82	21,25	24,64	27,82	31,06	35,03
	3	14,19	17,29	20,86	24,49	27,92	30,93	34,59
		14,46	17,16	20,79	24,56	27,59	30,66	35,05
	mean	14,26	17,54	21,05	24,68	27,86	31,15	34,76

In order to facilitate an interpretation of obtained results, they were also illustrated graphically in the following Figure 6.6

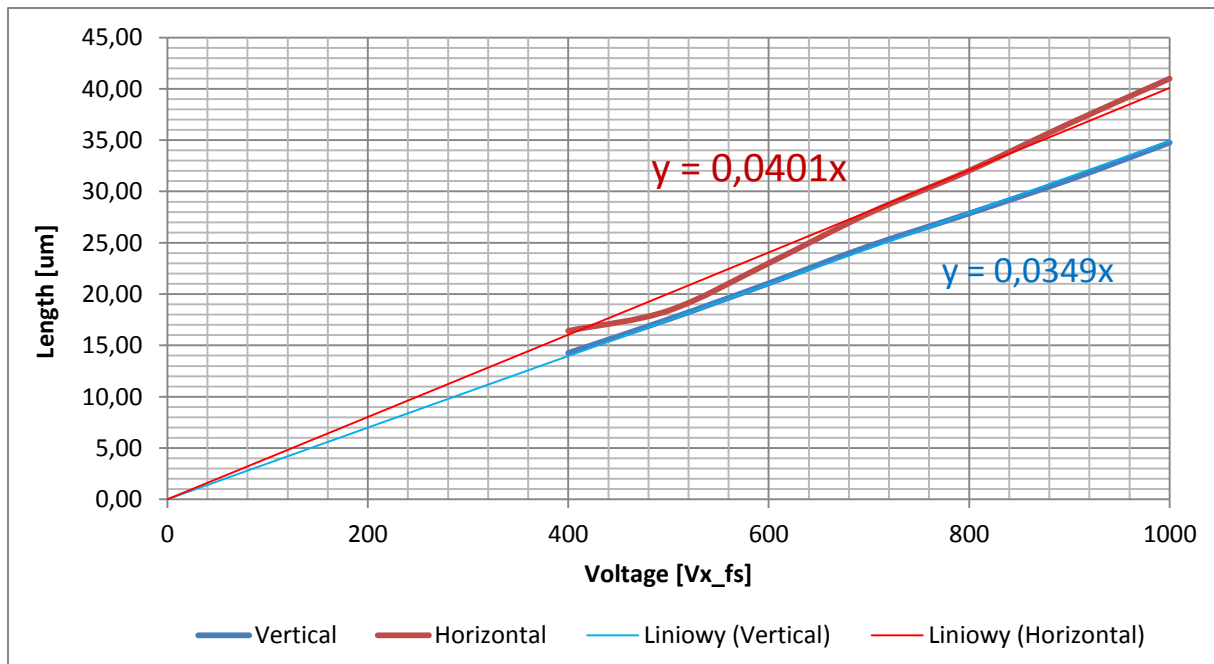


Figure 6.6 Dimensions of the ablated area as a function of voltage applied to scanning mirrors.

The obtained graph shows that both dimensions of the ablated area can be approximated as linear functions of the voltage applied to scanning mirrors. However, as it might be expected, the vertical dimension shows superior linearity than horizontal dimension. It is definitely a result of previously mentioned irregularities on the right edge of ablated area, which hindered length measurements. Moreover, as it was previously observed, the horizontal length is bigger than the vertical. Furthermore it increases faster with increase of the voltage. It may indicate some inaccuracies in operation of scanners or individual mirrors are out of tune (one of the mirrors move slightly larger distance for the same voltage applied).

6.4 EXPERIMENT – INVESTIGATING INFLUENCE OF A PULSE WIDTH ON AN ABLATION OF PMMA

The final part of this project was to investigate an influence of the pulse width on ablation of PMMA coating. However, before the start of the experiment some preparations and assumptions had to be made.

At the beginning of the experiment, the optical isolator was inserted back to the setup. Performed test revealed, that ablation is impossible without this device because the pulse operation of the laser is suppressed by the returning beam. Since the isolator extends the pulse, autocorrelation measurements were repeated and the obtained pulse width was 245 fs.

Furthermore, average power measurements were performed in order to investigate what fraction of light is lost on the components of the LSM. Firstly, a power meter was placed before the LSM (after the neutral density filter, which in that case was adjusted on full transmission) and the measured average power was 420 mW. Thereafter, the intensity, which leaves the objective, was measured and the obtained power was 30 mW. This simple measurement shown that components of the LSM are losing almost 93% of the incoming

light. It may indicate that some equipment used in the setup was not correctly selected for parameters of the system. It is worth noting that the energy of the laser pulse for maximum power (measured just after the laser unit) is 8 nJ.

Another assumption was related to the objective. It was decided to use an objective with magnification 40X and numerical aperture 0,68 because this device was already tested in ablation mode. Knowing properties of the objective, a size on an individual spot can be calculated using the formula for diffraction limit:

$$d = \frac{\lambda}{2 NA} = \frac{780 \text{ nm}}{2 \cdot 0,68} = 573 \text{ nm}$$

In order to verify an influence of the pulse width on ablation of PMMA, it was decided to perform two series of ablation. During the first series an ablation was performed without modulation of the pulse. In the second series, a 10 mm thick beamsplitter cube was inserted to the system, what should result in a significant incensement of the pulse width due to dispersion. Moreover, during both series the ablation was performed on the flat part of the sample as well as on the nano-structures. It has been done to investigate the impact of enhanced field, which is described in [21] [24] and verify if an extension pulse width affects field mapping [22]. After performing the ablation the sample has been transported to a cleanroom, where it was investigated using SEM.

6.4.1 ABLATION FOR UNMODULATED PULSE (WITHOUT THE BEAMSPLITTER CUBE)

At the beginning of the experiment, ablation was performed on the flat part of the sample (without nano-structures). Parameters of the software were set to provide 100 scanning spots in x and y directions of the scan and the duration of the one square-shaped scan was set to 10 s. The longer time of the scan was selected to allow adjusting of the focus, which was found very difficult. Furthermore, it was decide to apply a small voltage (300 V_{x_fs}) to scanning mirrors in order to save some space especially on nanostructures, whose area is relatively small. Moreover, ablation was performed for two different values of scanning cycles (2 and 6, which correspond to 15100 and 45300 pulses respectively) to investigate the incubation phenomena.

The main task was to find the ablation threshold. It was achieved by performing the ablation for different intensities of the laser beam, which was controlled using neutral density filter. The average power was decreased by 10 mW until the sings of the ablation started to vanish (the material was no longer removed). In the region close to the ablation threshold, the average power was changed by 5 mW. After a few attempts the ablation limit of PMMA for 2 scanning cycles was determined as 115 mW. As it was mentioned in the introduction, ablation thresholds are commonly described by fluence [m/cm^2] or intensity [W/cm^2]. However, since the goal was to compare threshold for modulated and unmodulated pulse and fluence is proportional to measured average power, the conversion was not performed. Hence, the average power is used as a laser ablation threshold unit. It is worth noting that, when the ablation for 2 scanning cycles was suppressed, for 6 scanning cycles it was still possible to

perform. It is the result of so called incubation. The following Figure 6.7 shows the ablation limit obtained for 2 scanning cycles and almost fully ablated square for 6 cycles.

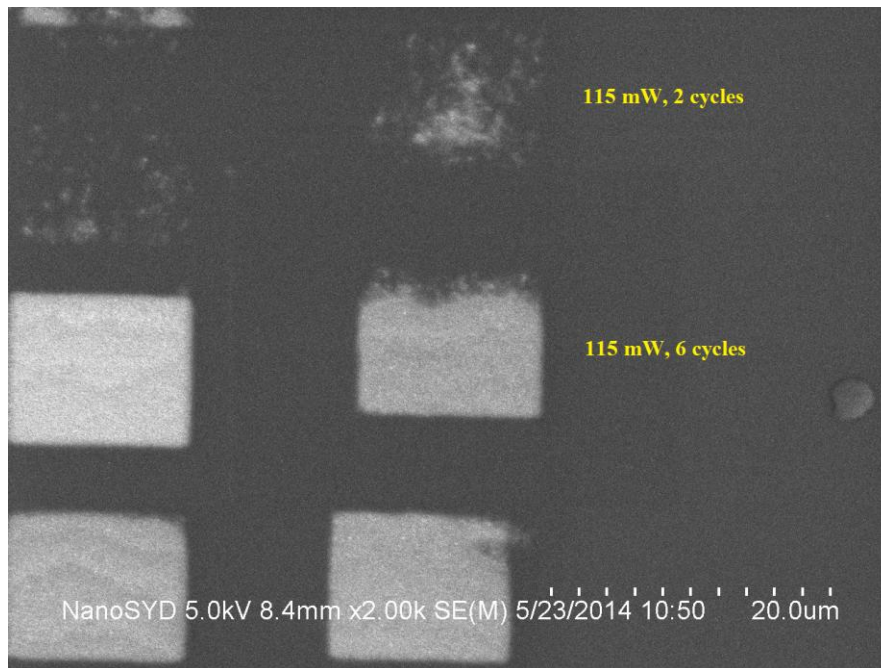


Figure 6.7 Ablated squares for unmodulated pulse on the flat part of sample.

The same procedure of experiment was repeated in case of nano-structures. The intensity of the laser beam was controlled using the neutral density filter and the ablation threshold was searched. Results of this part of the experiment, which are illustrated in Figure 6.8, shows that for 2 scanning cycles, the PMMA is no longer removed for 95 mW. However, for 100 mW the first signs of ablation are starting to occur.

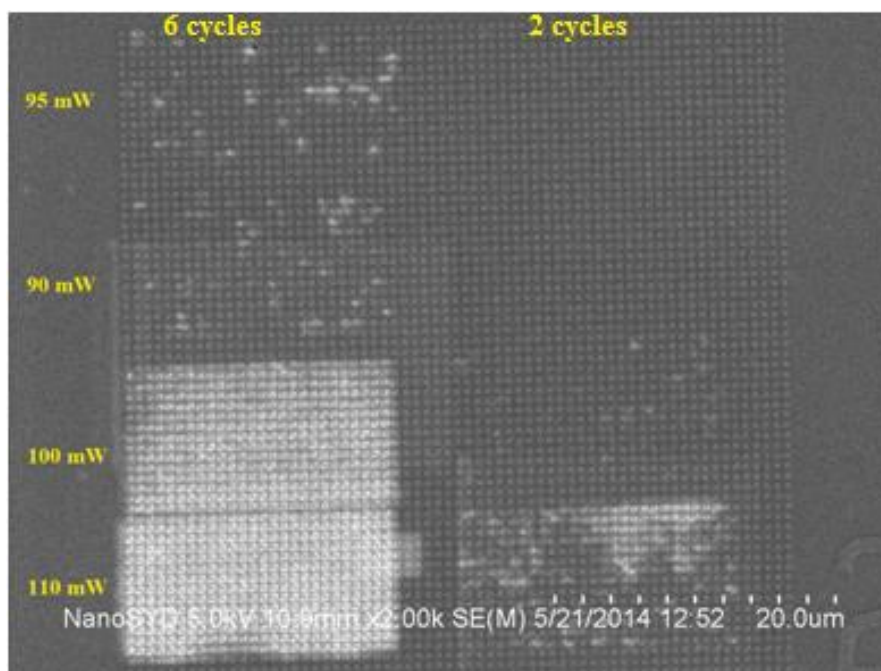


Figure 6.8 Ablated squares for unmodulated pulse on nano-structures part 1. Left column corresponds to 6 scanning cycles, while the right column corresponds to 2 cycles.

During the ablation on the nano-structures serious problems with focus were experienced. The reason is probably not uniform distribution of PMMA on the structures. Because of these problems it was decided to repeat this part of the experiment. The obtained results are presented in the following Figure 6.9.

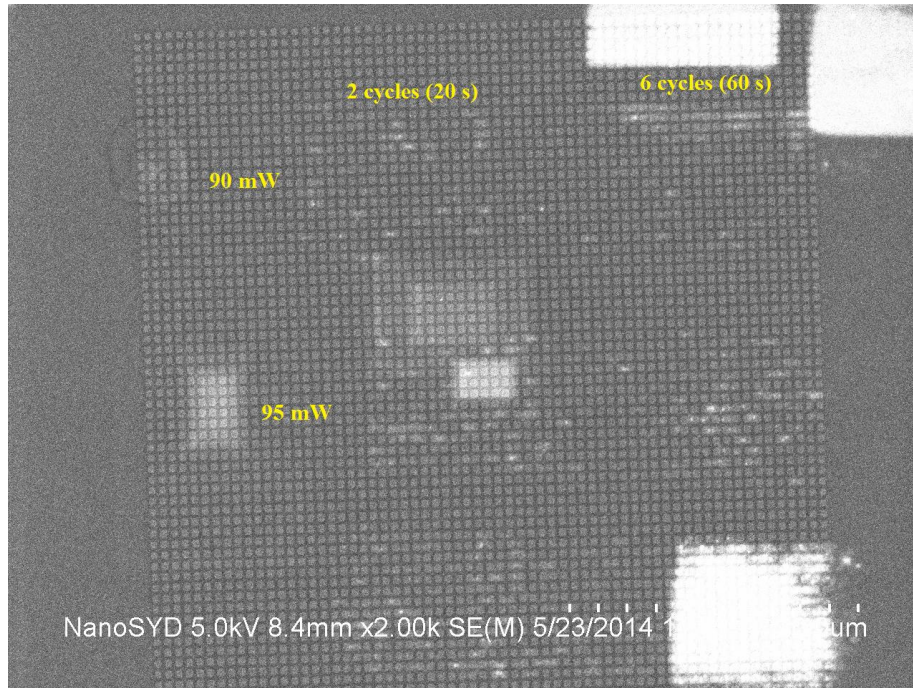


Figure 6.9 Ablated squares for unmodulated pulse on nano-structures part 2.

As it is presented in Figure 6.9, the ablation for 2 scanning cycles still occurs for 90 mW, which was not observed in the previous attempt. Taking that into account, the ablation threshold for 2 scanning cycles on nano-structures was determined as 90 mW. It is worth noting that obtained values are much smaller than in case of flat surface (115 mW). It is a result of the local field enhancement caused by occurrence of localised surface plasmons [24].

6.4.2 ABLATION FOR MODULATED PULSE (WITH THE BEAMSPLITTER CUBE)

Since the second series of ablation was performed with extended pulse width, it has been started with a pulse width measurement. The measurement revealed that beamsplitter cube extends the pulse duration about 31%. Subsequently, this part of experiment followed the same procedure as in the case of unmodulated pulse and the process parameters remained unchanged. The experiment was started on the flat part of the sample and the ablation threshold was searched. During experiment, it was observed that the ablation is hindered in comparison to the process with unmodulated pulse. Ablation could be performed only for 150 mW (maximum available power) and for 6 scanning cycles. The following Figure 6.10 shows the ablated areas made during this part of the experiment. Comparing these results to the ablation threshold obtained in the first experiment, there is a relatively big difference in favour of the unmodulated pulse.

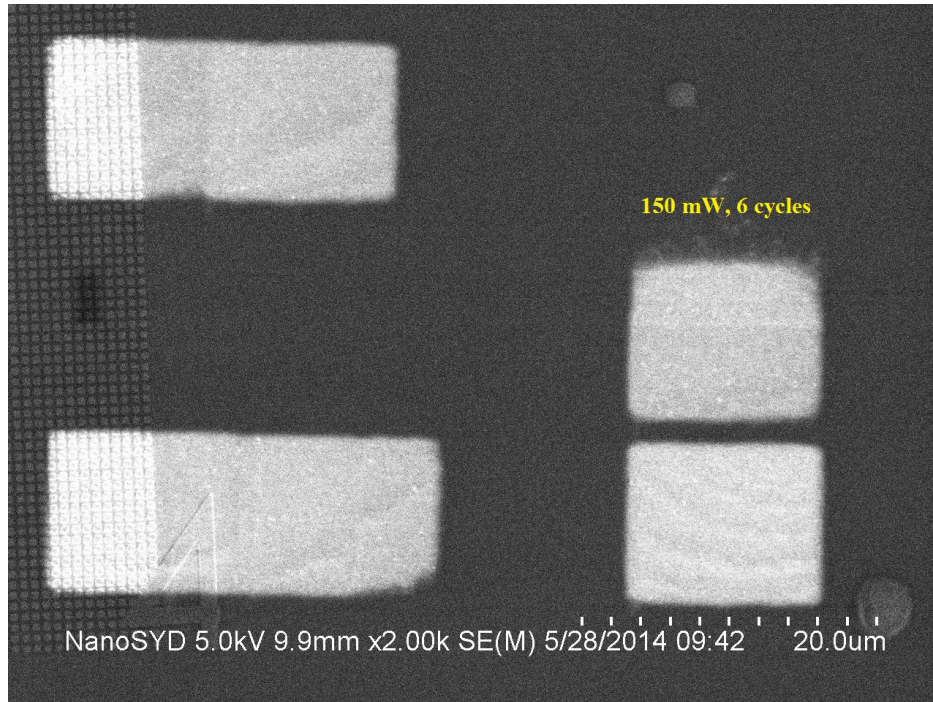


Figure 6.10 Ablated squares for modulated pulse on the flat part of the sample.

Once again the entire procedure was repeated. This time the ablation was performed on the nano-structures using modulated pulses. Since the previous research shown a big difference in ablation threshold of the modulated and unmodulated pulse, at the beginning of this experiment the ablation was performed for larger intensity values and only for 6 scanning cycles. The results are presented in the two following figures.

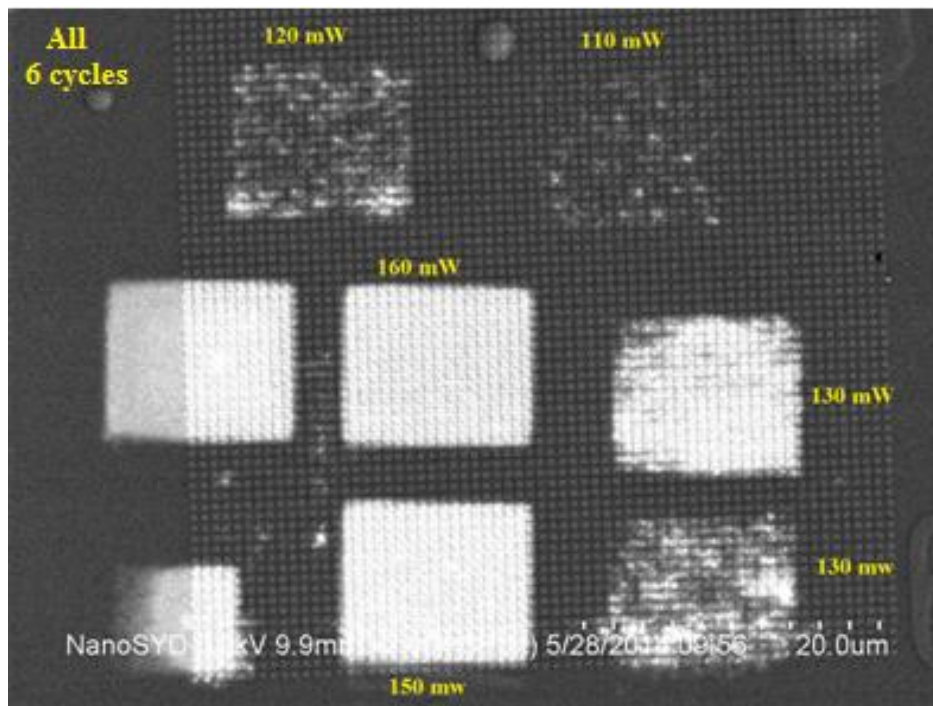


Figure 6.11 Ablated squares for modulated pulse on nano-structures. All square were ablated for 6 scanning cycles.

As it is presented in Figure 6.11, the difference in ablation threshold in comparison to the unmodulated pulse is not as big as it had been expected after the previous experiment. The square ablated using a 110mW average power still has clear signs of ablation. Taking that into account, it may be indicated that some serious problems occurred during the previous experiment. The reason for obtained difference in results may be a tilt of the sample or problems with finding a focus, which is quite a difficult task. In order to precisely determine the ablation threshold some further tests were performed. Their results are illustrated in Figure 6.12.

Two squares ablated using the same power of 130 mW, are worth a special attention. There is a significant difference in their appearance. It is a result of serious problems with finding a focus, which hinder the ablation process. Moreover, an operation of a shutter used for introducing the laser into LSM is also a big issue. The shutter is controlled manually, which results in a significant error of exposure duration. Situation presented in the Figure 6.11 should indicate how huge impact have issues with a focus and a shutter on performed experiments.

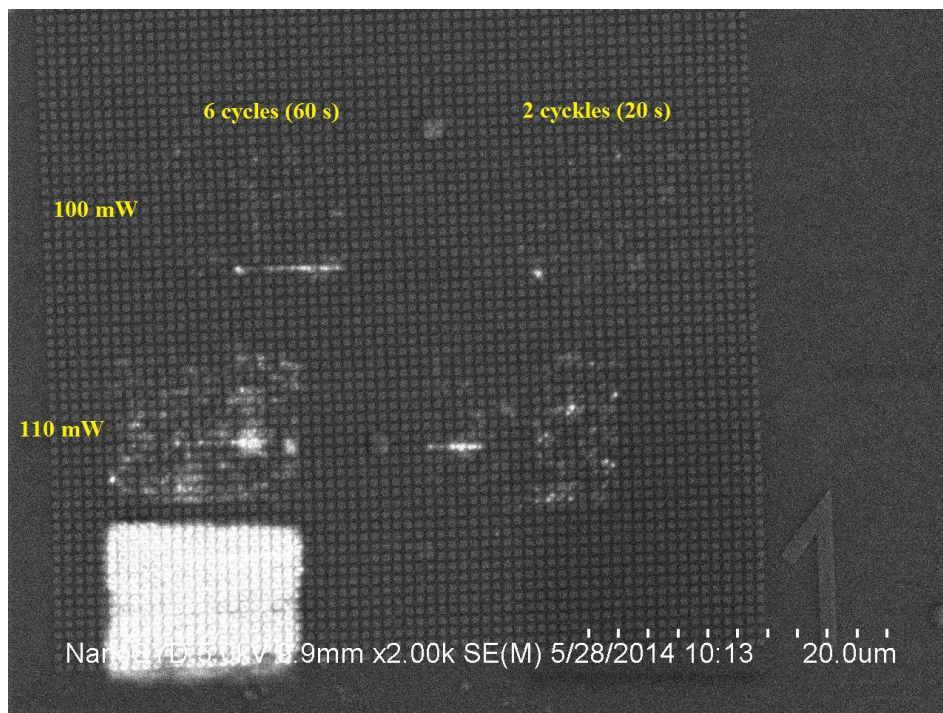


Figure 6.12 Ablated squares for modulated pulse on nano-structures.

Experimental results presented in the above figure confirm that the difference in the ablation threshold is not as big as it had been suggested by ablation without nano-structures. For 2 cycles of scanning the PMMA is still removed for 100 mW. Comparing this value with the result obtained for unmodulated pulse (90 mW), it can be stated that the ablation threshold is slightly smaller in favour of unmodulated pulse. It indicates that, for increased pulse width, the ablation threshold is also increased. The obtained result is consistent with the result of similar research, which investigated the influence of the pulse width on ablation of copper [32].

The last important matter that should be considered is related with an investigation of the sample by SEM. A long exposure for electron beam weakens bonds of PMMA, which results in local removing of the material. This situation is illustrated in Figure 6.13. In order to suppress this process, PMMA should be coated with a thin film of material, which is not affected by electron beam.

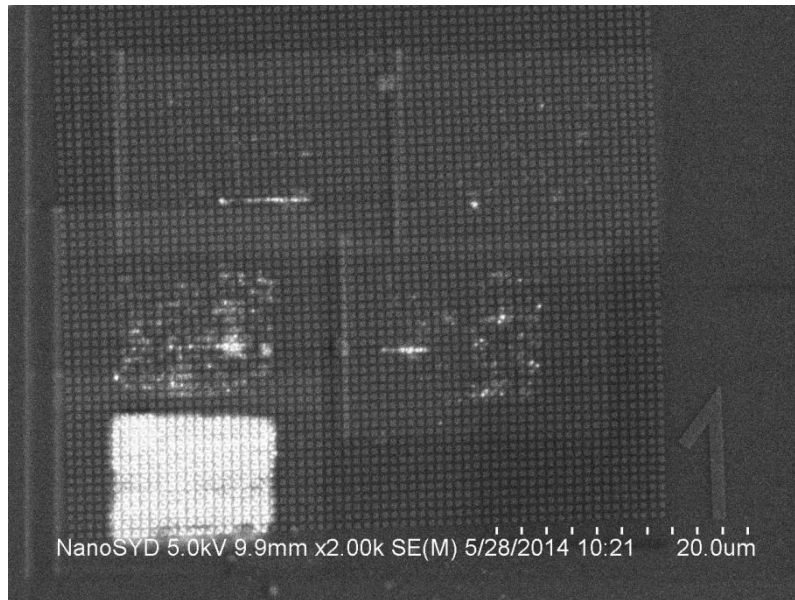


Figure 6.13 Local changes in a PMMA coating caused by electron beam.

7 CONCLUSIONS AND FURTHER IMPROVEMENTS

Comparing the work performed during this project with a list of predefined goals, it can be concluded that all assigned tasks were completed. The existing LSM setup has been upgraded by incorporating an intensity autocorrelation system. Thereby the functionality of the entire setup has been extended with pulse width measurements and basic diagnostics. Moreover, developed software for intensity autocorrelation system provides automatic measurement and allows controlling its parameters using the computer. Finally the new functionality - pulse width measurements have been used in the ablation mode of LSM in order to investigate the influence of pulse width on ablation of PMMA coatings. Detailed conclusions and improvement ideas related to individual milestones of the project are presented in dedicated sections:

➤ **Implementation of the intensity autocorrelation system.**

Considerations concerning various structures of autocorrelation system have led to the selection of the most optimal configuration in respect of used components. Moreover, the overall design of the system is well fitted in the LSM setup. Numerous tests revealed that the designed structure allows an easy access to all components of the system, which makes an adjustment process, is easy to perform. All optical components used in the system (considering replacements performed during test) were selected in terms of femtosecond applications. A small step size of the sliding table used for controlling the delay of the beam, provides great theoretical resolution of the system ($\sim 3,3$ fs). A special attention should be paid to two movable platforms (for lens and protective screen), which were designed and constructed during the project. Their presence ensures an easy positioning of the mounted components. The only improvement that can be introduced to the system is related to the mirror, which is stuck to the frame using wax. During one of tests the mirror has simply fallen down (fortunately without damaging it). In order to prevent this situation in the future, the mirror has to be stuck using some more adhesive medium or a special frame has to be used.

➤ **Developed software.**

Control over intensity autocorrelation measurements is provided by the designed software. Since two different measurement mechanisms were considered, two versions of the program were created. Performed tests revealed that both mechanisms give similar results (relative difference $< 2\%$) and the repeatability on measurements is very high (relative standard deviation $\sim 0,45\%$). Communication with the user was provided by easy in use and intuitive user's interface. Numerous tests did not reveal any abnormalities in the operation of the software. Despite the fact that the software is working correctly there are some minor improvements that can be applied. First of them is related to a communication with the user. The software does not directly inform about the execution stage of the program. The user should be informed if the program is ready to use by the user's interface and not, as it is applied now, by the behaviour of equipment (LabJack and the sliding table). The situation can be improved by implementing a diode in the interface that change its color depending on which state is actually executed. Another improvement aim to put together two versions of the program based on different measurement methods. Before tests, it was not sure if the

continuous measurement approach is going to work correctly therefore, two programs were created. After confirming a correct operation of this approach, both programs can be put together and the measurement method will depend on a user's choice.

➤ **Test of the intensity autocorrelation system.**

First tests of the autocorrelation system revealed that obtained autocorrelation function is distorted. In order to improve the measured signal and eliminate distortions, various tests and experiments were made. All components of the system were carefully tested and due to observed irregularities, some of them (optical isolator, beamsplitter, lens, BBO crystal) were replaced or removed from the system. Moreover, the geometry of the system was changed in order to prevent potential reflections. A special attention should be paid to test with a DC motor, which was intended to verify an influence of vibrations as well as geometry issues. All performed tests have contributed to improvement of the measured signal and reduced distortions. However, it has not been succeeded to remove all irregularities from autocorrelation function. The laser was the last remaining potential source of the problem. Performed measurements of the laser spectrum and a profile of the pulse may indicate potential problems with laser operation. Unfortunately, results of these measurements cannot be used to unambiguously confirm that theory. Since more reliable tools and measurement techniques were not available during this project it has been assumed that the laser operation is a cause of distortions of autocorrelation function. Taking that into account it is highly recommended to perform maintenance of the laser unit in order to fix the problem.

➤ **Laser ablation of PMMA**

During the experiment, ablation threshold for unmodulated pulse (2 scanning cycles, without structure) has been determined as 115 mW (average power). It was observed that for the same average power and a longer exposure time the ablation was conducted, what indicates the occurrence of an incubation phenomenon. Subsequently, the ablation threshold (2 scanning cycles, with structure) for structured part of the sample has been determined as 90 mW. Obtained result is consistent with these described in [14] [29] and it proves presence of the field enhancement on the nano-structures. Subsequently, the same experiment was performed for pulse extended by 31%. The ablation threshold (2 scanning cycles, without structure) has been found as 150 mW (it was found that problems with focus probably had a negative impact on this measurement). The ablation has been performed also on the nano-structures and in that case ablation threshold has been determined as 100 mW. There is a small difference between the ablation threshold for unmodulated and modulated pulses (90 mW and 100 mW respectively). Hence, it was observed that the incensement of the pulse duration increases the ablation threshold. It may indicate that the pulse width has the influence on the ablation of PMMA (at the end of the conclusions there is a comment to this statement!).

During the ablation experiment, some inconveniences and deficiencies associated mainly with the structure of the LSM has been observed. First of all there are some significant problems with finding a focus, which hinders the ablation and interfere the results (as it was presented in Figure 6.11). This issue can be avoided by performing a z-scan (axis

perpendicular to the sample) together with scanning along x and y axes. Another possible improvement is related with shatter. Manual opening and closing a shatter definitely results in a significant error in performed measurements. It is recommended to replace the manual shatter with an automatic one (it has already been ordered). It happens a few times that, the material was ablate only in one part of the sample, which was probably caused by a tilt of the sample either local (not uniform layer) or global (sample mounting). This problem can be avoided by adding two degrees of freedom to the sample mount (rotations around x and y axes) however; this solution would be hard to implement and probably very costly. Last but not least, a problem with characterization of the sample using SEM was observed. Electron beam was removing material during imaging. Therefore it is recommended to coat the sample with a material, which cannot be affected by the electron beam, before using the SEM.

Taking into account all described problems and inconveniences with the operation of the LSM in the ablation mode, it can be conclude that the uncertainty of the performed measurements is significant. Therefore, observed influence of the pulse width on the ablation threshold cannot be unambiguously confirmed. In order to confirm these results, all specified deficiencies and problems with the LSM setup has to be firstly eliminated.

8 INDEX OF FIGURES

FIGURE 2.1 SIMPLE LASER GEOMETRY. HR – HIGH REFLECTOR, OC – OUTPUT COUPLER, Z – DIRECTION OF LASER EMISSION [1].	2
FIGURE 2.2 OPERATION OF THE LASER IN A FREQUENCY DOMAIN A) MULTIMODE B) SINGLE-MODE [1].	3
FIGURE 2.3 SECOND HARMONIC GENERATION A) GENERAL CONCEPT B) ENERGY-LEVEL DIAGRAM.	5
FIGURE 2.4 SAMPLE OF COLLINEAR GEOMETRY OF AN AUTOCORRELATION SYSTEM [2].	7
FIGURE 2.5 SAMPLE OF NONCOLLINEAR GEOMETRY OF AN AUTOCORRELATION SYSTEM FOR BACKGROUND-FREE MEASUREMENTS [2].	8
FIGURE 3.1 SCHEMATIC DRAWING OF THE LABORATORY STAND.	10
FIGURE 3.2 TWO POSSIBLE CONFIGURATION OF AUTOCORRELATION SYSTEM A) BEAM REFLECTED IN THE DIRECTION OF THE INTENSITY SENSOR B) BEAM REFLECTED IN THE OPPOSITE DIRECTION.	11
FIGURE 3.3 CONSIDERED LOCATIONS FOR AUTOCORRELATION SYSTEM.	12
FIGURE 3.4 CONSIDERED SYSTEM CONFIGURATION FOR POSITION 2.	12
FIGURE 3.5 CONSIDERED CONFIGURATIONS OF THE SYSTEM FOR POSITION 1.	13
FIGURE 3.6 MIRROR MOUNTED TO A KINEMATIC MOUNT USED FOR GUIDING THE LASER BEAM TO THE AUTOCORRELATION SETUP A) POST ASSEMBLED B) POST DISASSEMBLED C) MIRROR STUCK TO THE FRAME.	14
FIGURE 3.7 SLIDING TABLE USED FOR MODIFYING LENGTH OF THE LASER PATH A) MANUFACTURER`S IMAGE [2] B) WITH MIRRORS ON A RAIL.	16
FIGURE 3.8 A) LENS MOUNTED TO THE SLIDING TABLE B) BBO CRYSTAL EMBEDDED IN ROTARY FRAME.	17
FIGURE 3.9 EQUIPMENT USED FOR INTENSITY MEASUREMENTS A) ELECTROMETER WITH ANALOGUE DISPLAY, POWER SUPPLIER (ON THE TOP OF THE AMPLIFIER) AND LABJACK – ANALOGUE-DIGITAL CONVERTER B) PHOTOMULTIPLIER.	18
FIGURE 3.10 BEAM-TERMINATING, PROTECTIVE SCREEN WITH A SLIT A) TEMPORARY SOLUTION MADE FROM CARTON B) FINAL SOLUTION EMBEDDED ON THE SLIDING-TABLE.	19
FIGURE 3.11 LIGHT SPECTRA MEASUREMENTS PERFORMED FOR VARIOUS OPTICAL FILTERS. DEUTERIUM ARC LAMP USED AS A LIGHT SOURCE.	20
FIGURE 3.12 LIGHT SPECTRA MEASUREMENTS PERFORMED FOR VARIOUS OPTICAL FILTERS. HALOGEN LAMP USED AS A LIGHT SOURCE.	20
FIGURE 3.13 ENTIRE AUTOCORRELATION SETUP WITH DESIRED LASER PATH.	21
FIGURE 3.14 COMPLETED AUTOCORRELATION SYSTEM.	22
FIGURE 4.1 SIGNAL FLOW DIAGRAM OF THE MEASUREMENT SYSTEM. SOLID LINES – DATA FLOW. DASHED LINES – POWER SUPPLY.	23
FIGURE 4.2 STATE MACHINE APPLIED IN THE SOFTWARE.	25
FIGURE 4.3 IMPLEMENTATION OF INITIATION STATE.	26
FIGURE 4.4 PROCESS DIAGRAM FOR CONTINUOUS MEASUREMENTS.	28
FIGURE 4.5 PROCESS DIAGRAM FOR STEP MEASUREMENTS.	29
FIGURE 4.6 USER INTERFACE – CONTROL TAB.	31
FIGURE 4.7 USER INTERFACE – CONTINUOUS MEASUREMENT SOFTWARE, MEASUREMENT TAB.	31

FIGURE 4.8 USER INTERFACE – STEP MEASUREMENT SOFTWARE, MEASUREMENT TAB.....	32
FIGURE 5.1 GANTRY USED IN ADJUSTMENT PROCESS.	34
FIGURE 5.2 SPECTRUM MEASUREMENTS IN A DIFFERENT PARTS OF THE SYSTEM A) AFTER LASER B) AFTER OPTICAL ISOLATOR C) AFTER A BEAMSPLITTER – STATIONARY DELAY LOOP D) AFTER A BEAMSPLITTER – CONTROLLED DELAY LOOP.	37
FIGURE 5.3 IMPLEMENTATION OF BANDWIDTH CALCULATOR.....	37
FIGURE 5.4 USER INTERFACE OF BANDWIDTH CALCULATOR.	38
FIGURE 5.5 THE RESULT OF THE VERY FIRST MEASUREMENT PERFORMED USING AUTOCORRELATION SYSTEM.	39
FIGURE 5.6 AUTOCORRELATION FUNCTION AFTER REMOVING THE OPTICAL ISOLATOR FROM THE SETUP A) WITHOUT FITTED FUNCTION B) WITH FITTED FUNCTION.....	39
FIGURE 5.7 AUTOCORRELATION FUNCTION OBTAINED WITH A COMPENSATING MIRROR APPLIED IN THE SETUP.	40
FIGURE 5.8 THE MOST OPTIMAL PROFILE OF AUTOCORRELATION FUNCTION OBTAINED DURING GEOMETRY CHANGES.....	41
FIGURE 5.9 TRANSMISSION COEFFICIENT OF BEAMSPLITTER APPLIED IN THE AUTOCORRELATION SYSTEM [13].	42
FIGURE 5.10 AUTOCORRELATION FUNCTION OBTAINED AFTER REPLACING THE BBO CRYSTAL.	43
FIGURE 5.11 AUTOCORRELATION FUNCTION FOR VARIOUS VOLTAGES APPLIED TO THE DC MOTOR MOUNTED TO THE LAST MIRROR IN THE CONSTANT DELAY LOOP A) 0 V – MOTOR TURNED OFF B) 1,5 V C) 3 V AND D) 4,5 V.	44
FIGURE 5.12 APPROXIMATE PULSE SHAPE OBTAINED USING GHz OSCILLOSCOPE.	45
FIGURE 5.13 INTENSITY AUTOCORRELATION FUNCTION OBTAINED USING A) CONTINUOUS APPROACH B) STEP APPROACH.....	46
FIGURE 6.1 SCHEMATIC DRAWING OF THE LSM SETUP [20]. M – MIRROR, PM – PERISCOPE MIRROR, SM – SCANNING MIRROR, D – DICHROMATIC MIRROR, F – ADJUSTABLE NEUTRAL DENSITY FILTER.	48
FIGURE 6.2 LSM SETUP.....	49
FIGURE 6.3 SCHEMATIC DRAWING OF THE NANO-SQUARES ARRAY LOCATED ON THE SAMPLE [20].	50
FIGURE 6.4 SAMPLE USED IN THE ABLATION EXPERIMENT.....	51
FIGURE 6.5 SEM IMAGES OF ABLATED SQUARES FOR DIFFERENT VALUES OF VOLTAGE APPLIED TO SCANNING MIRRORS A) 1000 B) 800 C) 600 D) 400.....	52
FIGURE 6.6 DIMENSIONS OF THE ABLATED AREA AS A FUNCTION OF VOLTAGE APPLIED TO SCANNING MIRRORS.....	54
FIGURE 6.7 ABLATED SQUARES FOR UNMODULATED PULSE ON THE FLAT PART OF SAMPLE.	56
FIGURE 6.8 ABLATED SQUARES FOR UNMODULATED PULSE ON NANO-STRUCTURES PART 1. LEFT COLUMN CORRESPONDS TO 6 SCANNING CYCLES, WHILE THE RIGHT COLUMN CORRESPONDS TO 2 CYCLES.	56
FIGURE 6.9 ABLATED SQUARES FOR UNMODULATED PULSE ON NANO-STRUCTURES PART 2.	57
FIGURE 6.10 ABLATED SQUARES FOR MODULATED PULSE ON THE FLAT PART OF THE SAMPLE..	58
FIGURE 6.11 ABLATED SQUARES FOR MODULATED PULSE ON NANO-STRUCTURES. ALL SQUARE WERE ABLATED FOR 6 SCANNING CYCLES.....	58

FIGURE 6.12 ABLATED SQUARES FOR MODULATED PULSE ON NANO-STRUCTURES..... 59
FIGURE 6.13 LOCAL CHANGES IN A PMMA COATING CAUSED BY ELECTRON BEAM. 60

9 INDEX OF TABLES

TABLE 2-1 THE MOST COMMON PULSE PROFILES WITH CORRESPONDING AUTOCORRELATION FUNCTIONS AND DECONVOLUTION FACTORS [2].	8
TABLE 5-1 THICKNESS OF THE BBO CRYSTAL REQUIRED FOR CERTAIN THE PULSE DURATION [12].	42
TABLE 5-2 RESULTS OF MEASUREMENTS OBTAINED USING CONTINUOUS METHOD WITH CORRESPONDING STATISTICS.	46
TABLE 5-3 RESULTS OF MEASUREMENTS OBTAINED USING STEP METHOD WITH CORRESPONDING STATISTICS.	47
TABLE 6-1 HORIZONTAL DIMENSION OF THE ABLATED ARE DEPENDING ON VARIOUS VOLTAGES APPLIED TO SCANNING MIRRORS.	53
TABLE 6-2 VERTICAL DIMENSION OF THE ABLATED ARE DEPENDING ON VARIOUS VOLTAGES APPLIED TO SCANNING MIRRORS.	53

10 REFERENCES

- [1] A. M. Weiner, in *Ultrafast Optics*, John Wiley & Sons, Inc., 2009, pp. 10-22.
- [2] J-C. Diels, W. Rudolph, "Ultrashort Laser Pulse Phenomena," Elsevier, 2006, pp. 9-12.
- [3] A. M. Weiner, in *Ultrafast Optics*, Hoboken, John Wiley & Sons, Inc., 2009, p. chapter 2.
- [4] R. W. Boyd, in *Nonlinear Optics Third Edition*, Elsevier, 2008, p. chapter 1.
- [5] Dr. Rüdiger Paschotta, "RP Photonics Encyclopedia," [Online]. Available: http://www.rp-photonics.com/phase_matching.html. [Accessed 25 05 2014].
- [6] Angela Goodacre, Dennis Donley and Jiwei Jai, Olympus America Inc., "Combining Second-Harmonic Generation with Multiphoton Imaging," *Biophotonics*, 2010.
- [7] A. Weiner, "Ultrafast Optics," Hoboken, John Wiley & Sons, Inc., 2009, pp. 99-104.
- [8] J-C. Diels, W. Rudolph, "Ultrashort Laser Pulse Phenomena," Elsevier Inc, 2006, pp. 457-459.
- [9] Swamp Optics, [Online]. Available: http://www.swampoptics.com/tutorials_autocorrelation.htm. [Accessed 17 05 2014].
- [10] L. Urecht and T. Lippert, "Photoablation of polymer materials," in *Photochemistry and Photophysics of Polymer Materials*, 2010, John Wiley & Sons, Inc..
- [11] E. G. Gamaly, A. V. Rode, V. T. Tikhonchuk and B. Luther-Davies, "Ablation of solids by femtosecond lasers: ablation mechanism and ablation thresholds for metals and dielectrics," *Phys. Rev. A* 23, 2001.
- [12] F. Di Nisoa, C. Gaudiuso, T. Sibillano, F.P. Mezzapesa, A. Ancona and P.M. Lugarà, "Influence of the Repetition Rate and Pulse Duration on the Incubation Effect in Multiple-Shots Ultrafast Laser Ablation of Steel," *Physics Procedia*, vol. 41, p. 698–707, 2013.
- [13] S. Baudach, J. Bonse, J. Kruger, W. Kautek, "Ultrashort pulse laser ablation of polycarbonate and polymethylmethacrylate," *Applied Surface Science*, Vols. 154-155, p. 555–560, 200.
- [14] J. Fiutowski, C. Maibohm, O. Kostiuenco, J. Kjelstrup-Hansen and H.-G. Rubahn, "Near-field mapping by laser ablation of PMMA coatings," *Proc. of SPIE Vol. 8096 809629-1*, 2014.

- [15] Tai-Chang Chen, Robert B. Darling, “Laser micromachining of the materials using in microfluidics by high precision pulsed near and mid-ultraviolet Nd:YAG lasers,” *Journal of Materials Processing Technology*, vol. 198, p. 248–253, 2008.
- [16] E. Ina, N. Matsumoto, E Shikada, F. Kannari, “Laser ablation deposition of crystalline copper-phthalocyanine thin films,” *Applied Surface Science*, Vols. 127-129, p. 574–578, 1998.
- [17] “MedlinePlus,” U.S. National Library of Medicine, [Online]. Available: <http://www.nlm.nih.gov/medlineplus/ency/article/007368.htm>. [Accessed 31 05 2014].
- [18] Zaber Technologies, [Online]. Available: http://www.zaber.com/products/product_detail.php?detail=T-LSR150B#tabs. [Accessed 02 05 2014].
- [19] “International Standard IEC 60825-1 Safety of laser products Part 1: Equipment classification, requirements and user's guide, Edition 1.2,” 2001.
- [20] [Online]. Available: http://www.zaber.com/wiki/Software/ASCII_Labview_Driver. [Accessed 10 05 2014].
- [21] [Online]. Available: <http://labjack.com/support/u12/users-guide/4>. [Accessed 14 05 2014].
- [22] Dr. Rüdiger Paschotta, “RP Photonics Encyclopedia,” [Online]. Available: http://www.rp-photonics.com/time_bandwidth_product.html. [Accessed 20 05 2014].
- [23] Clark-MXR Inc., [Online]. Available: <http://www.cmxr.com/Education/TBproduct.html>. [Accessed 18 05 2014].
- [24] Seong Kyeong Photonics, [Online]. Available: http://www.skphotonics.com/pdf/la_pdf/Isolator.pdf. [Accessed 22 05 2014].
- [25] J-C. Diels, W. Rudolph, in *Ultrashort Laser Pulse Phenomena*, Elsevier, 2006, p. chapter 2.
- [26] ThorLabs, [Online]. Available: http://www.thorlabs.de/newgrouppage9.cfm?objectgroup_id=898. [Accessed 24 05 2014].
- [27] Eksma Optics, [Online]. Available: <http://eksmaoptics.com/femtoline-components/femtoline-nonlinear-laser-crystals/thin-bbo-crystals-for-shg-of-ti-sapphire-laser-wavelength/#attributes>. [Accessed 24 05 2014].
- [28] C. Maibohm, “PhD. Thesis,” in *Generation and characterization of functionalized*, 2010,

p. chapter 5.

- [29] J. Fiutowski, C. Maibohm, O. Kostiučenko, J. Kjelstrup-Hansen, H.-G. Rubahn, “Mapping of gold nanostructure-enhanced near fields via laser scanning second-harmonic generation and ablation,” *Journal of nanophysics*, 2012.
- [30] J. Fiutowski, C. Maibohm, J. Kjelstrup-Hansen, and H.-G. Rubahn, “Laser ablation of polymer coatings allows for electromagnetic field,” *APPLIED PHYSICS LETTERS* 98, 193117, 2011.
- [31] A. Hohenau, J. R. Krenn, F. Garcia-Vidal, S. G. Rodrigo, L. Martin-Moreno, J. Beermann, and S. I. Bozhevolnyi, “Spectroscopy and nonlinear microscopy of gold nanoparticle arrays on gold films,” *Phys. Rev. B*, 75, 085104, 2007.
- [32] M. Hashida, A.F. Semerok, O. Gobert, G. Petite, Y. Izawa and J.F. Wagner, “Ablation threshold dependence on pulse duration for copper,” *Applied Surface Science*, Vols. 197-198, p. 862–867, 2002.

11 APPENDICES

APPENDIX A – DATASHEET OF TSUNAMI LASER

Tsunami

Specifications

Table 3-1 lists performance specifications for fs configurations. Table 3-2 lists those for ps configurations. Table 3-3 lists the electrical, mechanical and physical specifications. Specifications for the optional Lok-to-Clock system are found in Table 8-1 in chapter 8. Figure 3-5 and Figure 3-6 earlier in this chapter show the tuning curves for typical fs and ps systems, respectively.

	710 nm Blue (B)	790 nm Standard (S)		850 nm Mid (M)	900 nm⁷ Long (L)	1053 nm⁷ X-Long (X)
Average Power² with < 12 W TEM ₀₀ pump with < 10 W TEM ₀₀ pump with 6 W TEM ₀₀ pump	400 mW 375 mW 300 mW	1.1 W 1.0 W 500 mW	1.5 W 1.0 W 500 mW	1.1 W 1.0 W 500 mW	600 mW 500 mW 300 mW	250 mW N/A N/A
Peak Power² with < 12 W TEM ₀₀ pump with < 10 W TEM ₀₀ pump with 6 W TEM ₀₀ pump	> 37 kW > 35 kW > 28 kW	> 165 kW > 150 kW > 75 kW	> 140 kW > 95 kW > 50 kW	> 165 kW > 150 kW > 75 kW	> 55 kW > 47 kW > 28 kW	> 25 kW N/A N/A
Pulse Width^{3,8}	< 130 fs	< 80 fs	< 130 fs	< 80 fs	< 130 fs	< 130 fs
Tuning Range (nm) with < 12 W TEM ₀₀ pump with < 10 W TEM ₀₀ pump with 6 W TEM ₀₀ pump	690 – 790 690 – 790 690 – 790	720 – 850 720 – 850 735 – 840		780 – 900 780 – 900 800 – 900	840 – 1000 840 – 1000 850 – 990	970 – 1080 N/A N/A
Repetition Rate⁴	82 MHz					
Noise^{5,7}	< 2%					
Stability^{6,7}	< 5%					
Spatial Mode	TEM ₀₀					
Beam Diameter at 1/e² points	< 2 mm					
Beam Divergence, full angle	< 0.6 mrad					
Polarization	> 500:1 vertical					

¹ Specifications subject to change without notice and only apply when Tsunami is pumped by a Spectra-Physics Lasers BeamLok™ 2040E, 2080, or 2060 argon ion laser.

² Specifications apply to operation at the wavelength noted.

³ A sech² pulse shape (0.65 deconvolution factor) is used to determine the pulse width as measured with a Spectra-Physics Lasers Model 409 autocorrelator.

⁴ Laser operation is only specified at 82 MHz, or 80 MHz for the Model 3960C.

⁵ rms, measured in a 10 Hz to 2 MHz bandwidth.

⁶ Percent power drift in any 2-hour period after 1 hour warm-up and less than ± 3°C temperature change.

⁷ Specifications guaranteed with environmental package.

⁸ Pulse widths below 50 fs and between 150 fs and 1 ps are also available. Contact your local Spectra-Physics Lasers representative for more details.

APPENDIX B – BLOCK DIAGRAM OF STEP MEASUREMENT PROGRAM

**APPENDIX C – BLOCK DIAGRAM OF CONTINUOUS
MEASUREMENT PROGRAM**